

# Elucidating the role of long-distance electron transfer by cable bacteria in freshwater sediments and contaminated aquifers

## **Dissertation**

zur Erlangung des akademischen Grades einer Doktorin  
der Naturwissenschaften (Dr. rer. nat.)  
an der Fakultät für Biologie, Chemie und Geowissenschaften  
der Universität Bayreuth

vorgelegt von

**Corinna Sachs**

aus Celle

Bayreuth, 2022

Die vorliegende Arbeit wurde in der Zeit von Oktober 2016 bis April 2019 am Institut für Grundwasserökologie am Helmholtz Zentrum für Gesundheit und Umwelt München und von Mai 2019 bis Februar 2022 (mit krankheitsbedingter Unterbrechung von März 2021 bis Mai 2021 und einer Unterbrechung aufgrund einer Weiterbildung von September 2021 bis Dezember 2021) an der Universität Bayreuth am Lehrstuhl für Ökologische Mikrobiologie unter Betreuung von Herrn Professor Dr. Tillmann J. Lüders angefertigt.

Vollständiger Abdruck der von der Fakultät für Biologie, Chemie und Geowissenschaften der Universität Bayreuth genehmigten Dissertation zur Erlangung des akademischen Grades einer Doktorin der Naturwissenschaften (Dr. rer. Nat.).

Dissertation eingereicht am: 02.03.2022

Zulassung durch die Promotionskommission: 06.04.2022

Wissenschaftliches Kolloquium: 26.09.2022

Amtierender Dekan: Prof. Dr. Benedikt Westermann

Prüfungsausschuss:

Prof. Dr. Tillmann J. Lüders	(Gutachter)
Prof. Dr. Heike Feldhaar	(Gutachterin)
Prof. Dr. Dirk Schüler	(Vorsitz)
Prof. Dr. Eva Lehndorff	

## Abstract

Contamination of freshwater resources by hydrocarbons is a worldwide problem, and leads to damage of ecosystems and diminishing of drinking water supplies. Biodegradation is a possible way to remove pollutants from the environment, and certain microbes are able to metabolize and efficiently break down contaminants. In anoxic sediment, anaerobic hydrocarbon degradation predominantly occurs at redox gradients, where microbes rely on alternative electron acceptors, other than oxygen, for biodegradation, but are subject to limited electron acceptor availability. Recently discovered cable bacteria (CB) can overcome such limitation by forming filaments for long-distance electron transfer (LDET). These filaments enable CB to perform oxygen-dependent, electrogenic sulphur oxidation (e-SOX), they spatially separate redox half reactions over cm-distances, and consequentially allow them to overcome diffusion limitation and redox stratification in aquatic sediments. However, their unique geochemical requirements render CB notoriously difficult to cultivate, complicating investigations on their ecology. It is the aim of this thesis to establish a viable cultivation approach for the enrichment of freshwater cable bacteria, to investigate the occurrence and/or diversity of cable bacteria, and to elucidate the role of LDET in biodegradation of toluene.

In the first part of this doctoral thesis, I focus on a viable cultivation strategy for freshwater CB and introduce a new “agar pillar” approach to selectively enrich and investigate CB populations from aquatic sediments in laboratory columns. Within sediment columns, a central agar pillar is embedded, providing a sediment-free gradient system in equilibrium with surrounding sediment. Sediments from different freshwater systems (a streambed, a meromictic sulfidic lake, a polluted aquifer, river and lake sediments from mining-impacted Fichtelgebirge region) were incubated with the agar pillar approach. Microsensor profiling during column incubation revealed multiple characteristics of e-SOx, such as a suboxic zone between oxic surface and sulfidic sediments, as well as the establishment of electric potentials. Bacterial communities in agar pillars and surrounding sediment were analysed over depth by PacBio full-length 16S rRNA gene amplicon sequencing, allowing for a very accurate phylogenetic placement of detected populations. Putative CB affiliated with *Desulfobulbaceae* were detected in nearly all incubations and sediment types. Indeed, the selective niche of the agar pillar was preferentially colonized by CB from surface water sediments, but not so for groundwater sediments. While aquifer sediments hosted putative CB affiliated with *Desulfurivibrio* spp., CB clearly within the genus *Ca. Electronema*, representing several potentially novel species, prevailed in surface freshwater sediment columns. CB were seemingly linked to co-enriched fermenters, hinting at a possible role of e-SOx populations as an electron sink for heterotrophic microbes. Absence of CB resulted in similar microbiomes of agar pillar and surrounding sediment, suggesting agar pillar colonization by fermenters

may indeed be linked to LDET. These findings add to the current understanding of the diversity and ecology of cable bacteria in freshwater systems, highlighting a differentiation of CB from distinct surface and groundwater sediments. In conclusion, the agar pillar provides a new cultivation strategy that may facilitate enrichment of redox gradient-dependent microorganisms, including previously unrecognized CB populations.

In the second part of this thesis, I focus on the role of LDET in microbial toluene biodegradation. In a <sup>13</sup>C-toluene microcosm incubation experiment with freshwater sediment, I followed toluene degradation with a combination of biogeochemical and molecular biology methods utilizing by DNA-stable isotope probing (DNA-SIP). A subset of my incubations included filter membranes at relevant depths to prevent CB growth. The results of this multipronged approach allowed to identify toluene degraders and compare contaminant degradation between the same sediment with and without a possible involvement of LDET by CB. Depth-resolved microprofiling showed signatures of LDET in microcosms without filters, while headspace analysis revealed significantly more toluene degradation in microcosms when no filters were present. Microbial community analysis suggested that predominantly members of *Gammaproteobacteria*, specifically *Rhodocyclaceae*, *Comamonadaceae*, *Burkholderiaceae* and *Moraxellaceae*, and *Alphaproteobacteria*, specifically, *Beijerinckiaceae*, degraded toluene. These microbial groups were more abundant in microcosms without filters as compared to microcosms including filters, hinting at a presumed indirect impact of LDET for contaminant degradation.

Concluding, this thesis provides important new insights into the diversity and ecology of cable bacteria in freshwater systems, as well as a so far mostly unrecognised impact of LDET within sedimentary microbial communities. A possible function of CB-mediated e-SOx and LDET as an electron sink for heterotrophic microbes is considered relevant for potential future remediation endeavours of contaminated sediments. Previous strategies for contaminant removal by providing electron acceptors for anaerobic biodegradation are viable, but resource-intensive. Instead, the further exploration and harnessing of the potential of LDET by CB, intrinsically present within sedimentary systems, could offer an attractive alternative.

## Zusammenfassung

Die Kontamination von Süßwasserressourcen durch Kohlenwasserstoffe ist ein weltweites Problem und führt zur Schädigung von Ökosystemen und zur Verringerung der Trinkwasserversorgung. Der biologische Abbau ist ein möglicher Weg, um Schadstoffe aus der Umwelt zu entfernen, und bestimmte Mikroben sind in der Lage, Schadstoffe zu verstoffwechseln und effizient abzubauen. In anoxischen Sedimenten tritt der anaerobe Kohlenwasserstoffabbau überwiegend an Redoxgradienten auf, wo Mikroben für den biologischen Abbau auf andere Elektronenakzeptoren als Sauerstoff angewiesen sind, aber einer begrenzten Verfügbarkeit von Elektronenakzeptoren unterliegen. Kürzlich entdeckte Kabelbakterien (CB) können diese Einschränkung überwinden, indem sie Filamente für den Elektronentransfer über große Entferungen (LDET) bilden. Diese Filamente ermöglichen es CB, eine sauerstoffabhängige, elektrogene Schwefeloxidation (e-SOX) durchzuführen, sie trennen Redoxhalbreaktionen räumlich über cm-Abstände und ermöglichen es ihnen folglich, Diffusionsbeschränkungen und Redoxschichtungen in aquatischen Sedimenten zu überwinden. Ihre einzigartigen geochemischen Anforderungen machen es jedoch notorisch schwierig, CB zu kultivieren, was Untersuchungen zu ihrer Ökologie erschwert. Ziel dieser Arbeit ist es, einen praktikablen Kultivierungsansatz zur Anreicherung von Süßwasserkabelbakterien zu etablieren, das Vorkommen und/oder die Diversität von Kabelbakterien zu untersuchen und die Rolle von LDET beim biologischen Abbau von Toluol aufzuklären.

Im ersten Teil dieser Doktorarbeit konzentriere ich mich auf eine praktikable Kultivierungsstrategie für Süßwasser-CB und stelle einen neuen „Agarsäulen“-Ansatz vor, um CB-Populationen aus aquatischen Sedimenten in Laborsäuleninkubationen selektiv anzureichern und zu untersuchen. Innerhalb der Sedimentmikroskopen ist eine zentrale Agarsäule eingebettet, die ein sedimentfreies Gradientensystem im Gleichgewicht mit dem umgebenden Sediment darstellt. Sedimente aus verschiedenen Süßwassersystemen (ein Bachbett, ein meromiktischer sulfidischer See, ein belasteter Aquifer, Fluss- und Seesedimente aus der Bergbau-beeinflussten Region des Fichtelgebirges) wurden mit dem Agarsäulenansatz inkubiert. Mikrosensormessungen entlang der Sediment- und Agarsäule während der Inkubation zeigten mehrere Eigenschaften von e-SOX, wie eine suboxische Zone zwischen der oxidischen Oberfläche und sulfidischen Sedimenten, sowie die Etablierung elektrischer Potentiale. Bakteriengemeinschaften in Agarsäulen und umgebenden Sedimenten wurden über die Tiefe durch PacBio-16S-rRNA-Gen-Amplikon-Sequenzierung in voller Länge analysiert, was eine sehr genaue phylogenetische Platzierung der nachgewiesenen Populationen ermöglichte. Mutmaßliche mit *Desulfobulbaceae* assoziierte CB wurden in fast allen Inkubationen und Sedimenttypen nachgewiesen. Tatsächlich wurde die selektive Nische der Agarsäule bevorzugt von CB aus

Oberflächenwassersedimenten besiedelt, nicht jedoch aus Grundwassersedimenten. Während Aquifersedimente mutmaßliche CB beherbergten, die mit *Desulfurivibrio* spp. assoziiert sind, gehören CB aus Oberflächen-Süßwasser-Sedimentsäulen eindeutig zur Gattung *Ca. Electronema*, und weisen potenziell neue CB-Spezies auf. Ein Vorhandensein von CB war mutmaßlich mit co-angereicherten Fermentern verbunden, was auf eine mögliche Rolle von e-SOx-Populationen als Elektronensenke für heterotrophe Mikroben hinweist. Das Fehlen von CB führte zu ähnlichen Mikrobiomen der Agarsäule und des umgebenden Sediments, was darauf hindeutet, dass die Besiedlung der Agarsäule durch Fermenter tatsächlich mit LDET in Verbindung gebracht werden könnte. Diese Ergebnisse tragen zum aktuellen Verständnis der Diversität und Ökologie von Kabelbakterien in Süßwassersystemen bei und unterstreichen eine Unterscheidung von CB von vielfältigen Oberflächensedimenten und Grundwassersedimenten. Zusammenfassend bietet die Agarsäule eine neue Kultivierungsstrategie, die die Anreicherung von redoxgradientenabhängigen Mikroorganismen, einschließlich bisher nicht erkannter CB-Populationen, erleichtern kann.

Im zweiten Teil dieser Arbeit konzentriere ich mich auf die Rolle von LDET beim mikrobiellen biologischen Abbau von Toluol. In einem <sup>13</sup>C-Toluol-Mikrokosmos-Inkubationsexperiment mit Süßwassersediment verfolgte ich den Toluolabbau mit einer Kombination aus biogeochemischen und molekularbiologischen Methoden unter Verwendung von DNA-Stable-Isotope-Probing (DNA-SIP). Ein Teil meiner Inkubationen umfasste Filtermembranen in relevanten Tiefen, um das CB-Wachstum zu verhindern. Die Ergebnisse dieses mehrgleisigen Ansatzes ermöglichten es, Toluolabbauer zu identifizieren und den Schadstoffabbau zwischen demselben Sediment mit und ohne eine mögliche Beteiligung von LDET durch CB zu vergleichen. Tiefenaufgelöste Mikroprofile zeigten Signaturen von LDET in Mikrokosmen ohne Filter, während die Analyse der Gasphase einen signifikant stärkeren Toluolabbau in Mikrokosmen zeigte, wenn keine Filter vorhanden waren. Die Analyse der mikrobiellen Gemeinschaft legte nahe, dass überwiegend Mitglieder von *Gammaproteobacteria*, insbesondere *Rhodocyclaceae*, *Comamonadaceae*, *Burkholderiaceae* und *Moraxellaceae*, und *Alphaproteobacteria*, insbesondere *Beijerinckiaceae*, Toluol abbauen. Diese mikrobiellen Gruppen waren in Mikrokosmen ohne Filter häufiger als in Mikrokosmen mit Filtern, was auf einen vermuteten indirekten Einfluss von LDET auf den Schadstoffabbau hindeutet.

Abschließend liefert diese Arbeit wichtige neue Einblicke in die Diversität und Ökologie von Kabelbakterien in Süßwassersystemen, sowie in einen bisher weitgehend unerkannten Einfluss von LDET auf sedimentäre mikrobielle Gemeinschaften. Eine mögliche Funktion von CB-vermitteltem e-SOx und LDET als Elektronensenke für heterotrophe Mikroben wird als relevant für mögliche zukünftige Sanierungsbemühungen kontaminiertes Sedimente erachtet. Frühere Strategien zur

Schadstoffentfernung durch Bereitstellung von Elektronenakzeptoren für den anaeroben biologischen Abbau sind praktikabel, aber ressourcenintensiv. Stattdessen könnte die weitere Erforschung und Nutzung des Potenzials von LDET durch CB, welche in Sedimentsystemen intrinsisch vorhanden sind, eine attraktive Alternative bieten.

# Table of Contents

Abstract .....	3
Zusammenfassung .....	5
List of figures .....	12
List of tables .....	14
Abbreviations and symbols .....	15
Abbreviations .....	15
Symbols .....	16
1. Introduction .....	17
1.1. Redox stratification in aquatic sediments.....	17
1.2. Cable bacteria .....	17
1.2.1. Finding of spatial decoupling of redox half-reactions .....	17
1.2.2. Occurrence of cable bacteria.....	19
1.2.3. Physiology of cable bacteria .....	21
1.2.4. Phylogeny and evolution of cable bacteria .....	22
1.3. Long-distance electron transfer (LDET) in cable bacteria .....	23
1.4. Influence of cable bacteria on biogeochemistry of sediments .....	25
1.4.1. Cable bacteria impact element cycling in sediments .....	25
1.4.2. Influence of cable bacteria on microbial community and sedimentary biosphere .....	26
1.5. Contaminations in freshwater and groundwater sediments .....	27
1.5.1. Petroleum hydrocarbons and BTEX contaminants .....	28
1.5.2. Biodegradation of toluene in bacteria.....	30
1.5.3. Bioremediation .....	31
1.5.4. Cable bacteria and contaminated sites .....	31
1.5.5. POLLOX project outline.....	32
1.6. Thesis objectives .....	33

1.7.	Coordination and funding .....	35
2.	Materials and methods .....	36
2.1.	Sampling and site descriptions .....	36
2.1.1.	Streambed sediment near Garching.....	36
2.1.2.	Alpine Lake Alatsee.....	36
2.1.3.	The tar-oil contaminated site in Düsseldorf-Flingern.....	36
2.1.4.	Grassland soil.....	36
2.1.5.	Sampling sites in the Fichtelgebirge .....	37
2.2.	Microcosm design .....	38
2.2.1.	Upright laboratory incubation setup: Introducing the “Agar Pillar” technique.....	38
2.2.2.	Setup for toluene biodegradation .....	39
2.3.	Microcosm biogeochemistry.....	42
2.4.	Chemical analysis accompanying toluene biodegradation .....	43
2.4.1.	Toluene detection in liquid samples by HPLC.....	43
2.4.2.	Gas chromatography for total CO <sub>2</sub> .....	43
2.4.3.	Relative abundance of stable carbon isotopes via GC-IRMS .....	44
2.5.	Fluorescence <i>in situ</i> hybridization and microscopy .....	44
2.5.1.	Sample fixation .....	44
2.5.2.	FISH .....	44
2.5.3.	Microscopy .....	45
2.6.	DNA extraction and molecular methods.....	46
2.6.1.	DNA extraction from sediments and soil.....	46
2.6.2.	DNA extraction from agar.....	46
2.6.3.	PCR.....	47
2.6.4.	Microbial community fingerprinting.....	47
2.7.	Stable isotope probing (DNA-SIP) .....	48
2.7.1.	Stable isotopes .....	48

2.7.2. Isopycnic centrifugation of labelled and unlabelled DNA.....	48
2.8. Next generation sequencing .....	49
2.8.1. PacBio full-length 16S rRNA sequencing .....	49
2.8.2. Illumina 16S rRNA sequencing .....	52
2.9. Data handling and bioinformatics.....	52
2.9.1. 16S rRNA data handling from PacBio SMRT sequencing .....	52
2.9.2. 16S rRNA data from Illumina iSeq100 .....	53
2.9.3. Phylogenetic tree construction .....	54
3. Results .....	55
3.1. The “Agar Pillar” technique: Pre-experiments.....	55
3.2. Discovery of cable bacteria in aquatic sediments.....	57
3.2.1. Column biogeochemistry in investigated freshwater sediments .....	57
3.2.2. FISH and microscopy of filaments .....	60
3.2.3. Community composition via full-length 16S rRNA amplicon sequencing .....	62
3.2.4. Phylogenetic placement of 16S rRNA amplicon sequences .....	65
3.3. Cable bacteria in the aquatic sediments of the Fichtelgebirge.....	67
3.3.1. Biogeochemistry of columns from the Fichtelgebirge.....	67
3.3.2. FISH and microscopy in Fichtelgebirge samples .....	71
3.3.3. 16S rRNA amplicon sequencing and community analysis in Fichtelgebirge samples.....	72
3.3.4. Phylogeny of Fichtelgebirge samples with ARB .....	77
3.4. Testing the role of CB in anaerobic toluene degradation in lake sediments .....	77
3.4.1. Tracing of oxygen concentrations during microcosm incubation.....	77
3.4.2. Production of CO <sub>2</sub> and <sup>13</sup> CO <sub>2</sub> during sediment incubation .....	78
3.4.3. Biogeochemistry of toluene-degrading microcosms .....	80
3.4.4. Depth-resolved microbial communities .....	83
3.4.5. <sup>13</sup> C-isotope-labelling of toluene degraders.....	88
4. Discussion.....	93

4.1.	Tracing LDET and cable bacteria in freshwater sediments by gradient columns.....	93
4.1.1.	Establishing agar pillars with water-inundated soil columns .....	93
4.1.2.	Biogeochemistry and LDET in freshwater sediments .....	93
4.1.3.	Selective niche of the agar pillar.....	95
4.1.4.	Phylogenetic placement of terrestrial cable bacteria.....	95
4.1.5.	Cable bacteria- and redox gradient-associated microbiomes .....	96
4.2.	Cable bacteria from acidic mining-impacted freshwater sediments of the Fichtelgebirge .	97
4.2.1.	The “Agar Pillar” approach in acidic freshwater sediments .....	97
4.2.2.	Phylogenetic placement of <i>Desulfobulbaceae</i> from mining-impacted freshwater .....	97
4.2.3.	Biogeochemistry and LDET in Acidic Mining-Impacted Freshwater Systems .....	98
4.2.4.	Cable bacteria-associated microbiomes from mining-impacted freshwater systems.....	99
4.3.	Toluene degradation in a freshwater sediment microbial community affected by LDET..	100
4.3.1.	Biogeochemistry in Microcosms Amended with Toluene and Control .....	100
4.3.2.	CO <sub>2</sub> -Enrichment in Microcosms .....	101
4.3.3.	Depth-Resolved Microbial Community Composition in Microcosms .....	102
4.3.4.	Toluene-Degrader Community Identified by DNA-SIP.....	103
5.	Synopsis and outlook .....	105
6.	References.....	108
	Appendix 1: Supporting Information.....	125
	Appendix 2: Bioinformatics Example.....	133
	Manuscripts and Conference Contributions .....	135
	Manuscripts.....	135
	Conference Contributions .....	135
	Authorship Clarification .....	137
	Acknowledgments.....	139
	Statutory Declaration / Eidesstattliche Erklärung .....	141

## List of figures

Figure 1: Schematic drawing of biogeochemical profile in sediment with cable bacteria.....	18
Figure 2: Schematic drawing of cable bacteria filament cross section.....	24
Figure 3: Overview of structural diagrams of the BTEX hydrocarbons .....	29
Figure 4: Current perspective of biodegradation at fringes of groundwater contaminant plumes.....	33
Figure 5: Schematic drawing of the agar pillar gradient column setup.....	39
Figure 6: Schematic drawing of microcosm design for DNA-SIP experiment with labelled toluene.....	42
Figure 7: Scheme of PacBio full-length 16S rRNA amplicon sequencing preparation.....	49
Figure 8: Scheme of amplicon sequencing on the PacBio Sequel System.....	51
Figure 9: Geochemical depth-profiles measured in water-inundated soil incubations .....	56
Figure 10: Microbial community composition in of water-inundated grassland soil samples.....	56
Figure 11: Geochemical depth profiles in column incubations of Garching streambed sediments.....	58
Figure 12: Geochemical depth profiles in column incubations of Lake Alatsee sediments. ....	59
Figure 13: Geochemical depth profiles in column incubations of Flingern aquifer sediments.....	60
Figure 14: Fluorescent microscopy of filamentous cable bacteria detected in sediment columns. ....	61
Figure 15: Community composition of streambed microcosms. ....	63
Figure 16: Community composition of lake sediment microcosms. ....	64
Figure 17: Community composition of aquifer sediment microcosms. ....	65
Figure 18: Phylogenetic placement of full-length 16S rRNA gene reads of presumed species-level cable bacteria groups .....	66
Figure 19: Geochemical depth profiles in column incubations of Lake Fichtelsee sediments. ....	68
Figure 20: Geochemical depth profiles in column incubations of Lake Weißenstädter See sediments. ....	69
Figure 21: Geochemical depth profiles in column incubations of River Eger sediments. ....	70
Figure 22: Geochemical depth profiles in column incubations of Stream Lehstenbach sediments.....	71
Figure 23: Fluorescence microscopy images from Fichtelgebirge gradient columns.....	72
Figure 24: Microbial community composition in Lake Fichtelsee microcosms. ....	73

Figure 25: Microbial community composition in Lake Weißenstädter See microcosms. ....	74
Figure 26: Microbial community composition in River Eger microcosms. ....	75
Figure 27: Microbial community composition in Stream Lehstenbach microcosms.....	76
Figure 28: Phylogenetic placement of iSeq 16S rRNA amplicon reads within the Desulfobulbaceae....	77
Figure 29: Oxygen concentrations of microcosms during incubation. ....	78
Figure 30: CO <sub>2</sub> concentrations in microcosm headspace. ....	79
Figure 31: Atom % <sup>13</sup> CO <sub>2</sub> in microcosm headspace. ....	80
Figure 32: Geochemical depth profiles measured in control microcosm incubations. ....	81
Figure 33: Geochemical depth profiles measured in microcosm incubations with <sup>12</sup> C-toluene. ....	82
Figure 34: Geochemical depth profiles measured in microcosm incubations with <sup>13</sup> C-toluene. ....	83
Figure 35: Community composition in inoculum and microcosms with and without toluene. ....	86
Figure 36: Community composition in <sup>13</sup> C-toluene microcosms with and without filters. ....	87
Figure 37: Community composition in fractions of SIP experiment sampled on day 8.....	89
Figure 38 Community composition in fractions of SIP experiment sampled on day 15.....	91
Figure 39: Visible changes over incubation time in upright flooded microcosms.....	126
Figure 40: CO <sub>2</sub> concentrations in microcosm headspace (GC). ....	127
Figure 41: Volume % <sup>13</sup> CO <sub>2</sub> in microcosm headspace. ....	128
Figure 42: Relative abundance of selected families at 5-10 mm in SIP fractions over density. ....	130
Figure 43: Relative abundance of selected families at 20-25 mm in SIP fractions over density. ....	131

## List of tables

Table 1: Cable bacteria and where to find them.....	19
Table 2: Overview of treatments in toluene DNA-SIP experiment.....	40
Table 3: Conditions for analysis of CO <sub>2</sub> content in headspace samples .....	44
Table 4: Oligonucleotide probes that were used for cable bacteria detection.....	45
Table 5: Overview of PCR primer sets used in this study .....	47
Table 6: Pairwise 16S rRNA sequence similarity of freshwater cable bacteria .....	66
Table 7: Summary of PacBio sequencing results and number of reads in each sample .....	125
Table 8: Preparation of freshwater medium.....	127
Table 9: Refractive index and calculated density from DNA-SIP experiment.....	128
Table 10: Comparative enrichment of taxonomic groups in “heavy” fractions. ....	132

## Abbreviations and symbols

### Abbreviations

<sup>13</sup> C <sub>7</sub> toluene	Toluene in which all carbon atoms are the heavy stable isotope <sup>13</sup> C	DNA	Deoxyribonucleic acid
AFM	Atomic/scanning force microscopy	cDNA	Complementary DNA
BayCEER	Bayreuth Center of Ecology and Environmental Research	dsDNA	Double-stranded DNA
BTEX	Benzene, Toluene, Ethylbenzene, Xylene	ssDNA	Single-stranded DNA
CCS	Circular consensus sequence	dNTP	Deoxyribose nucleoside triphosphate
DAPI	4',6-Diamidin-2-phenylindol		
FISH	Fluorescence in situ hybridization	ATP	Adenosine triphosphate
EB	Elution buffer	CTP	Cytidine triphosphate
EP	Electric potential	GTP	Guanosine triphosphate
ERC	European Research Council	UTP	Uridine triphosphate
CB	Cable bacteria		
COMI	Research Unit Comparative Microbiome Analysis	PCR	Polymerase chain reaction
DIET	Direct interspecies electron transfer	qPCR	Quantitative PCR
DIET	Direct interspecies electron transfer	RT-PCR	Reverse transcriptase PCR
DNA	Deoxyribonucleic acid	RT-qPCR	Reverse transcriptase quantitative PCR
EFM	Electrostatic force microscopy		
FAM	Carboxyfluorescein	RNA	Ribonucleic acid
FIB-SEM	Focused ion beam-scanning electron microscopy	rRNA	Ribosomal RNA
GC	Gas chromatography	SSU rRNA	Small subunit ribosomal RNA
HMGU	Helmholtz Zentrum München	16S	SSU rRNA found in prokaryotes
HPLC	High pressure liquid chromatography	18S	SSU rRNA found in eukaryotes
IGOE	Institute for groundwater ecology	mRNA	Messenger RNA
KEGG	Kyoto encyclopaedia of genes and genomes		
LB	Luria broth; rich growth medium		
LDET	Long-distance electron transfer		
NGS	Next generation sequencing		
OMICs	Umbrella term for molecular biology disciplines including genomics, proteomics, metabolomics, metagenomics and transcriptomics		
PacBio	Pacific Biosciences		

PAH	Polyaromatic hydrocarbon
PCI	Phenol-chloroform-isoamyl alcohol
PEG	Polyethylene glycol
PHCs	Petroleum hydrocarbons
PLFA	Phospholipid fatty acids
POLLOX	Anaerobic pollutant degradation with oxygen
QIIME	Quantitative insights into microbial ecology
SDS	Sodium dodecyl sulfate
SEM	Scanning electron microscopy
SIP	Stable isotope probing
SMRT	Single-molecular real-time
Taq polymerase	Thermostable DNA polymerase from the thermophilic bacterium <i>T. aquaticus</i>
TEA	Terminal electron acceptor
TEM	Transmission electron microscopy
TRFLP	Terminal restriction fragment length polymorphism

## Symbols

Å	Ångström = $10^{-10}$ m = 100 pm
c	Concentration
ρ	Density
mV	Millivolts
n	Refractive index
T	Temperature
t	Time
d	Days
$\Sigma H_2S$	Total Sulphide = $[H_2S] + [HS^-] + [S^{2-}]$

## 1. Introduction

### 1.1. Redox stratification in aquatic sediments

All living organisms need to harness energy and conserve it, in order to sustain processes in cell functioning, growth and cell division (Sikkema *et al.*, 2019). On a molecular level, energy conservation equals coupling of chemical reactions, specifically of exergonic reactions, which release energy, to endergonic reactions, which utilize energy (Lane and Martin, 2010). In these redox reactions, electrons are transferred between reactants. While animals are limited to the use of organic carbon as electron donor and oxygen as electron acceptor, microbes have more diverse metabolisms and are able to use a much broader spectrum of redox reactions for energy conservation. How much energy can be gained is determined by electrochemical potential difference between oxidation and reduction (Nernst equation) of the redox reaction, as well as the supply of reacting agents (McCarty and Criddle, 2012). For conserving energy by redox reactions, the bacterial cell therefore needs access to electron donor and electron acceptor (McCarty and Criddle, 2012) and catalyzes the reaction, harnessing its energy. In the environment, chemical interphases are characterized by presence of both electron donor and acceptor, and are therefore hotspots for microbial life (Hong *et al.*, 2019).

Aquatic sediments are habitats generally perceived as redox stratified, reaching from higher values at the surface to more negative values in deeper zones (Borch *et al.*, 2010). The vertical zonation in typical organic-rich surface freshwater sediments follows the redox regime, and thus a succession of increasingly less energetically-favourable electron acceptors:  $O_2$ ,  $NO_3^-$ , Mn(IV), Fe(III),  $SO_4^{2-}$  (Froelich *et al.*, 1979; Shotyk, 1988; Davison, 1993; Urban *et al.*, 1994; Thomsen *et al.*, 2004; Koretsky *et al.*, 2006). Molecular oxygen, the energetically most favourable electron acceptor, is available in sediment porewater due to its solubility in water. By diffusion, oxygen is transported from the overlying water column to the sediment surface, where it is rapidly depleted within upper sediment due to respiration in organic matter degradation (Jost *et al.*, 2015). Below the upper oxic zones of aquatic sediments, alternative electron acceptors, other than oxygen, are utilized by microorganisms, following the succession of their electrochemical energy yield (Berner, 2020).

### 1.2. Cable bacteria

#### 1.2.1. Finding of spatial decoupling of redox half-reactions

Long-distance electron transfer (LDET) over centimetre distances by cable bacteria was first discovered in 2010 (Nielsen *et al.*, 2010). It was noticed that in marine sediment with overlying oxic water, oxygen

reduction occurred in the upmost sediment layer coupled to sulphide oxidation in the deeper sulfidic sediment layer (see Figure 1). This observation was astonishing, as both sediment layers were > 1 cm distance apart from each other. As the sediment sample was defaunated, this could not be explained by animal movement or shifting of sediment. The speed and rate of the redox half-reactions taking place was explicable by electron transmission, but not by diffusion of molecules. In the biogeochemical profile, a pH peak indicative of electron-driven oxygen reduction was also found. After all other explanations were ruled out, the only remaining hypothesis was that the present filamentous bacteria were able to transfer the electrons from sulphide oxidation onto oxygen, thereby using up protons from the surrounding environment.

This peculiar lifestyle discovered for cable bacteria is called electrogenic sulphur oxidation (e-SOx) and manifests in the geochemical depth profile of the sediment as a pH peak at oxic/anoxic interphase, while the pH becomes more acidic below the suboxic zone (defined as an anoxic sediment layer without detectable sulphide (Froelich *et al.*, 1979; Berner, 1981)). Over time, e-SOx-sediments show development and extension of a suboxic zone through downward shift of the onset of the sulfidic zone (Meysman *et al.*, 2015; Sulu-Gambari *et al.*, 2016) due to sulphide oxidation. Both of these observations can be taken as hints for ongoing LDET.

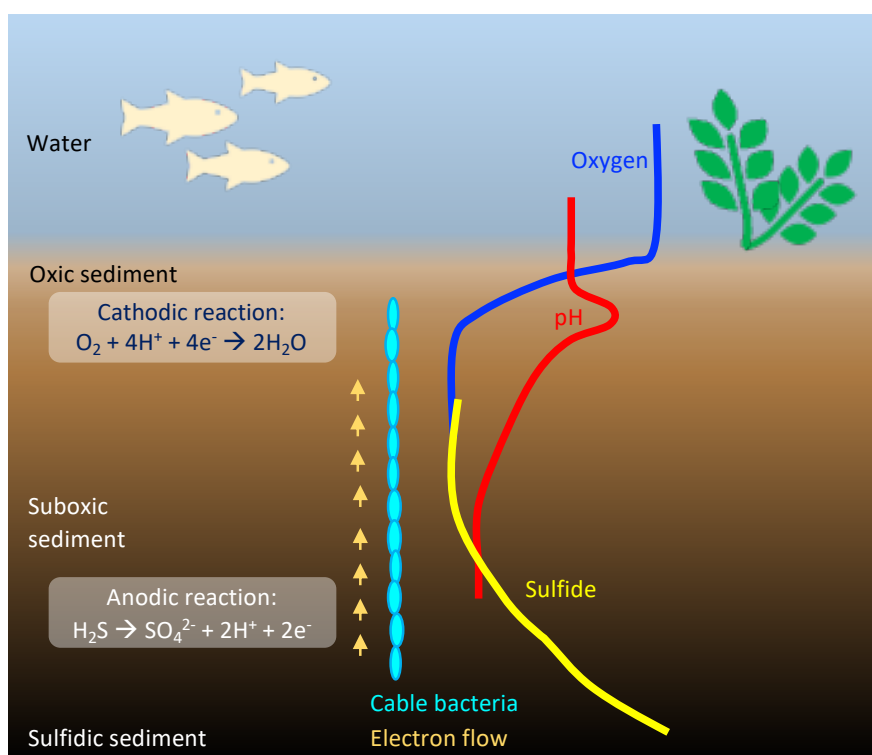


*Figure 1: Schematic drawing of biogeochemical profile in sediment with cable bacteria. On the left, the cathodic and anodic redox half reactions within the sediment layers are depicted, while on the right, typical geochemical profiles of oxygen (blue), pH (red) and sulphide (yellow) are shown over depth.*

### 1.2.2. Occurrence of cable bacteria

After their initial discovery in a Danish harbour sediment, cable bacteria and LDET were found to occur worldwide in marine, brackish and freshwater sediments and also in groundwater. The following table (Table 1) summarizes habitats, for which cable bacteria occurrence is documented in the literature.

*Table 1: Cable bacteria and where to find them.*

Type of sample	Site description and localization	Reference
Marine system		
Marine sediment	Aarhus bay, Denmark	(Nielsen <i>et al.</i> , 2010) (Pfeffer <i>et al.</i> , 2012) (Risgaard-Petersen <i>et al.</i> , 2012) (Marzocchi <i>et al.</i> , 2014) (Schauer <i>et al.</i> , 2014) (Jiang <i>et al.</i> , 2018) (Otte <i>et al.</i> , 2018) (Kjeldsen <i>et al.</i> , 2019) (Marzocchi <i>et al.</i> , 2020)
Marine sediment	Tokyo bay, Japan	(Trojan <i>et al.</i> , 2016)
Marine coastal sediment	Intertidal bivalve reefs, Mokbai site, near island of Texel in Wadden Sea, Netherlands	(Malkin <i>et al.</i> , 2017) (Geerlings <i>et al.</i> , 2019)
Marine sediment	Baltic Sea (varying bottom water redox conditions)	(Hermans <i>et al.</i> , 2019)
Marine sediment	East Gotland Basin, Baltic Sea	(Marzocchi <i>et al.</i> , 2018)
Harbor sediment	Messina Harbor, Italy	(Matturro <i>et al.</i> , 2017)
Marine coastal sediment	Coastal zone Station 130, Belgium	(Malkin <i>et al.</i> , 2014) (Cornelissen <i>et al.</i> , 2018)
Marine sediment	Black Sea sediment at 12 m depth	(Geerlings <i>et al.</i> , 2019)
Marine sediment	Yaquina Bay, Oregon, USA	(Li <i>et al.</i> , 2020)
Marine sediment	Florida Bay, USA	(Yin <i>et al.</i> , 2021)
Harbor sediment	Marselisborg Marina in Aarhus Harbor, Denmark	(Dam <i>et al.</i> , 2021)
Sea rhizosphere	Marine plant root sediment, Aggersund, Denmark	(Scholz <i>et al.</i> , 2021)
Sea rhizosphere	Marine plant root sediment, Arcachon Bay, France	(Scholz <i>et al.</i> , 2021)
Brackish water		
Salt marsh sediment	Intertidal sand flat, Rattekaai salt marsh, Oosterschelde tidal inlet, Netherlands	(Malkin <i>et al.</i> , 2014) (Malkin and Meysman, 2015) (Meysman <i>et al.</i> , 2019) (Geerlings <i>et al.</i> , 2019) (Geerlings <i>et al.</i> , 2020) (Eachambadi <i>et al.</i> , 2020)
Mangrove sediment	Mangrove sediment near Melbourne, Australia	(Burdorf <i>et al.</i> , 2016)

Salt marsh sediment	New England salt marsh, Buzzards Bay, MA, USA	(Larsen <i>et al.</i> , 2015)
Coastal bottom waters	Seasonally hypoxic basin, Den Osse basin, Netherlands	(Seitaj <i>et al.</i> , 2015)
Brackish sediment	Cocksdorp intertidal flat, Netherlands	(Cornelissen <i>et al.</i> , 2018)
River estuary	Periodical hypoxic bottom, Yarra River Estuary, Melbourne, Australia	(Kessler <i>et al.</i> , 2019)
River estuary	Swan River estuary, Western Australia	(Martin <i>et al.</i> , 2019)
River delta	Pearl River Delta, contamination with PAHs, China	(Liu <i>et al.</i> , 2021)

Freshwater		
River sediment	River (bank) sediment, Giber Å, Denmark	(Risgaard-Petersen <i>et al.</i> , 2015) (Scholz <i>et al.</i> , 2019)
Mudlake sediment	Eutrophic pond in Vennelystparken, Aarhus University, Denmark	(Cornelissen <i>et al.</i> , 2018) (Kjeldsen <i>et al.</i> , 2019) (Scholz <i>et al.</i> , 2020)
Lake sediment	Skanderborg Sø, shallow, eutrophic, alkaline, dimictic lake, Eastern Jutland, Denmark	(Sandfeld <i>et al.</i> , 2020)
Lake sediment	Vilhelmsborg Sø, shallow, eutrophic, alkaline, dimictic lake, Eastern Jutland, Denmark	(Kessler <i>et al.</i> , 2019) (Sandfeld <i>et al.</i> , 2020)
Lake sediment	Brabrand Lake, Aarhus, Denmark	(Dam <i>et al.</i> , 2021)
Lake rhizosphere	Aquatic plant root sediment, Lake Cadagno, Switzerland	(Scholz <i>et al.</i> , 2021)
Lake rhizosphere	Aquatic plant root sediment, oligotrophic sulfide-rich Lake Hampen, Denmark	(Scholz <i>et al.</i> , 2021)
Lake rhizosphere	Sulfidic aquatic plant root sediment, Lake Knud, Denmark	(Scholz <i>et al.</i> , 2021)
Lake sediment	Prealpine Lake Alatsee bank sediment, meromictic lake, Germany	This work
Creek sediment	Creek bank mud, near Garching, Germany	This work
Lake sediment	Mining-impacted iron-rich and acidic Lake Fichtelsee, Germany	This work
Lake sediment	Eutrophic recreational lake Weißenstädter See, Germany	This work
River sediment	River Eger, Czech Republic	This work

Groundwater		
BTEX-contaminated aquifer	Contaminated site, Düsseldorf/Flingern, Germany	(Müller <i>et al.</i> , 2016) (Müller <i>et al.</i> , 2019) This work

Considering the worldwide distribution of cable bacteria in marine as well as freshwater settings, they appear to be global players in aquatic sediments. Although they remained unnoticed until 2010, cable bacteria are part of ecosystems and via their electrogenic lifestyle have the ability to shape them. Apart from the worldwide possible impact of cable bacteria on aquatic sediment life and element cycling, their global distribution also means that they are adapted to various environments, especially a wide range of salinity (from freshwater over brackish habitats to full marine salinity). Moreover, they were found to occur in a range of climate zones from mid-latitude colder climates over subtropical to tropical climates.

While a number of studies has demonstrated the presence of CB in freshwater systems (see Table 1) to date (Risgaard-Petersen *et al.*, 2015; Müller *et al.*, 2016; Sandfeld *et al.*, 2020; Dam *et al.*, 2021; Liu *et al.*, 2021; Scholz *et al.*, 2021), the factors controlling their growth and ecology in freshwater systems remain poorly understood and freshwater cable bacteria still remain comparatively less well studied. This thesis aims to add to the current understanding of the diversity and ecology of cable bacteria in freshwater systems, and to a differentiation of CB from distinct surface and groundwater sediments.

Cable bacteria have proven difficult to cultivate. The first stable enrichment culture of CB, *Candidatus Electronema aureum* strain GS, has recently been presented (Thorup *et al.*, 2021). However, there is still no pure culture of any cable bacteria to date, and their supposed strict dependence on opposing gradients of oxygen and sulphur complicates sustaining them in culture.

### 1.2.3. Physiology of cable bacteria

The physiology of bacteria was more closely investigated in several recent studies. It is important to differentiate between *Ca. Electronema/Electrothrix* cable bacteria and groundwater cable bacteria (*Desulfurivibrio*-affiliated), also with regard to their respective lifestyle.

A comprehensive study (Kjeldsen *et al.*, 2019) combined *Ca. Electronema/Electrothrix* cable bacteria metagenomics with experimental approaches to untangle physiological properties in cable bacteria. In sum, from combining genomics and proteomics, they deduct that cable bacteria lack the genes characteristic of other sulphide oxidizing microorganisms, such as genes encoding the Sox pathway, or reversely operating dissimilatory sulphite reductase (rDSR). Instead, cable bacteria exhibit all genes from canonical sulphate reduction (DSR) pathway, and it is hypothesized that they inverse the pathway for sulphide oxidation, similar to previously described *Desulfurivibrio alkaliphilus* (Thorup *et al.*, 2017). A previous hypothesis from early cable bacteria research was that cable bacteria were able to conserve energy by cathodic oxygen respiration. This seemed plausible, as oxygen in aerobic respiration is

considered the electron acceptor with the greatest theoretical energy yield due to its redox potential. However, Kjeldsen *et al.* present data, suggesting this not to be the case. Energy conversion in cable bacteria seems to be realized only by the cells in the anoxic sediment layer (anodic cells). The pathway of energy conversion in cable bacteria is not experimentally proven, but through OMICs data, Kjeldsen *et al.* suggest (in brief) that quinol oxidation by complexes bound to the periplasmic membrane creates a proton gradient across the membrane and ATP can be gained. They further propose that under conditions where oxygen (or nitrate) might not be available as electron acceptor to cathodic cells, energy is conserved via sulphur disproportionation.

For groundwater cable bacteria, growing with nitrate as electron acceptor and elemental sulphur and thiosulfate as electron donor, sulphur disproportionation was suggested as energy conservation method (Müller *et al.*, 2019). Findings in this study are derived from metagenome data of one culture (1MN, consisting of a 1-methylnaphthalene degrader and CB) and substrate turnover experiments with said culture. The authors suggest that energy in groundwater cable bacteria is conserved by substrate-level phosphorylation as last step of a reversed sulphate reduction pathway. During this step, sulphate is formed and ATP is generated from adenosine-5'-phosphosulfate (APS) by the enzyme sulphate adenylyltransferase working in reverse. As is the case (see above) for freshwater and marine cable bacteria (Kjeldsen *et al.*, 2019), for groundwater cable bacteria, too, the authors find no support for energy conversion being directly coupled to LDET (oxygen or nitrate reduction) in cathodic cells.

#### 1.2.4. Phylogeny and evolution of cable bacteria

Although the first stable enrichment culture of CB, *Candidatus Electronema aureum* strain GS, has recently been presented (Thorup *et al.*, 2021), to this day, there is still no pure culture of any cable bacteria. Their supposed strict dependence on opposing gradients of oxygen and sulphur complicates sustaining them in culture. The reported cable bacteria species are therefore all *Candidatus* genera and species. Phylogenetic analysis of picked cable bacteria filaments revealed that they form a distinctive sister clade to the *Desulfobulbaceae* family (Trojan *et al.*, 2016). Within the cable bacteria, there are two main branches, dividing them into species found primarily in marine and brackish environment and a branch containing the species from freshwater habitats. The marine branch of cable bacteria genera was named *Candidatus Electrothrix*, while the freshwater cable bacteria genera were named *Candidatus Electronema* (Trojan *et al.*, 2016).

A special case are the so-called groundwater cable bacteria. Phylogenetically, these are not affiliated with the *Ca. Electrothrix/Electronema* branch within the *Desulfobulbaceae* family, but with

*Desulfurivibrio* spp. The 1MN culture, presented as groundwater CB culture (Müller *et al.*, 2019), is an enrichment derived from a former coal gasification site.

The “normal” *Desulfobulbaceae* family represents primarily single-celled bulbous-shaped (hence the name) sulphate-reducing bacteria, but many species within this family grow by sulphur disproportionation and some members are capable of sulphide oxidation (Kuever, 2014). Therefore, it seems plausible that the extraordinary lifestyle of cable bacteria evolved in this specific family. In their comprehensive metagenomic study, Kjeldsen *et al.*, 2019 showed that roughly 20 % of the genes specific to cable bacteria could not be assigned to any known ancestor, concluding that these must be derived either from a genetically undescribed donor lineage, or that they origin from evolution within the cable bacteria lineage. The authors further suggest that cable bacteria evolution was driven by considerable horizontal gene transfer in combination with moderate exchange and divergence of ancestral genes. However, this implies, that the trait “electric conduction along filaments” might also have evolved within other phylogenetic lineages. Indeed, the groundwater cable bacteria (Müller *et al.*, 2016, 2019) (see above) are physiologically as well as phylogenetically different from the *Ca. Electrothrix/Electronema* clade *sensu stricto*, albeit still within *Desulfobulbaceae* family. Additionally, recent findings (Yang *et al.*, 2021) showed extracellular LDET in Gram-positive *Lysinibacillus varians* filaments via nanowire-like appendages. In this example, the *L. varians* filaments were grown on electrodes and conducted electrons bidirectionally over 1 mm-distances, thus employing a mechanism of electric conduction different from cable bacteria. Still, even if LDET is more wide-spread in nature than anticipated after cable bacteria discovery, the mechanism of LDET in *Ca. Electronema/Electrothrix* cable bacteria with electricity-conducting fibres running within the shared periplasm of filament-forming individual cells is -so far- assumed to be unique in nature.

Within this thesis, cable bacteria from marine and freshwater sites (Phylogeny: *Ca. Electrothrix* and *Ca. Electronema* clade), as well as groundwater cable bacteria are referred to and freshwater and groundwater cable bacteria are part of the investigations. As there are phylogenetic and physiological differences between them, differentiation is needed (and given) when they are referred to.

### 1.3. Long-distance electron transfer (LDET) in cable bacteria

Long-distance electron transfer (LDET) is by literal definition the movement of electrons, which equals an electrical current, over a comparatively long range. In context of microbiology, LDET means electron transport over millimetre to centimetre distances, with 1 cm representing roughly the 10.000-fold of

a singular average 1- $\mu\text{m}$ -in-diameter bacterial cell. To scale this range to cell-size, illustrates the enormity of what “long-distance” means in the microbial world.

After the initial finding of filamentous bacteria responsible for e-SOx and acting as biological cables (hence the name), the question focused on how cable bacteria were able to transfer electric currents across centimetre distances. A first indication was found by visualizing the filaments (Pfeffer *et al.*, 2012) via AFM (atomic force microscopy), SEM (scanning electron microscopy), TEM (transmission electron microscopy) and EFM (electrostatic force microscopy) of individual cable bacteria filaments, that were picked from sediment samples. One individual cable or filament was comprised of several hundreds or thousands of individual cells. Ridges, that run along the whole filament, were observed, formed by fibres located within periplasmic space. Affiliated with Gram-negative *Desulfobulbaceae*, CB have two membranes. Notably for a CB filament, each cell has an individual inner cell membrane, while sharing the outer cell membrane with the whole filament (Pfeffer *et al.*, 2012). It was suspected that these fibres must be associated to the biological structures responsible for conducting the electricity. A further study (Jiang *et al.*, 2018) investigating the conducting fibres in cable bacteria revealed the junctions between individual cells within the filaments by AFM. A study of the cell envelope of cable bacteria (Cornelissen *et al.*, 2018) further investigated the fibres via various microscopic techniques, including SEM, TEM, cryo electron microscopy, FIB-SEM and AFM in order to generate a model of the cell envelope structure of cable bacteria (see Figure 2). They also could extract intact fibre sheaths of cable bacteria filaments and compared them to full filaments. Although it was possible to extract the fibre sheet formed of the fibres that possible conduct the electricity, the material is not identified yet.

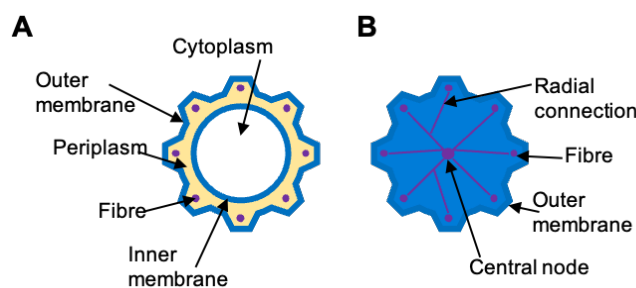


*Figure 2: Schematic drawing of cable bacteria filament cross section. A) Transverse cross section through one individual cell, depicting ridges and the fibres between inner and outer membrane. B) Transverse cross section at a cell junction between two individual cable bacteria cells, depicting the inner node. Graphic after Cornelissen *et al.*, 2018.*

In their comprehensive metagenomic study, Kjeldsen *et al.*, 2019 shed some light on the genetic foundation for the fibres and the associated supposed electron transfer mechanism. The so far known extracellular electron transfer (EET) mechanisms in *Geobacter* and *Shewanella* are based on

membrane-bound cytochromes (Shi *et al.*, 2009; Butler *et al.*, 2010) and therefore are metal-based. However, CB lack the homologs of the relevant *Geobacter* and *Shewanella* proteins, but encode complexes that might facilitate electron transfer coupled to quinol oxidation due to structural similarity (Kjeldsen *et al.*, 2019). The authors speculate that via this process, a proton gradient across the membrane develops and CB can conserve energy. While this might explain the electron transfer across membranes, there is more experimental evidence for electron transfer within the periplasm, which would transfer electrons from the membrane-bound complexes to the conducting fibres. It is hypothesized that periplasmic electron transfer in CB occurs via c-type cytochromes, indicated not only by genomic studies, but also by expression and resonance Raman microscopy (Kjeldsen *et al.*, 2019).

## 1.4. Influence of cable bacteria on biogeochemistry of sediments

### 1.4.1. Cable bacteria impact element cycling in sediments

By their unique lifestyle, cable bacteria have the ability to influence element cycling in the sediment that they inhabit. The most obvious impact is the influence on the sulphur cycle. By electrogenic sulphide oxidation (eSOx), cable bacteria deplete sulphide in anoxic sediment (sulfidic zone), producing sulphate. This can then be used as electron acceptor in anaerobic respiration by other microbes (Nielsen and Risgaard-Petersen, 2015; Sandfeld *et al.*, 2020). Such a cryptic sulphur cycling (Holmkvist *et al.*, 2011) has only been considered recently to play a role in sulphate recycling in freshwater sediments, characterized by low *in situ* sulphate concentrations (Holmer and Storkholm, 2001). Furthermore, the sedimentary pH profile is affected by cathodic oxygen consumption (pH peak, more alkaline conditions) and by anodic sulphide oxidation (proton formation, more acidic conditions)(Nielsen and Risgaard-Petersen, 2015). Especially the acidification of the suboxic zone leads to mineral dissolution, namely of iron(II) sulphide ( $\text{FeS}$ ) and calcium carbonate ( $\text{CaCO}_3$ ), which results in accumulation of mineral ions (ferrous iron  $\text{Fe}^{2+}$ , calcium  $\text{Ca}^{2+}$  and manganese  $\text{Mn}^{2+}$ ) in the porewater (Risgaard-Petersen *et al.*, 2012; Rao *et al.*, 2016; Sulu-Gambari *et al.*, 2016; van de Velde *et al.*, 2016). One study exploring formation of sedimentary minerals (Geerlings *et al.*, 2019) found that cable bacteria become mineralized due to their metabolism, resulting in a mineral crust covering the filaments. However, how severely this impacts the maintaining of cable bacteria lifestyle remains unresolved. But it can be speculated that both the bloom, as well as the collapse of a cable bacteria population in an aquatic sediment would have strong effects on sediment geochemistry.

#### 1.4.2. Influence of cable bacteria on microbial community and sedimentary biosphere

By impacting sediment geochemistry, cable bacteria can affect organisms around them. Discussed as “cables and friends”, the interactions of cable bacteria with other microorganisms in the environment is part of ongoing research. So far, specific interactions such as direct interspecies electron transfer (DIET) between CB and other microbes, have not been proven. However, CB are proposed to influence not only microbial communities around them, but also flora and fauna. Seitaj *et al.* (Seitaj *et al.*, 2015) suggest a “firewall” mechanism by CB, which includes CB-produced oxidized sedimentary iron minerals acting as binders for free sulphide in seasonally hypoxic basins. In these basins, the seasonal depletion of oxygen often leads to persistence of free sulphide (euxinia), which is toxic to marine life. In this way, CB contribute to saving marine life (Nielsen, 2016).

In several studies, cable bacteria occurred in close proximity with roots of aquatic plants, both in freshwater (Scholz *et al.*, 2019, 2021) rhizosphere, as well as in sea grass rhizosphere from brackish to marine systems (Martin *et al.*, 2019; Scholz *et al.*, 2021) and might also play a role in mangrove sediment (Burdorf *et al.*, 2016). By excreting oxygen through roots (radial oxygen loss), plants are hypothesized to protect their roots from constantly accumulating toxic free sulphide in the rhizosphere (Brodersen *et al.*, 2015). The oxygen leaking from these root shoots (the growing part of the roots) can serve as terminal electron acceptor (TEA) for cable bacteria in an otherwise anoxic environment similar to the oxic surface sediment layer in the “classic” cable bacteria conception as depicted in Figure 1. By electrogenic sulphide-oxidation (eSOx), cable bacteria are able to remove the toxic sulphide in plant root proximity while benefitting from the oxygen leaking from the plant root. In this supposed mutualistic process, both the cable bacteria, as well as the aquatic plants seem to benefit.

Apart from being neighbours to the roots of aquatic plants, cable bacteria were also found in close proximity to a second group of photosynthetic organisms: biofilm-forming algae (mainly diatoms) (Malkin and Meysman, 2015). In this case, the photosynthesis within the biofilm directly and rapidly affected the sulphide concentrations in the deeper sediment layers. Under light, the algae did photosynthesis and produced oxygen, which was then available as TEA to cable bacteria for eSOx.

For marine cable bacteria, one study (Vasquez-Cardenas *et al.*, 2015) reported high abundance of sulphur-oxidizing Epsilon- and Gammaproteobacteria in the sub-oxic zone, co-occurring with cable bacteria-activity. The authors suggest that these chemolithoautotrophs are metabolically linked to cable bacteria and coupled to their established electron transport network and might be able to benefit from their presence by using them as electron sink. For iron-cycling bacteria, such as Fe<sup>3+</sup>-

reducing *Geobacter* or *Shewanella*, co-occurrence with cable bacteria is documented (Otte *et al.*, 2018) in stratified marine sediment samples, suggesting possible interactions.

Indirect linkage of cable bacteria to the nitrogen cycle has been demonstrated (Kessler *et al.*, 2019) by cable bacteria-mediated iron sulphide dissolution, and subsequent higher bioavailability of Fe<sup>2+</sup>. This resulted in enhanced dissimilatory nitrate reduction to ammonium, while denitrification was occasionally decreased, which implies an impact of cable bacteria on nitrogen loss from the system.

The ongoing sulphur cycling mediated by cable bacteria via eSOx can lead to a shift in the microbial community, favouring sulphate reducers rather than methanogens (Scholz *et al.*, 2020), as sulphate reduction outcompetes methanogenesis under these conditions (Kristjansson *et al.*, 1982; Schönheit *et al.*, 1982). Thus, by replenishing the sulphate pool, cable bacteria activity might also prevent methane emissions from sediments.

### 1.5. Contaminations in freshwater and groundwater sediments

Freshwater is the foundation for life, not only human life, but all life on earth. This foundation, however, is threatened by widespread and increasing pollutant input into the environment. Among these are the petroleum hydrocarbons (PHC). By definition, hydrocarbons contain solely elemental carbon and hydrogen and can be divided into saturated, unsaturated and aromatic hydrocarbons (Wilkes and Schwarzbauer, 2010). Petroleum hydrocarbons formed as fossil resources over geological time scales from millions-of-years-old decomposition of buried dead organisms. While there are natural sources emitting petroleum hydrocarbons, such as natural oil seeps (Reed and Kaplan, 1977), most environmental contamination occurs due to human activities. Via leaks in pipelines or barrels, oil spills -like the Deepwater Horizon oil spill 2010 (Beyer *et al.*, 2016)- or inappropriate and often illegal disposal of PHCs, these pollutants can enter ecosystems. Sources of PHCs are often a legacy of petroleum or gasoline processing or transport and storage (Wilkes and Schwarzbauer, 2010; Lueders, 2017). In recent years, freshwater and groundwater resources have been increasingly contaminated through human activities and industrial progress (Weelink *et al.*, 2010). This represents not only a significant problem to the environment, but also a threat to the supply of clean drinking water.

For humans and other mammals, the toxicity of BTEX is well documented. Individual toxic effects of each BTEX component cover acute, chronic, genotoxic, carcinogenic, immunotoxic and teratogenic health effects (Varjani *et al.*, 2017), among others. Toluene, which is widely used as industrial solvent,

can enter the human body via inhalation of the airborne toluene fumes. It can cause neurotoxic effects, such as a feeling of being “high”, but long-term exposure may lead to visual restraints, cognitive dysfunctions, it can affect the central and peripheral nervous system and the respiratory system (Cohr and Stockholm, 1979), it affects the kidneys, the reproductive system and can lead to unconsciousness and even death (Devika and Rastogi, 2018). However, environmental contaminations with BTEX are often accompanied by more complex petroleum mixtures with increased toxicity for humans. When BTEX contaminants enter ecosystems, not only humans and other mammals are affected. In plants, petroleum exposure might lead to tissue necrosis due to hydrophobicity introduced by the contaminants (Ziółkowska and Wyszkowski, 2010). Plants are able to take up PHCs (Hunt *et al.*, 2019) and bioaccumulate them, thus introducing the contamination into the food web. Microbial communities in nature can be affected when facing a PHC contamination, and might shift towards an enrichment of specific degrader populations. High BTEX concentrations can lead to toxicity even among BTEX degrading microorganisms (Lueders, 2017), in which hydrocarbons accumulate in the lipid bilayer and alter membrane fluidity, leading to its non-specific permeabilization (Heipieper and Martínez, 2010).

Once in the environment, contamination with hydrocarbons, especially BTEX, is often persistent, as these molecules are chemically relatively stable. Removal can be achieved by physical processes (such as sorption), transport processes (such as diffusion, dispersion, advection) and abiotic transformation (Committee on Bioavailability of Contaminants in Soils and Sediments, 2003), or by degradation. Among these, biodegradation by microorganisms is considered the only sustainable mechanism to eliminate petroleum contaminants (Leahy and Colwell, 1990; Griebler and Lueders, 2009; Kleinstreuber *et al.*, 2012; Meckenstock *et al.*, 2015) from the environment.

#### 1.5.1. Petroleum hydrocarbons and BTEX contaminants

The IUPAC nomenclature of organic chemistry defines the following classifications for hydrocarbons (Favre and Powell, 2013):

- 1) Saturated hydrocarbons, only consisting of single bonds between carbon atoms and saturated with hydrogen. Acyclic saturated hydrocarbons have the formula  $C_nH_{2n+2}$ . Among these are straight chain (alkanes) and branched chain (paraffins) hydrocarbons, as well as cycloalkanes (naphthenes).
- 2) Unsaturated hydrocarbons, with one or more double or triple bonds between carbon atoms.
- 3) Aromatic hydrocarbons, with at least one aromatic ring

Petroleum hydrocarbons (PHCs) are a mixture of these compounds, consisting only of carbon and hydrogen (Moss *et al.*, 1995). They represent the main constituents of crude oil and fuel oils (together with non-hydrocarbons), such as diesel or gasoline. Two classes within the aromatic PHCs, which impact the environment (Abdel-Shafy and Mansour, 2016), are (1) monoaromatic hydrocarbons and (2) polycyclic aromatic hydrocarbons (PAHs). Within the PHCs' monoaromatic hydrocarbons, the compounds benzene, toluene, ethylbenzene and xylenes (BTEX, see Figure 3) are particularly relevant, because they are among the most common compounds in petroleum (Williams *et al.*, 2006). The US Agency for Toxic Substances and Disease Registry (ATSDR) lists BTEX as priority pollutants (2019: rank 6 benzene, rank 74 toluene, rank 137 ethylbenzene, rank 65 xylenes), based on their frequency, their known or suspected toxicity and their potential for human exposure (ATSDR and U.S. Department of Health & Human Services, 2019). Compared to PAHs, BTEX compounds are more soluble in water (Njobuenwu *et al.*, 2005; Lueders, 2017), thus they can spread more widely across an aqueous ecosystem.

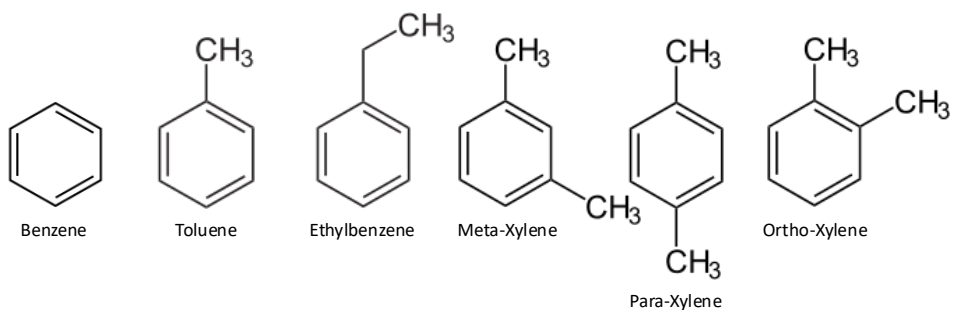


Figure 3: Overview of structural diagrams of the BTEX hydrocarbons

The monoaromatic BTEX compounds all have one aromatic ring (hence the name), with the delocalized  $\pi$ -electron system rendering them extremely stable. Benzene is structurally the simplest of the BTEX compounds, and the most stable. All six carbon atoms lie in the same plane, and the cyclic molecules have a fully conjugated double bond system (Wilkes and Schwarzbauer, 2010), which means that the atomic p orbitals overlap above and below the plane of the carbon ring. Electron density is equally allocated across the ring, as the  $\pi$ -electrons are mobile within the ring plane (Fuchs *et al.*, 2011). All of this makes aromatics chemically stable. Nonetheless, evolution equipped some living organisms with the capability to break the aromatic ring structure.

### 1.5.2. Biodegradation of toluene in bacteria

In nature, degradation of aromatic hydrocarbons can be achieved by aerobic or anaerobic bacteria. Although there are fungi able to degrade lignin (Kirk and Farrell, 1987), which has aromatic components, and some archaea are known for aromatic substrate degradation (Al-Mailem *et al.*, 2010; Fuchs *et al.*, 2011; Ramos-Padrón *et al.*, 2011), bacteria are the major degraders of aromatic compounds, such as BTEX. Research revealed multiple specialized catabolic pathways employed by these microbes to use the hydrocarbons as carbon sources and as electron donors. In general, aerobic and anaerobic degradation pathways can be differentiated.

So far, multiple different pathways for aerobic degradation have been found in microorganisms (Gülensoy and Alvarez, 1999). In brief, molecular oxygen is used as co-substrate in the initial attack on the aromatic ring structure, leading to addition of hydroxyl groups to the ring, and resulting in ring destabilization. The enzymes catalysing these reactions are mono- and di-oxygenases (Jindrová *et al.*, 2002). In a second oxygen-dependent step, the ring is cleaved and the opened ring offers further opportunities for final biodegradation.

Anaerobic biodegradation was long thought impossible and was only discovered in the 1980's (Vogel and Grbić-Galć, 1986; Lovley *et al.*, 1989; Evans *et al.*, 1991). The universal pathway that is known is chemically based on fumarate addition, in which the methyl group of toluene is added to fumarate, resulting in benzylsuccinate (Biegert *et al.*, 1996). The reaction is catalysed by benzylsuccinate synthase (Bss). After further activation and transformation reactions via numerous intermediates, the then activated benzoyl-CoA can be more easily degraded by microorganisms via ring cleavage and  $\beta$ -oxidation-like reaction to acetyl-CoA (Fuchs *et al.*, 2011; Rabus *et al.*, 2016). Compared to benzene, toluene can be degraded more easily, as the methyl group introduces a certain asymmetry to the otherwise fully symmetric -and thus stable- aromatic ring of benzene. The initial attack on the aromatic ring in benzene biodegradation is still less understood than for toluene (Lueders, 2017).

In the (aquatic) environment, anaerobic BTEX biodegradation pathways are more important than aerobic pathways, since surface water sediments are mostly anoxic compartments and groundwater often is devoid of oxygen (Lueders, 2017). Dissolved oxygen in porewater would either be rapidly used as terminal electron acceptor or concentrations are too low for complete oxidation of hydrocarbon contaminants (Biegert *et al.*, 1996).

Known anaerobic toluene degrading bacteria are found mainly among the taxonomic groups of *Burkholderiales* (now an order of *Gammaproteobacteria*, formerly affiliated with *Betaproteobacteria*),

former *Deltaproteobacteria* (now proposed to be split into new phyla: *Desulfobacterota*, *Myxococcota*, *Bdellovibrionota*, and SAR324 (Waite *et al.*, 2020)) and *Clostridia* (Lueders, 2017). In the environment, the electron acceptor availability often becomes the limiting factor controlling the activity of anaerobic degraders (Meckenstock *et al.*, 2015). In sediments and especially in aquifers limited mixing of electron acceptors and electron donors is a major obstruction *in situ*. Its recognition led to the formulation of the “plume fringe concept”, stating that main biodegradation activity occurs only at the fringes of a contaminant plume, as opposed to the longitudinal redox zonation concept (Meckenstock *et al.*, 2015).

#### 1.5.3. Bioremediation

Bioremediation describes the process of enhancing biodegradation of a contaminated site, often by stimulating the contaminant degrader population and enhancing degrading activity. As such, it represents a real-world application of biodegradation research. Understanding which microorganisms are able to degrade the contaminant and what they need to increase their degrading activity are essential factors for successful site remediation (Lueders, 2017). Advances in this research field might be directly applied in order to guarantee future drinking water supply and healthy freshwater ecosystems.

#### 1.5.4. Cable bacteria and contaminated sites

So far, a few studies have investigated the possible impact of cable bacteria on biodegradation of petroleum hydrocarbon-contaminated sites. Contaminant degradation is often limited by electron acceptor-availability (Meckenstock *et al.*, 2015). LDET between anoxic sediments and oxic overlying water, might enhance sulphate regeneration in the anoxic sediment, and by this, biodegradation of petroleum hydrocarbons.

Cable bacteria were found in hydrocarbon-contaminated sites. In a PAH-polluted river, cable bacteria were found to enhance biodegradation (Liu *et al.*, 2021). The oxygen concentration in the overlaying water above the contaminated sediment was artificially increased, leading to increase in cable bacteria presence. It was hypothesized that the observed accelerated PAH biodegradation was a result of interactions of cable bacteria with PAH degraders, as well as increased electron acceptor regeneration due to cable bacteria metabolism. Marzocchi *et al.* (Marzocchi *et al.*, 2020) compared biodegradation in artificially crude oil-contaminated marine sediment between different sediment cores. The idea was to increase biodegradation capacity of the intrinsic sediment microbiome by introducing a preferential route for electrons to flow from highly reduced to oxidized zones, either by “bioelectrochemical snorkel” (an electrically-conductive, non-polarized material, such as graphite, essentially an electrode), or by CB. Thus, the degrader community received access to otherwise out-of-reach oxygen as electron

acceptor. Cores that had a bioelectrochemical snorkel showed similar accelerated hydrocarbon biodegradation, to that observed in cores with CB present. The authors observed that high degradation rates were fuelled by LDET-induced sulphide removal and the authors highlighted CB as “overlooked players in the self-healing capacity of crude-oil contaminated sediments”. Especially considering their worldwide distribution, future bioremediation applications for hydrocarbon contaminated sites are imaginable, where the potential of CB could be harvested for this purpose. Both cases, the PAH-polluted river and the crude oil-contaminated marine sediment, highlight the impact of cable bacteria presence on contaminant biodegradation. This is supposed to occur mainly by indirect effects of cable bacteria metabolism on surrounding degraders, rather than direct contaminant degradation by cable bacteria.

Groundwater cable bacteria were found in a petroleum-contaminated aquifer, predominantly at the fringes of the contaminant plume (Müller *et al.*, 2016). In such environments, contaminant biodegradation is limited by diffusion-controlled electron acceptor availability, and therefore restricted to the plume fringe (Meckenstock *et al.*, 2015). Groundwater cable bacteria are hypothesized to overcome this limitation, as they could theoretically access electron acceptors outside the contaminant plume. By sulphide oxidation, groundwater cable bacteria might provide sulphate as electron acceptor for pollutant degrading microorganisms within the plume (Müller and Meckenstock, 2017).

#### 1.5.5. POLLOX project outline

This thesis contributed in parts to the larger research effort within the POLLOX project, which aimed to investigate possible scenarios for anaerobic pollutant degradation with oxygen. In groundwater and sediments, biodegradation is controlled by two central paradigms:

- 1) Breakdown of pollutants occurs primarily at the “hotspots”, which are redox gradients and interphases between compartments.
- 2) Local electron acceptor availability is the main limitation for biodegradation.

In the POLLOX project, these paradigms were questioned: At a contaminant plume fringe, CB could theoretically overcome redox stratification by de-coupling redox half reaction, enabling them to access oxygen as terminal electron acceptor in otherwise anaerobic and electron-acceptor-limited environment (see Figure 4). Investigating a possible role of LDET in biodegradation was an integral part of this thesis.

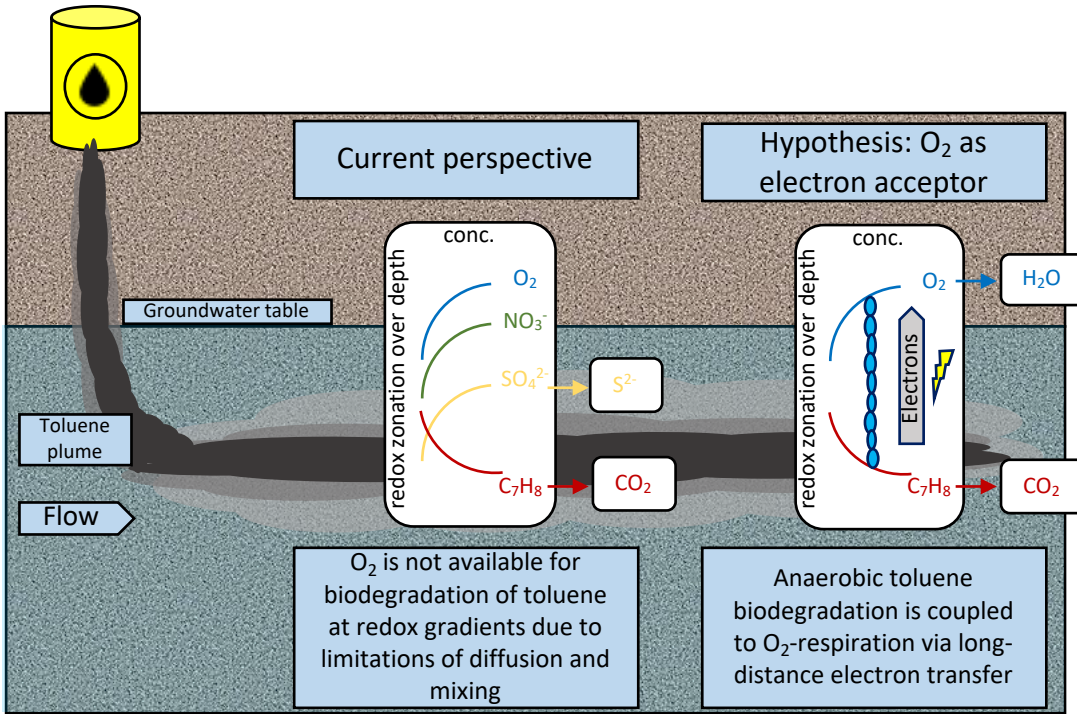


Figure 4: Current perspective of biodegradation at fringes of groundwater contaminant plumes. The hypothesis of POLLOX is depicted, proposing a new role for  $O_2$  in anaerobic biodegradation of pollutants.

## 1.6. Thesis objectives

Investigating cable bacteria remains challenging, as they have proven difficult to cultivate. The assumed strict requirement of cable bacteria for opposing concentration gradients of oxygen and sulphide complicates sustaining them in culture. A first step towards comprehensive cable bacteria research would therefore be the targeted enrichment, preferentially in a (semi-) natural, but sediment-free experimental compartment. Therefore, the **first objective and associated hypothesis** of this thesis were the following:

**Objective 1:** To develop and evaluate a novel cultivation method for targeted enrichment of cable bacteria.

**Hypothesis I:** Physicochemical properties of agar pillars, embedded in a sediment matrix, provide a selective niche for microorganisms relying on geochemical gradients and therefore present a viable cultivation approach for the enrichment of freshwater cable bacteria.

Long-distance electron transfer has a direct impact on biogeochemical transformations and elemental cycling in sediments (Risgaard-Petersen *et al.*, 2012). Via the ability to conduct electricity, cable

bacteria shape the geochemistry of their habitat, removing potentially harmful sulphide from deeper sediments and forming an extended suboxic zone (Seitaj *et al.*, 2015). Because of their unique conductive capacity, cable bacteria are thought to have a competitive advantage over other sulphur-oxidizing microbes in marine sediment (Meysman, 2018). Due to their ability to uncouple redox half reactions in e-SO<sub>x</sub>, CB can capitalize on diffusion gradients especially in environments with high organic loading and limited electron acceptor availability, including polluted sediments (Meckenstock *et al.*, 2015; Matturro *et al.*, 2017). While a number of studies has demonstrated the presence of CB in freshwater systems to date (Risgaard-Petersen *et al.*, 2015; Müller *et al.*, 2016; Sandfeld *et al.*, 2020; Dam *et al.*, 2021; Liu *et al.*, 2021; Scholz *et al.*, 2021), the factors controlling their growth and ecology in freshwater systems remain poorly understood. Hence, the **second objective and associated hypothesis** of this thesis was:

**Objective 2:** To track the distribution and diversity of cable bacteria in diverse freshwater environments by state-of-the art molecular biology and biogeochemistry methods.

**Hypothesis II:** Sediment origin and biogeochemistry control the occurrence and/or diversity of cable bacteria.

Electroactive microorganisms have been considered for their possible potential to bioremediation purposes in the past (Abbas *et al.*, 2019; Wang *et al.*, 2020; Tucci *et al.*, 2021). In anaerobic biodegradation, electron acceptor availability is seen as the main limitation (Meckenstock *et al.*, 2015). This could be overcome, by introducing electrodes into contaminated sediments (e.g. electro-bioremediation), which effectively act as electron acceptors and thus can overcome redox limitations for the degrader community (Zhang *et al.*, 2010; Yan and Reible, 2015; Yang and Chen, 2021). As CB can conduct electricity over cm-distances, they could be imagined as very small bioelectrodes (anodes), stretching throughout redox zones within the sediment. Anaerobic biodegradation of BTEX contaminants in freshwater sediments in presence of cable bacteria has not yet been studied, but cable bacteria might be essential as they can access oxygen as terminal electron acceptor. By either degrading contaminant directly, or indirectly providing an electron sink to other degraders, cable bacteria have the potential in increasing biodegradation within contaminated sediments. Consequently, the **third objective and associated hypothesis** of this thesis was the following:

**Objective 3:** To investigate the impact of long-distance electron transfer on biodegradation in toluene contaminated sediments and identify associated toluene degrading microorganisms.

**Hypothesis III:** Presence of long-distance electron transfer in sediments enhances biodegradation of toluene.

### 1.7. Coordination and funding

This thesis was started at the Institute of Groundwater Ecology (IGOE) of the Helmholtz Zentrum München (HMGU), which was closed in 2019. The work for this thesis was continued at the University of Bayreuth in the Department of Ecological Microbiology. Funding was granted by the European Research Council (ERC) in the frame of the “POLLOX” project (Anaerobic Pollutant Degradation With Oxygen, under FP7-IDEAS-ERC, grant agreement 616644, Principal Investigator: Tillmann Joachim Lüders) and after 06/2020 by the Department of Ecological Microbiology.

## 2. Materials and methods

### 2.1. Sampling and site descriptions

Various sampling sites were visited for the different work packages of this thesis. These are described in detail in the following to better illustrate the environments from which samples were chosen and how and when sampling took place. All of this are important information helping to place samples within their environmental context. All samples were stored anoxically in closed containers in the dark at 5-12°C until laboratory microcosm setup within 2 months after sampling.

#### 2.1.1. Streambed sediment near Garching

Freshwater sediment from a streambed was taken in October 2018 by manual shovelling from a side-branch of the Isar river near Garching, Germany (48°14'23.4"N 11°39'53.4"E). The small stream called Gießen is running below trees in close proximity to agricultural fields. The water temperature at the time of sampling was 13°C. The sediment was characterized by leaf litter and small branches from surrounding trees, as well as a strong sulfidic smell and a black coloring in anoxic zones. Mesofauna was present in form of worms < 1 cm length. Surface sediment was sampled up to 15 cm depth.

#### 2.1.2. Alpine Lake Alatsee

Freshwater sediment from the meromictic (i.e., water layers do not seasonally intermix) pre-alpine lake Alatsee (47°33'45.2"N 10°38'23.3"E) (Oikonomou *et al.*, 2014, 2015) was taken by shovelling from around 1 m depth in October 2018 by wading in from the bank. The water temperature at the time of sampling was 15 °C. Surface sediment was sampled up to 15 cm depth. This lake is known for its sulfidic monimolimnion and redox transition zone, with seasonal blooms of purple sulphur bacteria.

#### 2.1.3. The tar-oil contaminated site in Düsseldorf-Flingern

Contaminated aquifer sediment was sampled from 6-10 m depth below ground in November 2016 via drill-coring at a previously investigated tar-oil-contaminated aquifer in Flingern near Düsseldorf, Germany (51°13'20.6"N 6°49'05.6"E) (Wisotzky and Eckert, 1997; Anneser *et al.*, 2008; Pilloni *et al.*, 2019). Sediment from the upper fringe of the hydrocarbon plume at 7 m depth was used for column incubations.

#### 2.1.4. Grassland soil

To have an easily approachable sampling site mainly for pre-experiments, a grassland soil was chosen in close proximity to the Munich lab. Sampling was done by shovelling from beneath the grass sod of

a meadow in Neuherberg north of Munich, Germany ( $48^{\circ}13'25.0''N$   $11^{\circ}35'44.8''E$ ) starting in March 2017. The site was characterized by sandy and gravelly soil, characteristic for the area around Munich and by occurring pine needle deposits.

#### 2.1.5. Sampling sites in the Fichtelgebirge

The Fichtel Mountains (German: Fichtelgebirge) form a mountain range with elevations up to 1050 m and extend from north-eastern Bavaria to north-western Czech Republic. The region is known for ore-mining since the early Middle Ages and main products were metals, such as gold, tin, iron, silver and copper, but also minerals, earths and rock (Fikenscher, 1807; Besnard, 1854).

The lake Fichtelsee was artificially created by flooding a raised bog. Due to acidification, weathering of the ore-heavy rock stratum released sulphate and iron minerals into the lake. Sampling from lake Fichtelsee sediment ( $50^{\circ}00'58.4''N$   $11^{\circ}51'26.9''E$ ) took place in October 2019 by manual shovelling. The sampling site was surrounded by conifers and without heavy leaf input. The sediment was sandy with pebbles and was of brown colour. The pH of the lake was between 4 and 4.5 (by pH paper measuring) and the water is coloured in a deep brown. For the toluene biodegradation experiment a second field sampling at the same location took place in August 2020.

Lake Weißenstädter See is an artificial recreational lake. The phosphate-rich sediment and the increasing temperatures generated eutrophic conditions, resulting in a mass blue-green algae bloom in early 2000s (Meier *et al.*, 2003). Lake sediment samples from the south bank of lake Weißenstädter See ( $50^{\circ}05'45.2''N$   $11^{\circ}52'18.2''E$ ) were also taken in October 2019 by shovelling. The pH of the lake water was between 6 and 6.5. The sediment samples from this site had a strong sulfuric smell and black colour.

River Eger is one of the inflows of lake Weißenstädter See. Sediment was taken by shovelling from river Eger close to the Czech border ( $50^{\circ}06'51.6''N$   $12^{\circ}26'39.5''E$ ) in October 2019. The water showed pH values between 6 and 6.5. Leaf input occurred regularly due to trees along the river banks and the sediment smelled sulfidic with a black colour.

A small stream, that flows into the river Eger, is the stream Lehstenbach (Weyer *et al.*, 2018). Weathering processes in the boggy environment led to iron and tin occurrence. Microorganisms, such as sulphate-reducing *Desulfobacca* and iron-reducing *Geobacteraceae* were described for this site (Selle *et al.*, 2019). Sediment was sampled from the stream Lehstenbach ( $50^{\circ}07'49.7''N$   $11^{\circ}52'53.4''E$ ) close to research site Schlöppnerbrunnen bog in October 2019. Located in a mixed forest, leaf input

regularly takes place and the gravelly sediment smelled sulfidic, although it did not show a strong black colour. The pH ranged from 5.5 to 6 upon sampling.

## 2.2. Microcosm design

### 2.2.1. Upright laboratory incubation setup: Introducing the “Agar Pillar” technique

To set up the laboratory CB enrichment microcosms (see Figure 5), sediment or soil samples were sieved individually through an analysis sieve (Haver Boecker, stainless steel, mesh aperture 2 mm) to remove larger plant debris or gravel. Sparging with N<sub>2</sub>-gas was used to reduce oxygen exposure during sieving. Glass cylinder columns of 2.8 cm diameter and 12 cm height were prepared by sealing them from the bottom with a rubber stopper of a syringe (Omnifix®, Luer Lock Solo, 50 mL, Braun, Germany). Approximately 150 ml of the homogenized sediment slurry were augmented with 2 µmol/g (wet weight) of solid, anoxic FeS precipitate (prepared as described previously (Müller *et al.*, 2016)) until the slurry took a blackish colour. The bottom-sealed glass cylinders were filled up to 1 cm with the FeS-augmented sediment slurries as sulfidic bottom layer rich in electron donors. Then, a central agar pillar (Fig. 1) was cast before further sediment addition. For this, ethanol-rinsed cocktail straws (diameter 7 mm) were vertically placed into the glass cylinders, gently pressing them into the FeS-augmented bottom layer. A cardboard gauge with a central hole for the straw was used to maintain upright orientation, before further homogenized, non FeS-augmented sediment slurry was then filled on top of the bottom layer to surround the straw. Air bubbles were prevented while the slurry was filled up to ~2 cm below the upper rim of the cylinder. 1.5 % pre-boiled agar (microbiology grade, Carl Roth GmbH) cooled down to ~55°C was then filled into the straws. After the agar had solidified, the straws were carefully pulled, with minimal mechanical disturbance of the slurry and the fresh-made agar pillar. The agar pillars were then cut to end ~2 mm above the surrounding sediment surface, and columns were left to further settle and equilibrate. Columns (as depicted in Figure 5) were then submerged in a freshwater aquarium (~20 L) filled with non-sterile tap water and covered with a lid to minimize evaporation during incubation. The water was air-sparged during incubation by aquarium pumps (Tetra, Melle, Germany). For each sediment, triplicate columns were incubated at room temperature (samples described under 2.1.1 – 2.1.4.) or at 15°C (samples described under 2.1.5.) in the dark for 28 d. Microsensor profiling of diffusion gradients and signatures of LDET was done on days 3 and 28, both in agar and in surrounding sediment. Columns were sacrificed after 28 days.

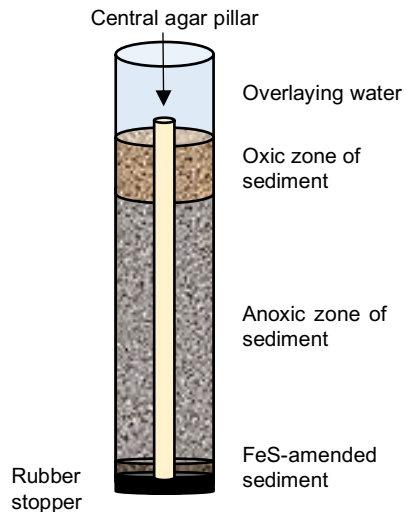


*Figure 5: Schematic drawing of the agar pillar gradient column setup. The glass cylinder was sealed at the bottom with a rubber stopper. Sediment samples were filled into the column around a central agar pillar, spanning the entire length of the column. Bottom layer sediments were amended with FeS. The columns were placed in freshwater tanks, so that they were always overlayed with water during incubation.*

For column sacrificing, the glass cylinders were fixed into a metal stand. Sediment subsections of 0-3 mm, 3-6 mm, 6-10 mm, 10-15 mm, 15-20 mm, 20-25 mm, 25-30 mm, 30-40 mm and 40-50 mm column depth were then sampled. Sacrificing was done by fitting a syringe plunger (50 mL Omnifix or 100 mL BD Plastipak) from below. The plunger was pressed against the syringe rubber stopper originally used to seal the glass cylinders. Thus, the entire sediment column, including agar pillars, was pushed out of the glass cylinder without disturbing depth stratification. The sediment was pushed into a sterile, second glass cylinder of the same diameter with an attached mm-scale. Each depth segment was then cut by using a thin sterilized metal plate and sliding it carefully between the two glass cylinders. The upper part of the sediment of a defined height was then carefully transferred to a sterile petri dish for further handling. From each subsampled sediment section, 500 µL were transferred into 500 µL of 4 % paraformaldehyde solution (1:1) for later fluorescence in situ hybridization (FISH). Further replicates of ~0.5 g were transferred into bead beating tubes for DNA extraction (storage at -80°C). Agar pillar segments were carefully rinsed of remaining sediment with sterile water. Approximately 500 µL of agar from inside the cross section were then squashed into 500 µL 4 % paraformaldehyde solution for FISH. For DNA extraction 0.1 - 0.2 g agar was used per depth-transect.

### 2.2.2. Setup for toluene biodegradation

As toluene is a highly volatile chemical, a closed system was designed in order to safely conduct the experiment. Several replicate columns were used, because sacrificing was conducted at determined time points during the incubation. Because cable bacteria were expected to develop over time, oxic

conditions needed to be monitored within the closed system during incubation. Four different setups were prepared (see Table 2).

*Table 2: Overview of treatments in toluene DNA-SIP experiment*

	<b>Control</b>	<b><sup>12</sup>C-Toluene</b>	<b><sup>13</sup>C-Toluene</b>	<b>Cable bacteria-free Control</b>
Amberlite XAD7 beads	1 g	1 g	1 g	1 g
Sediment	~100 g homogenized sediment slurry	~100 g homogenized sediment slurry	~100 g homogenized sediment slurry	~100 g homogenized sediment slurry
Toluene	-	Unlabelled toluene	Fully labelled <sup>13</sup> C <sub>7</sub> toluene	Fully labelled <sup>13</sup> C <sub>7</sub> toluene
Additions	-	-	-	Incl. 2 membrane filters at 5 and 10 mm depth to prevent filament formation
Micropyrolysis	Possible	Possible	Possible	Not possible
Function	Toluene-free control	Control with unlabelled (lighter) toluene	Follow toluene degradation via labelled C in microbial community (DNA-SIP)	Follow toluene degradation via labelled C in CB-free community (DNA-SIP)
Replicate microcosms	4	4	4	4

Gradient column setup (see Figure 6) was done in glass hybridization vessels of 3.8 cm diameter and 16 cm height (Labor Ochs, Bovenden/Lengern, Germany). Two oxygen sensor spots (PreSens Precision Sensing GmbH, Germany) were glued inside each vessel with silicone glue, one ~5 cm above bottom, the other beneath the top opening and allowed to set for >48 hours. Amberlite XAD7 beads (Sigma-Aldrich) were prepared by washing 5 times with absolute ethanol (Sigma-Aldrich) then 5 times with ultrapure water and dried at 90 °C for 3 days. Each vessel received 1 g of the so prepared beads, then they were transferred to an anoxic box and 5 ml autoclaved anoxic freshwater medium (see Appendix 1, Table 8) was added. A glass syringe rinsed with acetone and flushed with nitrogen gas was used to add 10 µL of either fully <sup>13</sup>C-labelled (<sup>13</sup>C<sub>7</sub>; Sigma-Aldrich) or unlabelled (<sup>12</sup>C; Sigma-Aldrich) toluene to each bottle, resulting in a total toluene concentration of ~ 20 mM before adsorption to XAD7 beads. Vessels were sealed gas-tight with Teflon-coated rubber septa (Labor Ochs, Germany) to prevent toluene loss. Control setups (toluene-free control) were prepared the same way, and received beads and freshwater medium, but no toluene. Incubation was at 15°C in the dark with gentle shaking (50 rpm) for 3 days to allow toluene adsorption to beads, after which the toluene concentration dropped to ~ 10 µM +/- 3 µM (measured by HPLC).

Sediment filling was done in an anoxic chamber to prevent oxidation of samples. Each vessel received ~10 ml or ~25 g (wet weight) of FeS-augmented sediment slurry (~2 µmol/g (wet weight) of solid, anoxic FeS precipitate, prepared as described previously (Müller *et al.*, 2016), until the slurry took a blackish colour). The FeS-augmented slurry was then homogenized with the beads. Upon this 1 cm thick bottom layer of sediment-bead mix, ~75 g of homogenized sediment sample was gently filled, resulting in a total of ~100 g sediment per vessel up to a height of ~4 cm. One group was set up including sterile filter membranes (hydrophilic polycarbonate membrane filters with 0.2 µm pore size; Sigma-Aldrich). These were carefully added at 5 mm and 10 mm sediment depth during preparation. Microcosms including filter membranes were intended as control without CB-growth (Pfeffer *et al.*, 2012; Schauer *et al.*, 2014). Filter membranes prevent bacteria from migrating through due to the pore size, while only having insignificant impacts on diffusional transport (Sayre, 1926). After sediment filling was complete, vessels were then removed from the anoxic chamber and ~20 ml oxic freshwater medium were filled carefully upon the sediment column. Vessels were sealed with aerated headspace.

During the incubation, oxygen levels in the water column above sediment surface as well as in the headspace were monitored by optode measurements (PreSens Precision Sensing GmbH, Germany) every 2-3 days (day 2, 6, 9, 16, and 22). Headspace within the microcosm was kept at atmospheric pressure. Headspace samples were taken on days 1, 3, 6, 9, 13, 16 and 22, and samples were handled as described below (see sections 2.4.2. and 2.4.3.).  $^{13}\text{CO}_2$  in the headspace was determined by IRMS (see below). One replicate column per treatment was opened on days 8, 15 and 29, to take microprofiles and afterwards sacrifice for depth-resolved sediment subsamples for molecular analysis. Depth-resolved sediment transect samples were taken from the following depths: 0-5 mm, 5-10 mm, 10-15 mm, 20-25 mm and 25-30 mm. The sediment transects were used for DNA extraction (see 2.6.1.). Microbial community profiling was done over all depths. DNA-SIP fractionation (see 2.7.2.) was done only for DNA collected from transects at 5-10 mm depth and 20-25 mm depth and only from day 8 and day 15, as for later timepoints label dilution due to cross-feeding (DeRito *et al.*, 2005) was anticipated.

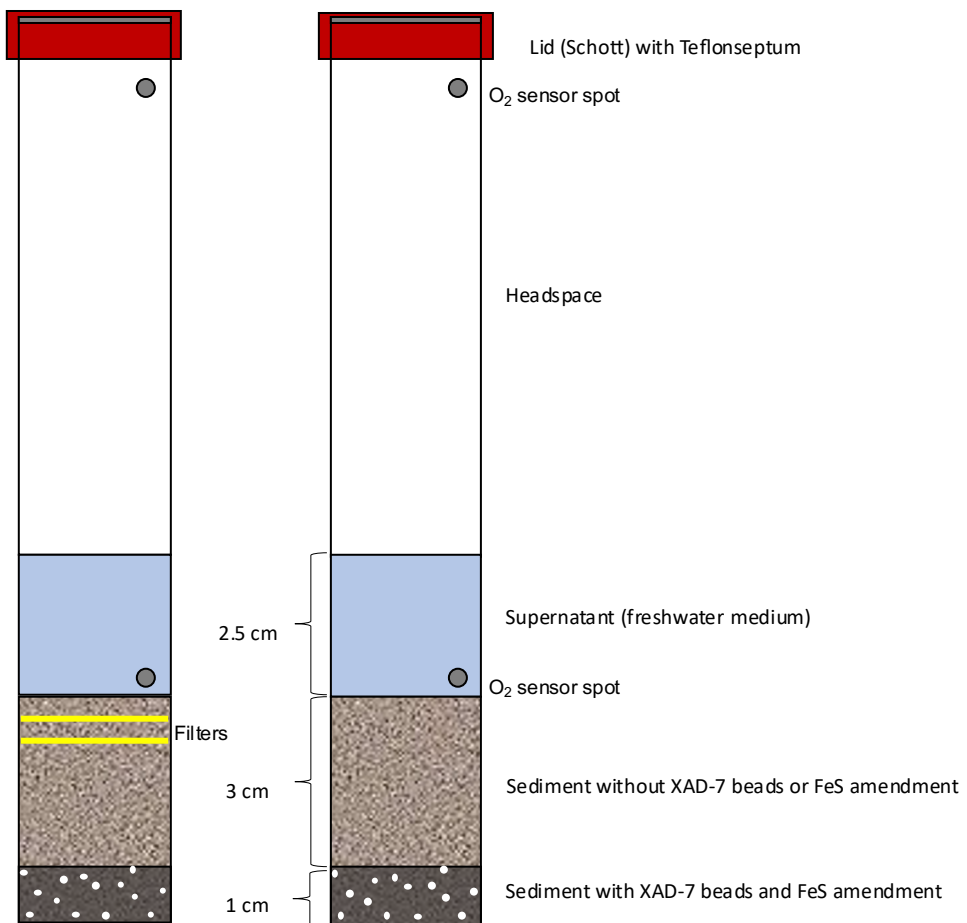


*Figure 6: Schematic drawing of microcosm design for DNA-SIP experiment with labelled toluene. Glass vessels were sealed with Teflon-coated rubber stoppers to prevent toluene loss. Sediment was filled anoxically with oxic freshwater medium as supernatant and atmospheric headspace. Oxic conditions were monitored within the sealed microcosms via sensor spots. Toluene was added to the sediment by binding it to XAD7 adsorber resin beads. Toluene-free control microcosms were additionally prepared.*

### 2.3. Microcosm biogeochemistry

Microprofiles of oxygen, sulphide and pH were measured with microsensors (~200-500 µm tip size for measurements in sediment, ~100-200 µm tip size for measurements in agar), purchased from Unisense (Aarhus, Denmark) (Revsbech and Jørgensen, 1986; Revsbech, 1989; Jeroschewski *et al.*, 1996). In replicate columns, electric potential measurements were always done using in-house prepared sensors (Revsbech and Jørgensen, 1986; Damgaard *et al.*, 2014) from Aarhus University. Calibration of microsensors was done according to the manufacturer's instructions, or raw signal was noted for electric potential measurements. After sensor equilibration and pre-polarization for at least 2 h, calibration was always done at the same temperature (usually 15 °C or room temperature) as the subsequent measurements would be done. In more detail, the oxygen sensors were calibrated by a 2-

point-calibration, using a solution of 0.1 M sodium ascorbate and 0.1 M NaOH ( $\sim$ 2 g sodium ascorbate in 100 ml of 0.1 M NaOH) as zero reading and aerated MilliQ water (minimum 5 min of vigorous bubbling with air) as atmospheric reading (oxygen-saturated water under atmospheric partial pressure conditions). The sulphide sensors were calibrated by a 4- or 5-point-calibration, always using MilliQ water as zero reading and a dilution series of a stock solution of  $S^{2-}$  ( $\sim$  0.01 M total sulphide) with concentrations for the expected measuring range. The stock solution was prepared anaerobically by dissolving 0.24 g  $Na_2S \cdot 9 H_2O$  in 100 mL of  $N_2$ -flushed water ( $pH < 4$ ) in a closed container. For pH measurements, either a pH sensor with integrated reference electrode was used or a micro electrode with external reference electrode were used. They were calibrated using a 3-point-calibration (at  $pH = 4$ ,  $pH = 7$ ,  $pH = 9.3$ ) with manufactured pH buffers covering the expected pH range.

All microsensor signals were recorded with the Sensortrace pro software (Unisense, Aarhus, Denmark) and data were exported to Excel. Total sulphide concentrations  $\sum H_2S = [H_2S] + [HS^-] + [S^{2-}]$  were calculated using the simplified equation after Jeroschewski *et al.* (Jeroschewski *et al.*, 1996):  $[H_2S] = [S_{tot}^{2-}] / (1 + K_1 / [H_3O^+])$  with  $pK_1 = 6.9518$  after Millero *et al.* (Millero *et al.*, 1988) For total sulphide concentrations, it was therefore important to measure the pH at the same depth as well. For EP, reverse profiles were taken (measuring from depth to the surface) to minimize noise. Profiling data from Excel were finally imported into SigmaPlot 14.0 to generate depth-resolved graphs. Mean values with standard deviation are shown.

## 2.4. Chemical analysis accompanying toluene biodegradation

### 2.4.1. Toluene detection in liquid samples by HPLC

Toluene concentrations in the aqueous phase were measured by high pressure liquid chromatography (HPLC) on a 1200 Series HPLC instrument (Agilent Technologies, Wilmington, DE, USA) with HPLC Prodigy-Column (5  $\mu m$  ODS-3 100 Å, LC Column 250 x 4.6 mm, Ea, and pre-column for C18 phase, both Phenomenex, CA, USA). The flow rate was 0.8 ml/s with 70% Acetonitrile (Acetonitril ROTISOLV® 2 min. 99,95 %, HPLC Ultra Gradient Grade, Carl Roth GmbH, Germany) at pH 6 as eluent buffer. 10  $\mu l$  sample were injected and measured at 194 nm wave length. Under these conditions, the retention time of toluene was  $\sim$ 7.7 min.

### 2.4.2. Gas chromatography for total $CO_2$

For total  $CO_2$  measurements, 100  $\mu l$  headspace was directly inserted into a gas chromatograph (Schambeck SRI 8610C, SRI Instruments, Earl St. Torrance, CA, USA) with column Hayesep-D 2 m x 1/8"

(SRI Instruments), so that the temperature of the incubations could be kept constant at 15 °C. Measurements were done in triplicates. Sample analysis conditions are given below (see Table 3) and Peak simple Software (version 4.20, SRI Instruments) was used for evaluation.

*Table 3: Conditions for analysis of CO<sub>2</sub> content in headspace samples*

Oven temperature	Detector	Detector temperature	Flow rate	Carrier gas
80 °C	Thermal conductivity detector (WLD)	175 °C	20 ml/min	Helium

#### 2.4.3. Relative abundance of stable carbon isotopes via GC-IRMS

For CO<sub>2</sub> stable isotope analysis, samples of 3.1 ml headspace were injected into exetainers (Exetainer® 3ml Vial - Flat Bottom, Labco, UK) for subsequent analysis. Isotope ratio mass spectrometry (IRMS), coupled to gas chromatography (GC) was applied to analyse natural relative abundances of stable C (<sup>13</sup>C/<sup>12</sup>C) isotopes. Measurements were done by BayCEER's Key Lab for Isotope Biogeochemistry at Bayreuth University. <sup>13</sup>CO<sub>2</sub> atom percent was calculated according to the following formula:

$$^{13}\text{CO}_2 \text{ atom \%} = ^{13}\text{CO}_2 / (^{13}\text{CO}_2 + ^{12}\text{CO}_2)$$

### 2.5. Fluorescence *in situ* hybridization and microscopy

#### 2.5.1. Sample fixation

Samples for later FISH analysis were fixed relying on protocol from MPI Bremen (Llobet-Brossa *et al.*, 1998). In brief, squashed agar slices from the agar pillar, sediment or soil samples were fixed ~ 1:1 overnight in fresh 4% paraformaldehyde solution (resulting in a final concentration of ~2%) at 4°C in the dark. After fixation, samples were washed 3x with 1xPBS pH 7.6 (centrifugation steps at 16.000xg for 5 minutes) and supernatant was poured off. Finally, sediment samples were stored in a 1:1 mix of 1xPBS / absolute ethanol at -20°C or -80°C until further processing.

#### 2.5.2. FISH

Many different conditions were tested for optimum probe hybridization to environmental samples. In the following, only the protocol for best conditions is described.

A dilution of 1:10 was used for analysis of sediment samples. A final volume of 20 µl was pipetted onto polysine-coated slides (Polysine® Slides, Menzel-Gläser, Thermo Scientific, Germany) or on microscopic

slides with wells (diagnostic, Menzel-Gläser, Thermo Scientific, Germany) with self-prepared gelatin-coating (70 °C warm solution of 0.075% gelatin, 0.01 % CrK(SO<sub>4</sub>)<sub>2</sub>). For the agar samples, a slice was squashed between an object slide and a cover slip. The slides were dried at 46 °C for 30-60 minutes. After applying the fixed sample onto the slide, they were dehydrated in consecutively increasing ethanol concentrations of 50 %, 80 % and 100 % for 3 minutes each. Subsequent hybridization occurred for at least 2.5 hours at 46 °C and was followed by a 20 min stringent washing step according to Pernthaler *et al.* (Pernthaler *et al.*, 2001). For details on FISH probes used to generate images for this thesis see below (see Table 4). Filamentous *Desulfobulbaceae* were detected with the specific family-level oligonucleotide probe DSB706 (Loy *et al.*, 2002) modified with Atto 647N using a hybridization stringency of 35 % formamide. For detection of total bacteria, the oligonucleotide probe mix EUB I-III was used (Daims *et al.*, 1999) coupled to Atto 488 with 35 % stringency (FISH probes were 5'-labelled mono-probes, biomers.net GmbH, Germany). Samples were counterstained with universal DNA stain 4',6-diamidino-2-phenylindole (DAPI) and embedded in antifade mounting medium, a 1:5 mix of Vectashield® H-1000 (Vector Laboratories, Burlingame, California, USA) and Citifluor (Electron Microscopy Sciences, Hatfield, Pennsylvania, USA).

Table 4: Oligonucleotide probes that were used for cable bacteria detection

Probe name	Sequence 5'-3'	Target organisms	Reference
DSB706	5'-ACCGGTATTCTCCGAT-3'	Most <i>Desulfobulbaceae</i>	(Loy <i>et al.</i> , 2002)
EUB338 I	5'-GCTGCCTCCGTAGGAGT-3'	<i>Eubacteria</i>	(Amann <i>et al.</i> , 1990)
EUB338 II	5'-GCAGCCACCCGTAGGTGT-3'	<i>Eubacteria</i>	(Daims <i>et al.</i> , 1999)
EUB338 III	5'-GCTGCCACCCGTAGGTGT-3'	<i>Eubacteria</i>	(Daims <i>et al.</i> , 1999)
Non-Eub	5'-ACTCCTACGGGAGGCAGC-3'	Negative control, for unspecific binding	(Wallner <i>et al.</i> , 1993)

### 2.5.3. Microscopy

Fluorescence microscopy was done with an Axioskop 2 plus (Zeiss, Jena, Germany) using specific filters (Zeiss filter sets 02, 10, 50). Imaging was realized using a Leica DFC9000 sCMOS camera (Wetzlar, Germany) and the Leica Application Suite X. Fluorescent images taken in different channels were overlaid in either LAS X software or imageJ software packages.

## 2.6. DNA extraction and molecular methods

DNA was usually extracted choosing the phenol-chloroform-isoamyl alcohol (PCI) method, as described previously (Lueders *et al.*, 2004), as it extracts all nucleic acids. Another advantage of the method is, that all nucleic acids in the environmental sample are supposed to be extracted equally, while commercially-available kits reportedly might introduce a bias during this step (Guo and Zhang, 2013; Teng *et al.*, 2018). If DNA from some microbial taxa is favourably extracted, then their number will be overrepresented in the community composition analysis and vice versa.

### 2.6.1. DNA extraction from sediments and soil

For highest DNA yield, sediment and soil samples were extracted using a phenol-chloroform-isoamyl alcohol (PCI) method, described previously (Lueders *et al.*, 2004). Between 0.2-0.5 g of sediment or soil were added to 2 ml screw-top tubes containing a 1:1 mix of 0.1 and 0.7 mm diameter zirconia-silica beads (Roth, Karlsruhe, Germany), suspended in 750 µl 120 mM NaPO<sub>4</sub> buffer (pH 8) and 250 µl TNS buffer (500 mM Tris pH 8.0, 100 mM NaCl, 10 % SDS (w/v)). Frozen samples were thawed at 50°C for 10 min with 600 rpm shaking. Bead-beating was done for 45 s at 6.5 m/s in a FastPrep-24 (MP Biomedicals, Solon, OH, USA) or for 60 s at 30 Hz in a TissueLyser II (QIAGEN, Hilden, Germany), then tubes were centrifuged at 20800 g for 5 min at 4 °C. Aqueous supernatants were transferred to Phase Lock Gel heavy tubes (Quantabio, Beverly, MA, USA) and extracted (10 s vortex) with one volume PCI, centrifuged at 20800 g for 5 min at 4 °C, transferred, and likewise extracted (10 s vortex) with 1 vol of 24:1 chloroform-isoamyl alcohol. After centrifugation, purified supernatants were mixed with 2 vol of 30 % polyethylene glycol (PEG 6000, Roth, Karlsruhe, Germany, in 2.5 M NaCl) and incubated over night at 4 °C. If low DNA yield was expected, glycogen (20 µl of 0.5 µg/µl in glycogen in TE buffer were added) was added to the PEG tubes in order to enhance later pellet visibility. DNA was precipitated by centrifugation at 20000 g for at least 30 min at 15-20 °C and PEG residues were washed off the (visible or non-visible) pellet with ice-cold fresh 70 % ethanol. The pellet was dried and resuspended in 25-50 µl EB (QIAGEN, Hilden, Germany). Extract quality was either checked by agarose gel electrophoresis (1.5 % agarose in 1xTAE buffer, 100 V, 30 min) or by Nanodrop Spectrophotometer (Thermo Fisher Scientific, Waltham, USA).

### 2.6.2. DNA extraction from agar

Nucleic acids were extracted from agar similarly than from sediments (see above). For higher yield in these low biomass samples, a second bead beating step was introduced for 20 s at 6 m/s in a FastPrep-24 (MP Biomedicals, Solon, Ohio, USA) or for 30 s at 26 Hz in a TissueLyser II (QIAGEN, Hilden, Germany).

### 2.6.3. PCR

DNA raw extracts from sediment or soil samples were diluted 10-100 times depending on quality (content of co-extracted PCR inhibitors, especially humic acids) and yield (DNA concentration) for use as PCR template. PCR reaction mixes differed depending on how the amplicon needed to be processed. If not stated otherwise, the reaction volume was 25 µL, consisting of nuclease-free water, 1.5 mM MgCl<sub>2</sub>, 0.1 mM dNTP mix, PCR buffer, 0.5 U Taq polymerase (Fermentas GmbH, Basel, Switzerland), 5 µg bovine serum albumin (Roche Diagnostics GmbH, Basel, Switzerland), 0.5 µM of each primer (see Table 5), and 1 µL template DNA. Cycling conditions were as followed: 5 min initial denaturation at 95 °C, followed by 25-35 cycles of amplification (denaturation at 95 °C for 45 s, annealing at 52 °C for 60 s, elongation at 72 °C for 90 s), then a final 72 °C extension for 5 min. PCR products were visualized by gel electrophoresis with Generuler 1 kb DNA as ladder (Thermo Fisher Scientific, Waltham, MA, USA).

*Table 5: Overview of PCR primer sets used in this study*

Primer name	Primer sequence 5'-3'	Target region	Purpose	Reference
PB-Ba-27f	5'-AGRGTGTYGATYMTGGCTCAG-3'	Bacteria full-length	PacBio	(Lane, 1991)
PB-Ba-1492r	5'- RGYTACCTTGTTACGACTT-3'	16S rRNA		(Lane, 1991)
IIIu-Ba-515f	5'-GTGYCAGCMGCCGCGTAA-3'	Bacteria 16S rRNA	Illumina	(Parada <i>et al.</i> , 2016)
IIIu-Ba-806r	5'-GGACTACNVGGGTWTCTAAT-3'	V4 region		(Apprill <i>et al.</i> , 2015)
Ba27f-FAM 907r	5'-FAM-AGAGTTGATCMTGGCTCAG-3' 5'-CCGTCAATTCTTGAGTTT-3'	Bacteria 16S rRNA (FAM-labelled fwd primer)	TRFLP	(Edwards <i>et al.</i> , 1989) (Muyzer <i>et al.</i> , 1995)

### 2.6.4. Microbial community fingerprinting

Fingerprinting of the microbial communities -when used- was realized by terminal-restriction fragment length polymorphism (TRFLP) analysis. For this, part of the 16S rRNA gene was amplified with primers Ba27F-FAM (5'FAM-AGA GTT TGA TCM TGG CTC AG -3') and 907r (5'-CCG TCA ATT CCT TTG AGT TT-3') as described previously (Pilloni *et al.*, 2011). The following cycling conditions were used for amplification: initial denaturation (94 °C, 5 min), followed by 24 or 28 cycles of denaturation (94 °C, 30 s), annealing (52 °C, 30 s) and elongation (70 °C, 60 s), followed by a final elongation step (70 °C, 5 min). Each PCR reaction with 50 µL total volume contained 1 × PCR buffer, 1.5 mM MgCl<sub>2</sub>, 0.1 mM dNTPs, 1.25 U recombinant Taq polymerase (all from Fermentas, St. Leon-Rot, Germany), 0.2 µg µL<sup>-1</sup> bovine serum albumin (BSA) (Roche, Penzberg, Germany), 0.5 µM of each primer (Biomers, Ulm, Germany) and 1 µL of template DNA. 80 ng of FAM-labelled amplicons were restricted at 37 °C for 2 h using 0.3 µL Mspl in Tango buffer in a total volume of 10 µL. Fragments were desalting with DyeEx 2.0 Spin Kit (QIAGEN, Hilden, Germany) and 1 µL of the desalting fragments was mixed with 13 µL HiDi Formamide

(Thermo Fisher Scientific) containing a 1:300 dilution of MapMarker-100 ROX Size Standard. Fragments were then denatured at 95 °C for 5 min and separated by capillary electrophoresis on ABI 3730 DNA analyser (Thermo Fisher Scientific). Data were then assessed with the Gene Mapper software 5.1 (Thermo Fisher Scientific) and analysed with T-REX online application. Results from community fingerprinting were here used only to pre-examine the community, upon which 16S rRNA amplicon sequencing was done. No community fingerprinting results are therefore shown in this thesis.

## 2.7. Stable isotope probing (DNA-SIP)

### 2.7.1. Stable isotopes

For DNA-SIP experiments, heavy carbon isotopes (<sup>13</sup>C) were used in comparison with light carbon isotopes (<sup>12</sup>C). Prepared microcosms (see 2.2.2.) were amended either with heavy, fully labelled toluene (<sup>13</sup>C<sub>7</sub>-toluene), meaning that every C-atom was a heavy isotope, or with unlabelled toluene (both purchased from Sigma-Aldrich). Microbial metabolism of toluene would then lead to incorporation of the <sup>13</sup>C or <sup>12</sup>C atoms into microbial DNA, upon cell division.

### 2.7.2. Isopycnic centrifugation of labelled and unlabelled DNA

Unlabelled and labelled DNA from sediment was extracted (see above for details) . After column sacrificing on day 9, 16 and 30, sediment was subsampled by depth and stored at -20°C for up to 4 weeks until nucleic acid extraction. Briefly, ~0.4 g sediment sample was extracted by bead beating (45 sec, 30 Hz, TissueLyser II, QIAGEN, Germany) in the presence of 120 mM NaPO<sub>4</sub> buffer. Aqueous supernatant was extracted successively with equal volumes of phenol-chloroform-isoamyl alcohol (PCI, 25:24:1(vol/vol/vol), Carl Roth, Germany) and chloroform-isoamyl alcohol (CI, 24:1(vol:vol), Carl Roth, Germany). DNA was precipitated with two volumes of polyethylene glycol (PEG 6000, Sigma). DNA concentrations of selected samples were measured on Qubit (dsDNA HS Assay Kit, Thermo Fisher Scientific, Germany) and DNA extracts containing ~2 µg DNA were loaded individually into CsCl (Calbiochem, Merck, Germany) centrifugation media (0.1 M Tris-HCl pH=8, 0.1 M KCl, 1 mM EDTA) in polyallomer QuickSeal tubes (Beckman, Germany). Sediment DNA extracts were isopycnically centrifuged (44 h, 20°C, 184000\*g in Optima ultracentrifuge, Beckman, Germany) as described previously (Lueders *et al.*, 2004). Centrifuged gradients were fractionated from bottom to top into 14 fractions. Refractive index (n) was measured by refractometer (Krüss, Hamburg, Germany) and used to calculate density (ρ) according to the following formula:

$$\rho = -11.293 * n^2 + 42.6513 * n - 35.9133$$

The densities of each fraction are given below (see Appendix 1, Table 9). DNA was recovered by precipitating with two volumes of polyethylene glycol (PEG 6000, Sigma), washed with cold 70 % EtOH, and subsequently resuspended in 25 µL EB (QIAGEN). 16S rRNA amplicons (515F to 806R) were prepared for Illumina sequencing resulting in fastq files for bioinformatic analysis (see below sections for detailed workflow).

## 2.8. Next generation sequencing

Next generation sequencing (NGS) of the 16S rRNA was used to determine the microbial community present in the samples. Two different technologies were applied: PacBio SMRT sequencing for full-length 16S rRNA sequencing and Illumina sequencing, resulting in shorter read-length for sequencing the V4 region of the 16S rRNA gene.

### 2.8.1. PacBio full-length 16S rRNA sequencing

To prepare 16S rRNA amplicons for subsequent PacBio SMRT Sequencing, the Unsupported Full-Length 16S Amplification, SMRTbell™ Library Preparation and Sequencing Protocol (@2016, Pacific Biosciences of California, Inc) was followed. In brief, the approach was to amplify the full-length 16S rRNA in a 1<sup>st</sup> PCR, using 16S primers (27F 5'-AGRGTTCATYMTGGCTCAG-3' and 1492R 5'-RGYTACCTTGTTACGACTT-3') tailed with universal sequences and connect the barcodes for multiplexing in a 2<sup>nd</sup> PCR via the tail, using PacBio® Barcoded Universal F/R Primers Plate – 96 set (see Figure 7). The resulting fragment would then be approximately 1600 bp (1465 bp 16 S rRNA + primers + tail + barcodes).

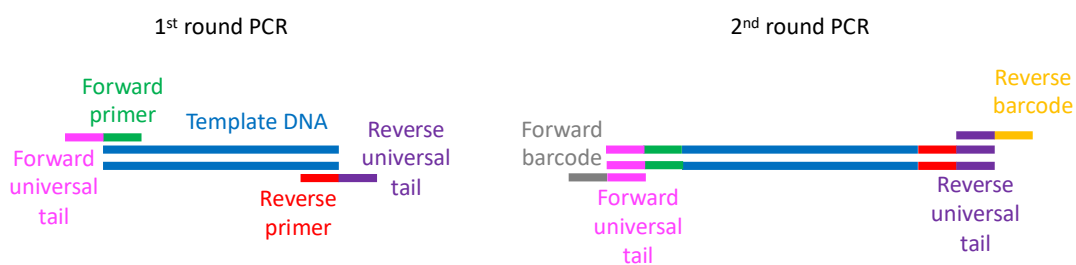


*Figure 7: Scheme of PacBio full-length 16S rRNA amplicon sequencing preparation using primers tailed with universal sequences (1<sup>st</sup> round PCR) and PacBio® Barcoded Universal F/R Primers Plate (2<sup>nd</sup> round PCR).*

In more detail, PacBio SMRT sequencing of bacterial 16S full-length amplicons was done as recently described for ~1 kb nitric oxide dismutase amplicons (Zhu *et al.*, 2020) using universal bacterial 16S primers (Ba27f: AGRGTTYGATYMTGGCTCAG / Ba1492r: RGYTACCTTGTACGACTT) (Lane, 1991) tailed with PacBio universal sequence adapters for the first round of amplification. PCR was done in triplicates in a total reaction volume of 25 µL each, consisting of nuclease-free water, KAPA HiFi Buffer for GC-rich samples (Kapa Biosystems, Roche, Basel, Switzerland), 10 mM dNTP, 50 µM forward and 50 µM reverse primer, 1 U µL<sup>-1</sup> KAPA HiFi Hot Start DNA Polymerase (Kapa Biosystems) and approximately 1 ng of template DNA. The first round of amplification was done with initial denaturation at 95°C for 5 min, followed by 23 cycles of denaturation (30 sec at 95°C), annealing (30 sec at 57°C) and elongation (60 sec at 72°C), and after 23 cycles a final extension at 72 °C for 5 min. Cycle number was increased to up to 27 whenever necessary due to low input template or contaminated DNA. Triplicates were pooled for subsequent purification. Amplicons were purified with the MicroElute® DNA Clean Up Kit (Omega Bio-tek Inc., Norcross, GA, USA) and quantified with a Fragment Analyzer (Agilent Technologies, Santa Clara, CA, USA) using the standard sensitivity kit (DNF-473). Special attention was given to the presence of primer dimers and if these could be detected, amplicons were purified again. The second round of amplification was done in a total reaction volume of 25 µL, consisting of nuclease-free water, KAPA HiFi Buffer for GC-rich samples (Kapa Biosystems, Roche, Basel, Switzerland), 0.3 mM dNTP, 0.3 µM Barcoded Universal Primers (using barcoded universal F/R primers plate – 96, Pacific Biosciences, Menlo Park, CA, USA), 1 U/ µl KAPA HiFi Hot Start DNA Polymerase (Kapa Biosystems) and approximately 0.5 ng template DNA from the first PCR (higher input led to increased chimera formation). Amplification was done in 20 cycles using the same conditions as in the first round. It was essential that cycle number was chosen as small as possible and a maximum of 20 cycles was used. Amplicons were then purified using PacBios' recommended magnetic bead protocol (AMPure PB beads, PacBio, Menlo Park, California, USA) according to manufacturer's instructions. Beads needed to be at room temperature and well homogenized before usage. 25 µL PCR reaction volume was filled up with 25 µL nuclease-free water and then, the 0.6-fold volume (30 µL) of bead solution was added. After the bead clean-up of amplicons, purified PCR products were checked and quantified in Fragment Analyzer (Agilent Technologies, Santa Clara, CA, USA) using the standard sensitivity kit (DNF-473).

SMRTbell library preparation was done according to standard manufacturer protocols. 20 to 25 barcoded amplicon samples per SMRTcell were multiplexed by equimolar pooling, following the guide “Preparing SMRTbell™ Libraries using PacBio® Barcoded Universal Primers for Multiplex SMRT® Sequencing” by Pacific Biosciences. The libraries underwent DNA damage repair, ends repair, followed by purification with AMPure PB beads as described above. Afterwards, blunt-ligation was performed,

followed by adding exonucleases in order to remove failed ligation products. Finally, the SMRTbell™Templates were purified again using the AMPure PB beads and both quality-checked, as well as quantified on fragment analyser. Sequencing of the pooled amplicon mixes was done on a PacBio Sequel II System using version 2.1 chemistry and 2.1 polymerase by COMI at Helmholtz Zentrum Munich.

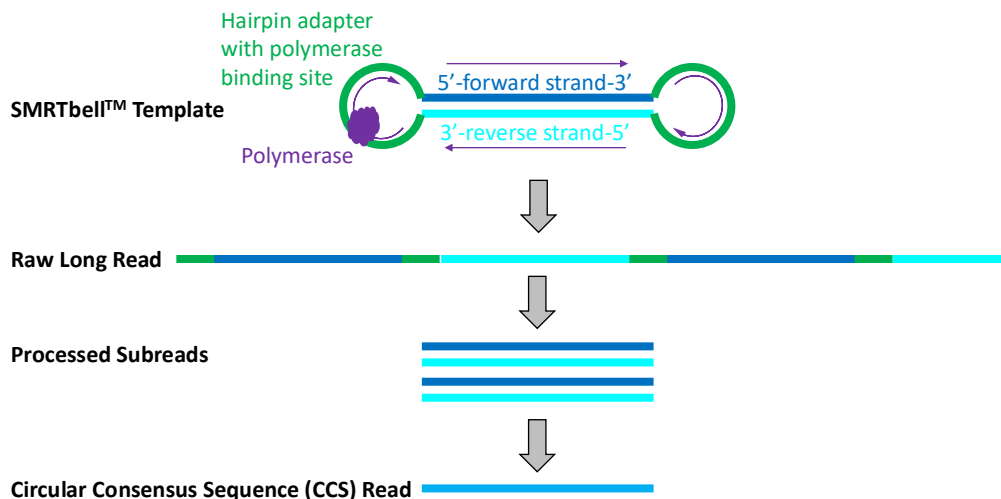


Figure 8: Scheme of amplicon sequencing on the PacBio Sequel System.

In PacBio SMRT sequencing, the hairpin loop with the polymerase binding sit is attached to the desired amplicon and together they form the SMRTbell template for the sequencing. Because, the whole template acts like a closed circle, the polymerase sequences the whole template many times, which is called multiple-pass sequencing. The result is one molecule made-up from a sequence of polymerase-incorporated nucleotides, which are both adaptor sequence and target sequence (see Figure 8). The subreads are both the forward as well as the reverse pass of the target sequence without adapter sequences. The comparatively high random sequencing error rate in PacBio sequencing for an individual pass (in 2013: ~11% (Korlach, 2013)) is overcome by the multiple passes (at least 3 passes are recommended), as individual subreads of the sequence of interest are merged together into a circular consensus sequence (CCS) read. Thereby, the error rate decreases dramatically and was indicated to be over 99% accurate for long reads (Wenger *et al.*, 2019), which is effectively close to zero for the ~1500 bp full-length 16S rRNA gene. This low error rate combined with the long read-length allows for detection of single nucleotide differences and thus considerably increases taxonomic and phylogenetic resolution down to the species level in environmental samples (Mosher *et al.*, 2014; Callahan *et al.*, 2019) and even strain level resolution can be achieved (Callahan *et al.*, 2019).

### 2.8.2. Illumina 16S rRNA sequencing

Illumina sequencing was done based on the protocol available from the Earth Microbiome Project (Thompson *et al.*, 2017) founded in 2010 (EMP, [www.earthmicrobiome.org](http://www.earthmicrobiome.org)). All polymerase chain reactions (PCR) were performed using the NEBNext High-Fidelity 2x PCR master mix (New England Biolabs, MA, USA). Primers for the first PCR with Illumina adapters targeting the bacterial V4 16S rRNA were purchased from Biomers (Ulm, Germany). Raw DNA extract was PCR amplified in a total reaction volume of 25 µl together with 0.5 µM forward primers (515F 5'-GTGYCAGCMGCCGCGTAA-3') (Parada *et al.*, 2016), and 0.5 µM reverse primers (806R 5'-GGACTACNVGGGTWTCTAAT-3') (Apprill *et al.*, 2015). Cycling conditions were as follows: denaturation at 95°C for 5 min followed by 25 cycles of amplification (denaturation 95°C for 30 sec, annealing 50°C for 30 sec, extension 72°C for 60 sec) and a final extension at 72°C for 5 min. PCR product was purified with NucleoMag PCR kit for PCR clean up with magnetic beads (Macherey-Nagel, Düren, Germany) and utilized as template for second Illumina PCR with indexed primers with KAPA 3G HotStart ready mix (Roche, Basel Switzerland). After purification, library preparation was realized with Nextera XT Index Kit v2 Set A (Illumina, San Diego, CA, USA). Sequencing was done on an Illumina iSeq100 with iSeq 100 i1 Reagent and Phi-X Sequencing Control Library (all Illumina). The samples from Fichtelgebirge (autumn 2019) and the subsequent incubations were sequenced in forward and reverse direction with lengths of ~ 150 bp each for later merging of full 16S V4 region while samples from Fichtelsee taken in August 2020 and the incubations for toluene SIP experiment were sequenced as forward reads, reaching a length of ~ 293 bp. Index PCR and sequencing were done by BayCEER's Keylab Genomics & Bioinformatics at Bayreuth University.

## 2.9. Data handling and bioinformatics

Both, PacBio as well as Illumina sequencing that were used during the work for this thesis, resulted ultimately in fastq files, a text-based format, containing the nucleotide sequence and its corresponding quality scores, encoded in ASCII characters. The detailed data handling, which differed for the NGS techniques, is described in the following paragraphs.

### 2.9.1. 16S rRNA data handling from PacBio SMRT sequencing

PacBio sequences produced in 2018 and 2019 were initially handled within the SMRTLink 6.0 portal to generate fastq files. In a first step, pooled samples were demultiplexed (manually in SMRTLink 5.0, after upgrade to version 6.0 in 2018, this happened automatically), followed by generation of circular consensus sequences (CCS). Settings for CCS generation for full-length 16S rRNA gene were as

followed: predicted accuracy = 0.995 or 0.999 (allowing for either 5 or 1 sequencing error(s) in 1000 bp, respectively), minimum number of passes = 3, minimal length = 1300 bp, maximal length = 2000 bp. All other parameters were at default. Fastq files from sampling locations described under 2.1.1.–2.1.4. were submitted to the NCBI Sequence Read Archive (SRA) database under submission ID: SUB9561533 and BioProject ID PRJNA726381. A summary of PacBio sequencing results is given (see Appendix 1, Table 7).

Quality control and denoising of the sequencing reads was performed with mothur v.1.43.0 (Schloss *et al.*, 2009), following previously described procedures (Schloss *et al.*, 2016; Wagner *et al.*, 2016). In a first step, fasta files were generated with the `fastq.info` command using the `pacbio=T` option. Primer and adapter sequences, as well as sequences outside the expected size range (<1350 bp and >1650 bp) were removed using the `trim.seqs` command. Further, putative chimeras were removed with the mothur-implemented Uchime algorithm (Edgar *et al.*, 2011). Unique sequences were generated using `unique.seqs` command. The resulting denoised, high-quality sequences were uploaded to the SILVAngs server (<https://ngs.arb-silva.de>; all settings at default; (Quast *et al.*, 2013)) for automated alignment against the SILVA SSU database (release 132) (Quast *et al.*, 2013; Yilmaz *et al.*, 2014) and taxonomic analysis. Resulting tables were converted to Excel and barplots showing relative abundance were constructed.

### 2.9.2. 16S rRNA data from Illumina iSeq100

Sequences from Illumina iSeq100 were handled differently from PacBio data, as they were much shorter and only covered the V4 region of the 16S rRNA gene. Demultiplexed fastq files were taken as raw data input for bioinformatic analysis. Analysis was done with RStudio version 1.4.1106 or higher (using R version 4.0.4 or higher) and packages dada2 (Callahan *et al.*, 2016) version 1.22.0, ggplot2 (Wickham, 2011) version 3.3.3, Biostrings version 2.58.0 and phyloseq (McMurdie and Holmes, 2013) version 1.34.0. Either paired end reads were used (for microcosms from Fichtelgebirge region), or longer, single end (forward) reads were used (for microcosm data from the toluene experiment). The workflow was as followed: fastq files (either forward and reverse reads as paired-end data, or longer forward reads as single-end data) were read into RStudio and given their sample names. Primers were trimmed off with `removePrimers` command, allowing for a maximum of 3 mismatches and using the `orient=TRUE` option. The quality profiles were examined with `plotQualityProfile`. Based on inspection, the positions for truncation were determined. The `filterAndTrim` command was used with the determined `truncLen` in order to quality-filter the reads. For the denoising with the dada2 algorithm, the error rates were calculated with the `learnErrors` command and plotted for inspection afterwards. The core sample inference algorithm was then applied with the `dada` command and using

the learned error rates. Only afterwards, the paired-end forward and reverse reads were merged, using the `mergePairs` command with a minimum overlap of 10 bases. The chosen overlap for this merging was smaller than the recommended minimum of 12 bases, because the Illumina iSeq reads were only 150 bp long, each. After trimming off the primers, only a few bases remained for merging the forward with the reverse read.

For merged paired-end data and for single-end data, the sequence table was constructed with the `makeSequenceTable` command and chimeras were removed with the `removeBimeraDenovo` command using the “consensus” method. By means of a table that followed the reads through the pipeline and showed how many were filtered out, it was determined if the parameters were chosen in a reasonable manner. Taxonomy was assigned with the `assignTaxonomy` command using the Silva train set version 132 (Fichtelgebirge microcosms) and version 138 (toluene microcosms) and the `addSpecies` command was used with the corresponding Silva species assignment to assign taxonomy down to the species level. All subsequent data analysis was done within the `phyloseq` package. Microbial community barplots were realized in Excel and beautified using Inkscape.

An overview of the bioinformatic analysis done for the toluene microcosm data can be found below (see Appendix 2).

### 2.9.3. Phylogenetic tree construction

*Desulfobulbaceae*-affiliated full-length 16S rRNA sequences were aligned using the SINA online tool (Pruesse *et al.*, 2007) and added to the SILVA Release 138 SSU Ref database (Quast *et al.*, 2013) in ARB (Ludwig *et al.*, 2004). The alignment was inspected manually, using the built-in ARB alignment tool.

For PacBio full-length 16S rRNA amplicon reads, a phylogenetic tree was calculated, using maximum likelihood algorithms and support by 1000 bootstraps (using a 50% sequence variability filter for *Delta proteobacteria*). A selection of representative full-length *Desulfobulbaceae* 16S rRNA sequences from the SSU database was included as reference sequences. For shorter Illumina 16S rRNA amplicon reads, a phylogenetic tree of full-length 16S rRNA reference *Desulfobulbaceae* sequences from the SSU database was calculated, using maximum likelihood algorithms and support by 1000 bootstraps (including a 50% sequence variability filter for *Delta proteobacteria*). Illumina 16S rRNA amplicon reads were added using ARB’s parsimony algorithm. After exporting the tree as graphic, the phylogenetic tree was beautified for publication with adobe photoshop.

### 3. Results

#### 3.1. The “Agar Pillar” technique: Pre-experiments

As cable bacteria are not available in pure cultures to this day, enrichments from environmental samples are the next-best possible thing for experimental purposes. However, sediments can hamper post-incubation analysis of sample. For example, sediment particles may complicate microscopy or humic substances in DNA extracts from sediments might act as PCR-inhibitors. For these reasons, we tested another enrichment approach, called “agar pillar” technique, which enabled bacteria growth in gel-like agar, while maintaining sediment-like redox stratification for cable bacteria lifestyle.

To establish the microcosm setup with an included agar pillar, water-inundated grassland soil was chosen due to direct availability. Sieved and homogenized soil slurry was used for microcosm setup and microprofiling, microscopy and community analyses were performed. Microscopy of inundated soil incubations revealed filaments in both agar pillar and surrounding soil, but hybridization with Dsb706 probe for *Desulfobulbaceae* was not conclusive. Observed filaments were mostly shorter than 500 µm (no images shown).

The primary microprofiling of grassland soil columns (see Figure 9) on day 3 revealed  $\Sigma\text{H}_2\text{S}$  concentrations of up to  $\sim 11 \mu\text{M}$  in the soil and negligible sulphide concentrations in agar pillar ( $< 0.2 \mu\text{M}$ ). pH decreased steadily from  $\sim 8.5$  to  $\sim 8.1$  at 10 mm depth in the soil and more steeply from  $\sim 8.1$  to  $\sim 7.9$  at 5 mm depth in the agar. Hypoxic conditions prevailed in the first 3 and 6 mm in soil and agar, respectively. After 26 d of incubation,  $\Sigma\text{H}_2\text{S}$  concentrations stayed below  $1.2 \mu\text{M}$  both in soil and agar. pH decreased from  $\sim 8.3$  in the oxic zone to  $\sim 7.6$  at anoxic conditions both in soil and agar. Oxygen could no longer be detected below 5 mm depth in both compartments, while the oxygen gradient decreased steeper in soil than in agar. EP measurements were not conducted for the soil columns.

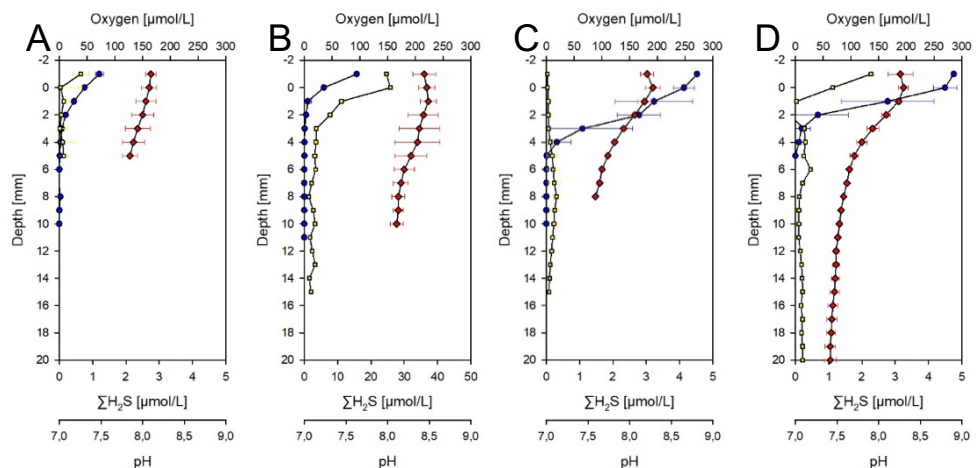


**Figure 9: Geochemical depth-profiles measured in water-inundated soil incubations.** Mean values with standard deviation are depicted. The colour coding is as follows: oxygen (blue), sulphide (yellow) and pH (red). The number of replicate profiles was three. A) Agar pillar, on day 3 of incubation. B) Soil, day 3. C) Agar pillar, day 26. D) Soil, day 26.

Microbiomes from columns with inundated soil (see Figure 10) showed the biggest distinctions between the upper oxic layer and deeper anoxic zones, especially in the agar pillar (oxic 0-3 mm, microoxic 3-6 mm, anoxic below 6 mm depth). The upper agar pillar was highly dominated by *Burkholderiaceae* (up to 54%), while members of the *Ruminococcaceae* became highly abundant below (up to 54% at 6-10 mm depth). In contrast, communities in soil were much more uniform and even over depth. Still, a small population of *Desulfobulbaceae* also seemed to be selected at the oxic/anoxic interphase in soil (up to 2% at 3-6 mm depth).

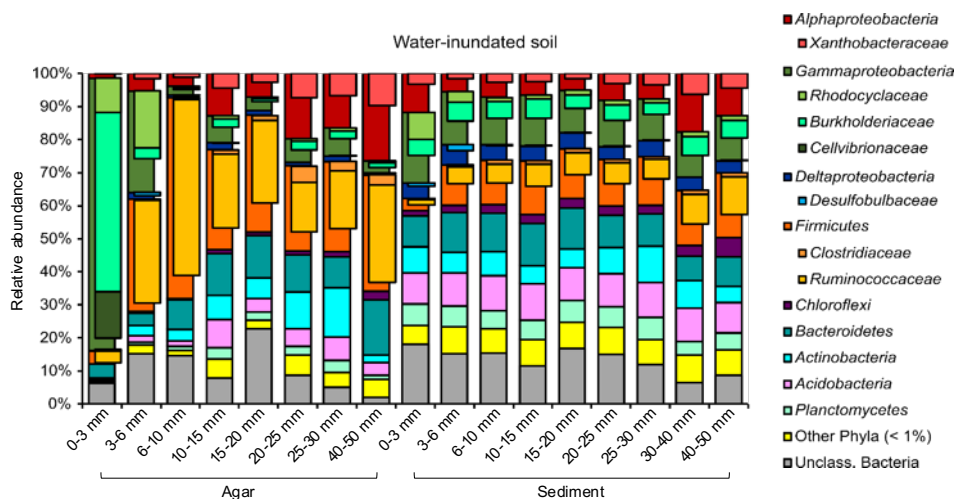


**Figure 10: Microbial community composition in water-inundated grassland soil samples:** 16S rRNA gene-based relative abundance of dominant bacterial groups (relative abundance >1%) observed in gradient incubations. Divided into depth transects of both agar pillar and soil after 4 weeks of incubation.

### 3.2. Discovery of cable bacteria in aquatic sediments

#### 3.2.1. Column biogeochemistry in investigated freshwater sediments

A variety of terrestrial freshwater habitats was selected for sampling to represent a broad spectrum of sites where cable bacteria could possibly occur. An agriculturally impacted side stream of the Isar river was chosen, furthermore sediment of a pre-alpine meromictic lake well-known for its sulfidic hypolimnion (Oikonomou *et al.*, 2014, 2015), and as comparative control site, a previously investigated hydrocarbon-polluted aquifer sediment (Müller *et al.*, 2016) was investigated. The three different sample sediments were incubated under oxygen/sulphide counter-gradients in comparative laboratory columns. Incubations lasted for 4 weeks and microsensor profiling of diffusion gradients and signatures of LDET was done after 3 and 28 days, respectively, both in agar and in surrounding sediment.

In streambed sediment columns,  $\Sigma\text{H}_2\text{S}$  concentrations strongly increased below 10 mm depth after 3 d, both in sediment and agar, rising up to  $\Sigma\text{H}_2\text{S}$  concentrations between  $\sim 17 \mu\text{M}$  and  $\sim 78 \mu\text{M}$  at 15 mm depth, respectively (see Figure 11). The pH decreased gradually from  $\sim 8.5$  in the oxic zone to  $\sim 7.3$  at 10 mm depth. The pH values were comparable between sediment and the agar pillar. Oxygen was completely depleted below 4.5 mm sediment depth, while a minimum of  $47 \mu\text{M}$  was reached at 12 mm depth in the agar pillar, suggesting the upper  $\sim 10$  mm of the agar pillar remain oxic. The EP measured on day 3 remained below 3 mV over all depths both in sediment and agar. After 28 d of incubation, sulphide profiles in streambed columns were markedly shifted.  $\Sigma\text{H}_2\text{S}$  concentrations started to increase to maximally  $4 \mu\text{M}$  only below 20 mm in sediments, while  $\sim 1.4 \mu\text{M}$  were present below 8 mm in the agar pillar. pH dropped from  $\sim 8.7$  to  $\sim 6.7$  at the oxic-anoxic interface and further decreased over depth with a steeper gradient in sediment. The start of the suboxic zone was at 3 mm depth in the sediment and at 6 mm in the agar pillar. An electric field was clearly present after 28 days, indicated by increasing electric potentials (starting at the oxic-anoxic interface) to  $\sim 17$  and  $\sim 14$  mV with depth in sediment and agar, respectively.

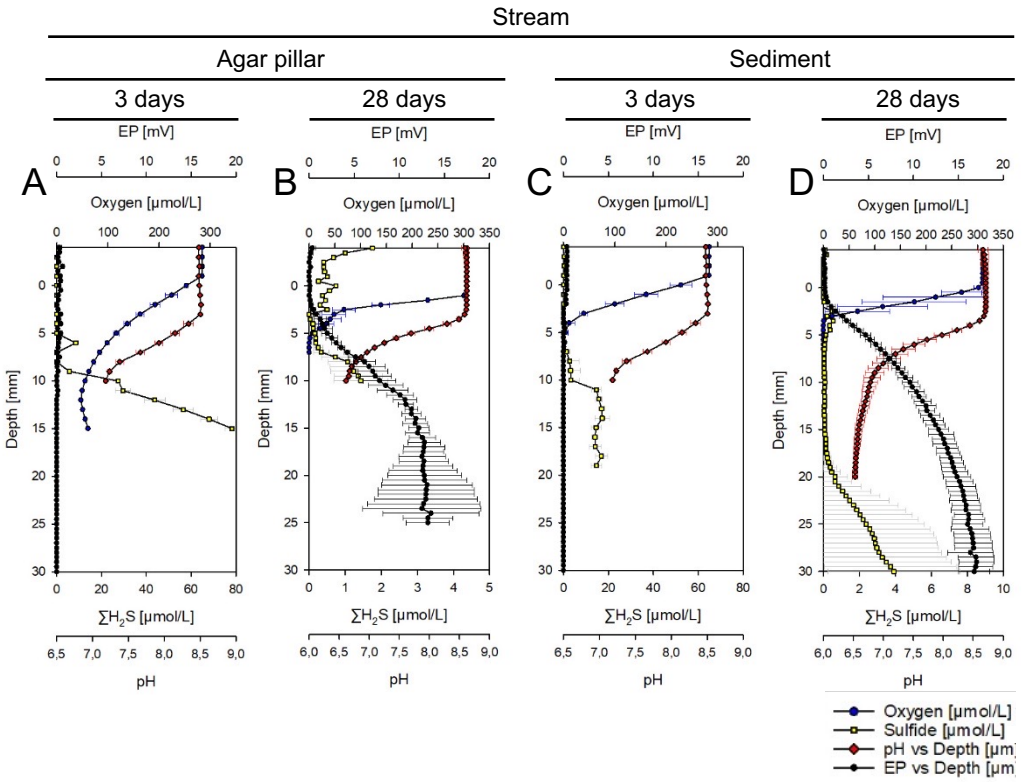


Figure 11: Geochemical depth profiles in column incubations of Garching streambed sediments. (A: agar pillar, 3d; B: agar pillar 28 d; C: sediment 3 d; D: sediment 28 d). Shown are means +/- standard deviations of triplicate profiles.

After 3 days, microprofiling of Alatsee sediments revealed an oxygen penetration depth not deeper than 5 mm in sediments, while oxygen penetrated up to 10 mm into the agar pillar (see Figure 12). Sulphide concentrations were near zero from the surface to a depth of 10 mm in the agar pillar, with the sulfidic zone starting below, while they increased from 0 to  $\sim 40 \mu\text{M}$  between 3 and  $\sim 15 \mu\text{m}$  depth in sediments, but decreased again below. The pH profiles in the agar pillar and sediment resembled each other, reaching minimum values of  $\sim 7.2$  at 8 mm depth. After 28 days, the sulphide gradient was shifted downwards by more than 10 mm (increasing below  $\sim 17 \mu\text{m}$  depth) in the sediment, with a marked suboxic zone detectable between 5 and 17 mm depth, while the suboxic zone started at 7 mm depth in the agar, extending at least 8 mm below. A minimal pH of  $\sim 6.5$  was reached below 10 mm

(agar) and 15 mm (sediment), respectively, and was slightly more acidic than at the start of the experiment.

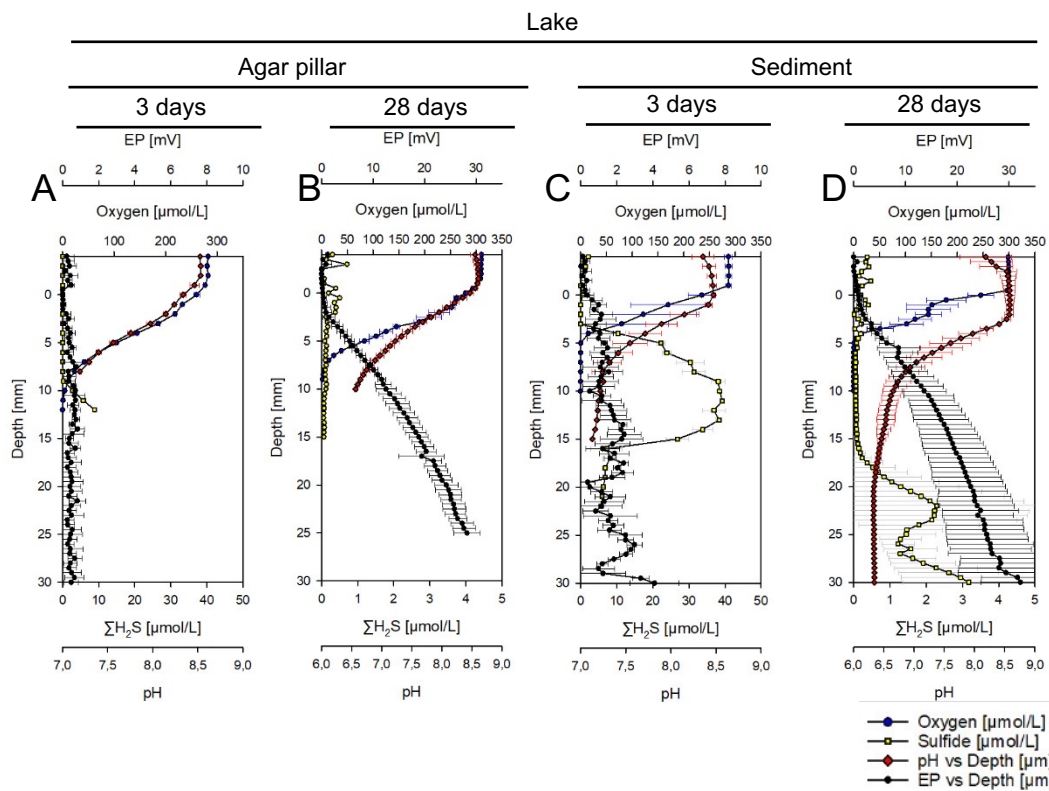


Figure 12: Geochemical depth profiles in column incubations of Lake Alatsee sediments. (A: agar pillar, 3d; B: agar pillar 28 d; C: sediment 3 d; D: sediment 28 d). Shown are means +/- standard deviations of triplicate profiles.

Microprofiling of aquifer sediments showed negligible  $\Sigma\text{H}_2\text{S}$  concentrations over depth after 3 days (see Figure 13). pH dropped from  $\sim 8.3$  to  $\sim 7.5$  over the first 10 mm in both sediment and agar. Oxygen concentrations decreased steadily over depth and anoxic conditions were reached at 8 mm in sediment and at  $\sim 10$  mm in the agar pillar. An electric field was not present, as indicated by EP values below 2 mV over depth. After 28 days of incubation,  $\Sigma\text{H}_2\text{S}$  concentrations remained below 3  $\mu\text{M}$  over depth both in sediment and agar, suggesting increasing sulphide concentrations to be found only below 30 mm sediment depth. pH in the oxic zone was  $\sim 8.4$  (sediment and agar) and dropped below the oxic/anoxic interphase to  $\sim 7.6$  (sediment at 20 mm) or  $\sim 7.9$  (agar at 10 mm). An electric field was detectable in the sediment, as indicated by an EP increase of  $\sim 4$  mV over depth. However, no electric field was present in the agar pillar.

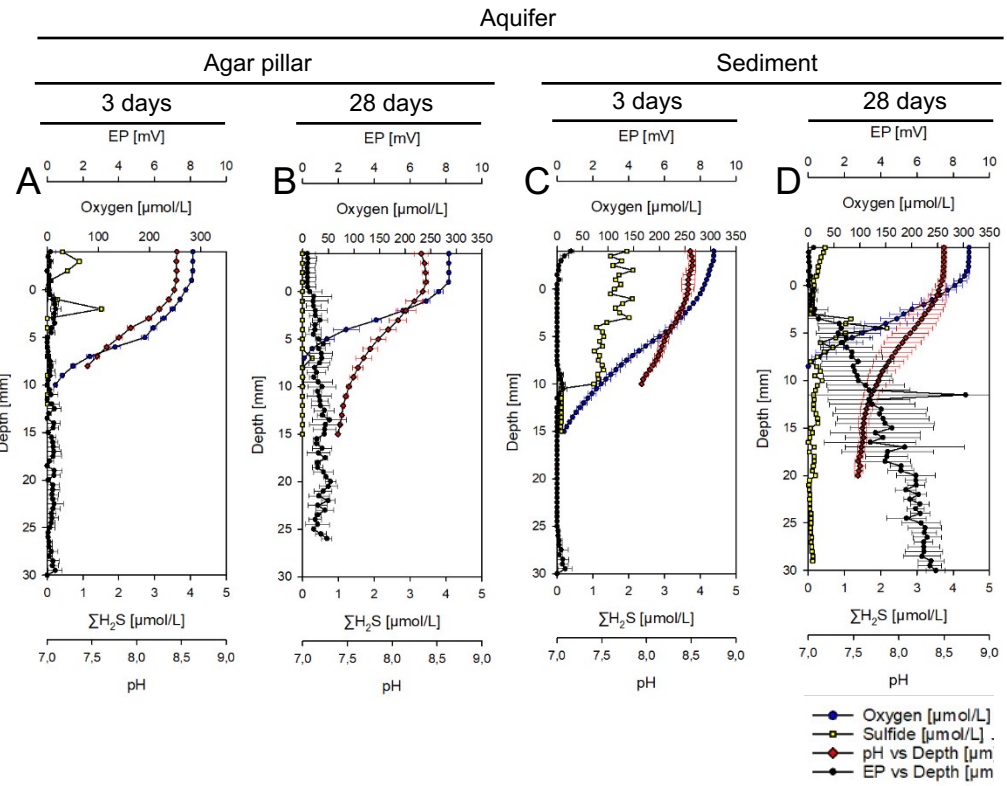


Figure 13: Geochemical depth profiles in column incubations of Flingern aquifer sediments. (A: agar pillar, 3d; B: agar pillar 28 d; C: sediment 3 d; D: sediment 28 d). Shown are means +/- standard deviations of triplicate profiles.

Comparing the three sites, a general observation was that oxygen penetrated deeper within the agar pillar than in the surrounding sediment, and that oxygen gradients were less steep in agar. The pH gradients in sediment and agar were mostly comparable. Geochemical profiles provided evidence for the establishment of a suboxic zone and the occurrence of LDET with time in all different column types, with interesting distinctions in patterns between the different locations. A characteristic pH peak as indicative for LDET by CB (Schauer *et al.*, 2014) was observed at times in individual columns, but was largely hidden when averaged values were calculated for triplicate columns. Still, the marked shift of the sulfidic zone into deeper zones over time, along with the establishment of an electric field, was interpreted as a strong indication of e-SOX by CB.

### 3.2.2. FISH and microscopy of filaments

The presence of *Desulfobulbaceae* filaments in incubated sediment samples was inspected by fluorescence *in situ* hybridization with probe Dsb706 (Loy *et al.*, 2002) (see Figure 14). Indeed, bacterial filaments resembling typical freshwater CB and hybridizing with the Dsb706 probe were detected in column depths between 3-10 mm for all columns, suggesting the presence of CB within the

*Desulfobulbaceae* family within all investigated sediments. For samples from agar pillars, filaments were also detected by FISH (shown for an Alatsee column in Figure 14 B), as well as additionally by light microscopy.

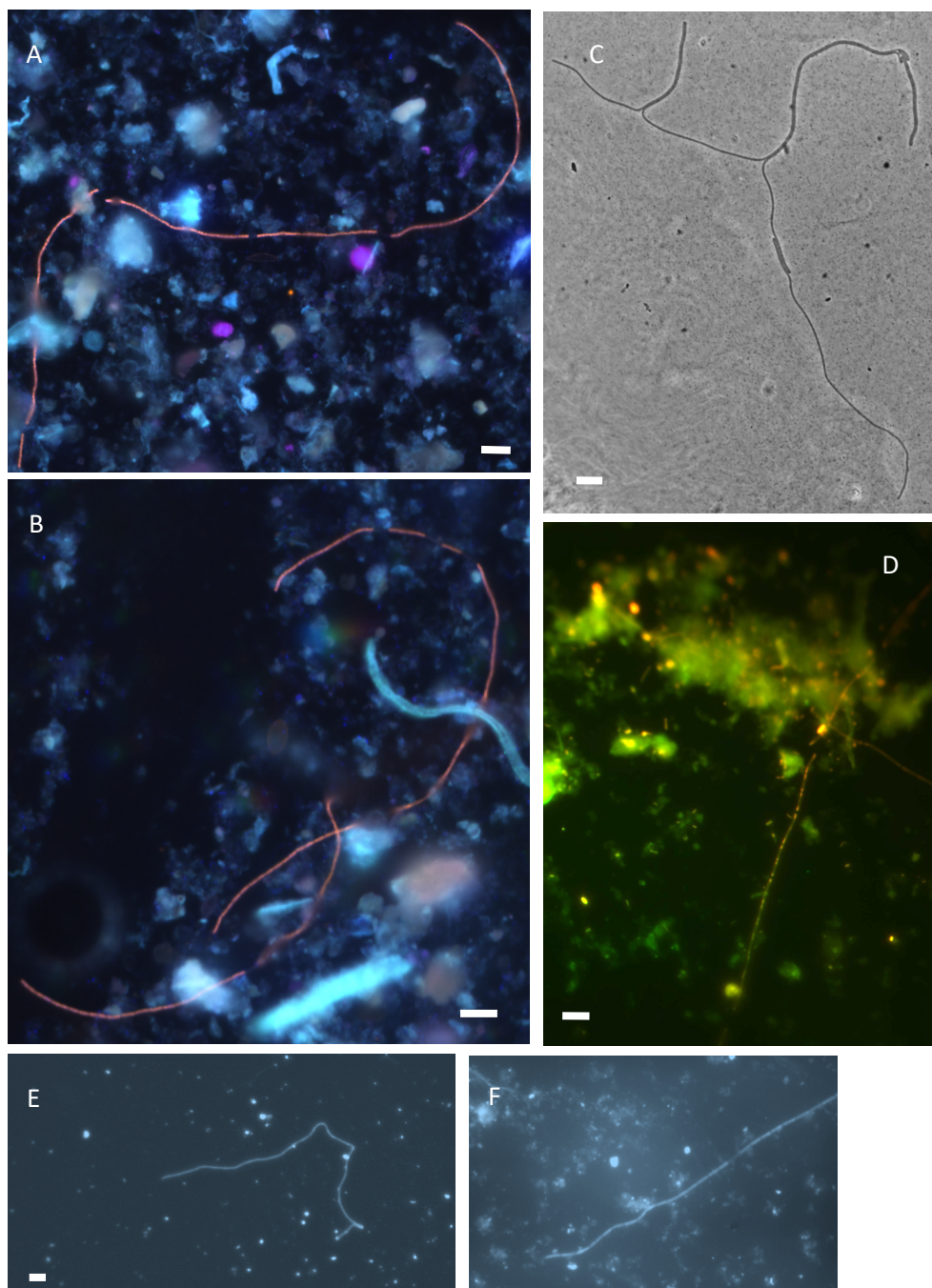
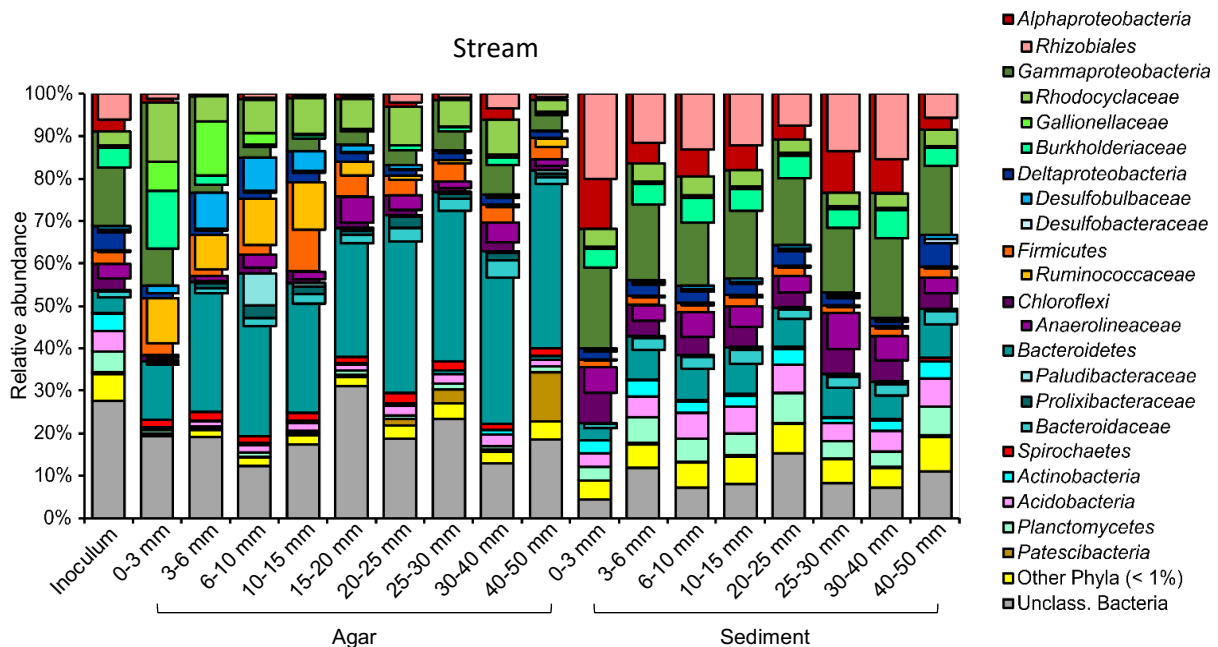


Figure 14: Fluorescent microscopy of filamentous cable bacteria detected in sediment columns. Scale bars are always 10 µm.  
 A: Micrographs of filaments from Garching streambed sediments. Filaments are visualized in an overlay of two images taken with filters for specific fluorescence of the DSB706 FISH probe (red) and 4',6-diamidino-2-phenylindole counterstaining (blue).  
 B: Micrographs of filaments from Lake Alatsee sediments. Other details are as in panel (A). C: Light microscopy image of a filament growing within an agar slide incubated within streambed sediment. D: Micrographs of filaments from Lake Alatsee agar pillar (6-10 mm depth). Filaments are visualized in an overlay of two images taken with filters for specific fluorescence of the DSB706 (red) and EUB I-III (green) FISH probes. E, F: Micrographs of filaments from Flingern aquifer sediments. Filaments are visualized in images taken with filters for the 4',6-diamidino-2-phenylindole fluorescence (blue).

### 3.2.3. Community composition via full-length 16S rRNA amplicon sequencing

The bacterial community was investigated by PacBio SMRT sequencing of full-length 16S rRNA genes in sediment and agar pillars. DNA of depth transects from all sites (both sediment and agar) was extracted and almost full-length 16S rRNA amplicons were sequenced using a PacBio Sequel SMRT sequencing strategy. Per sample, 1732-14819 reads (after QC) with average read length >1450 bp were obtained (for details see Table S1). Communities clearly differed between sites, column depth and between sediment or agar.

The initial bacterial community in the inoculum of the streambed sediment was characterized by a notable abundance of *Gammaproteobacteria* (22%), *Alphaproteobacteria* (9%), *Deltaproteobacteria* (6%), *Firmicutes*, *Chloroflexi*, *Bacteroidetes*, *Actinobacteria*, *Acidobacteria* and *Planctomycetes* (see Figure 15). After 28 days of column incubation, community profiles had clearly changed over depth. In the agar pillar, the uppermost oxic layer was dominated by *Gammaproteobacteria* (22%), amongst them members of the *Rhodocyclaceae*, *Gallionellaceae* and *Burkholderiaceae*. Below 3 mm (oxygen < 80 µM), members of the *Desulfobulbaceae* appeared significantly enriched compared to the surrounding sediment (up to 8%, or ~10x more; p = 0.006), as well as the initial inoculum (up to 8%, or ~10x more; p = 0.026). Within these *Desulfobulbaceae* sequences, full-length amplicons also allowed for the unambiguous identification of reads affiliated to the genus *Ca. Electronema* (up to 0.2% total abundance, see Figure 18). *Ca. Electronema* were significantly enriched in the agar pillar compared to the surrounding sediment (below 3 mm depth, ~10x enrichment, p = 0.041). The anoxic agar was dominated by members of the *Bacteroidetes* (up to 35%), *Firmicutes* (5-21%), but also *Deltaproteobacteria* (<10%) and *Chloroflexi* (<7%), whereas the uppermost oxic sediment layer (0-3 mm) was mainly colonized by *Alphaproteobacteria* (~30%), members of the *Rhizobiales* amongst them, *Gammaproteobacteria* (28%) and *Chloroflexi* (13%). The fraction of *Alphaprotobacteria* decreased over depth (to a minimum of 8%) while *Bacteroidetes* increased (up to 12%). Compared to the agar, *Firmicutes*, *Bacteroidetes* and *Spirochaetes* were less abundant while *Alphaproteobacteria* and *Chloroflexi* were more abundant in sediments. Distinctions in distribution over depth were not apparent.



**Figure 15: Community composition of streambed microcosms.** 16S rRNA gene-based relative abundance of dominant bacterial groups (relative abundance >1%) observed in gradient incubations of stream sediment samples. Divided into inoculum, and depth transects of both agar pillar and sediment after 4 weeks of incubation.

In lake Alatsee sediments (see Figure 16) the upper agar pillar was dominated by *Alphaproteobacteria* (mainly *Beijerinckiaceae* up to 23%) and *Gammaproteobacteria* (up to 54%). Below 30 mm, the community was more diverse with *Gammaproteobacteria* (mainly *Aeromonadaceae*, up to 20%), *Firmicutes* (up to 8%) and also *Desulfobulbaceae* (up to 2%) detected. Unfortunately, some agar pillar samples from Alatsee were degraded and overgrown with a black fungus after 28 days, so that DNA extraction failed and no amplicon data could be generated between 3 and 30 mm depth. Bacterial communities in sediments were rather similar over depth. They were dominated by *Gammaproteobacteria* (up to 36%) with mainly *Burkholderiaceae* and *Rhodocyclaceae*, while members of *Alphaproteobacteria* (up to 9%), *Deltaproteobacteria* (up to 12%, ~1% *Desulfobulbaceae*, including reads affiliated to *Ca. Electronema*, see Figure 18), *Chloroflexi* (up to 5%), *Bacteroidetes* (up to 5%), *Acidobacteria* (up to 5%) were also present. The number of unclassified taxa was higher than for other examined sites (up to 30%).

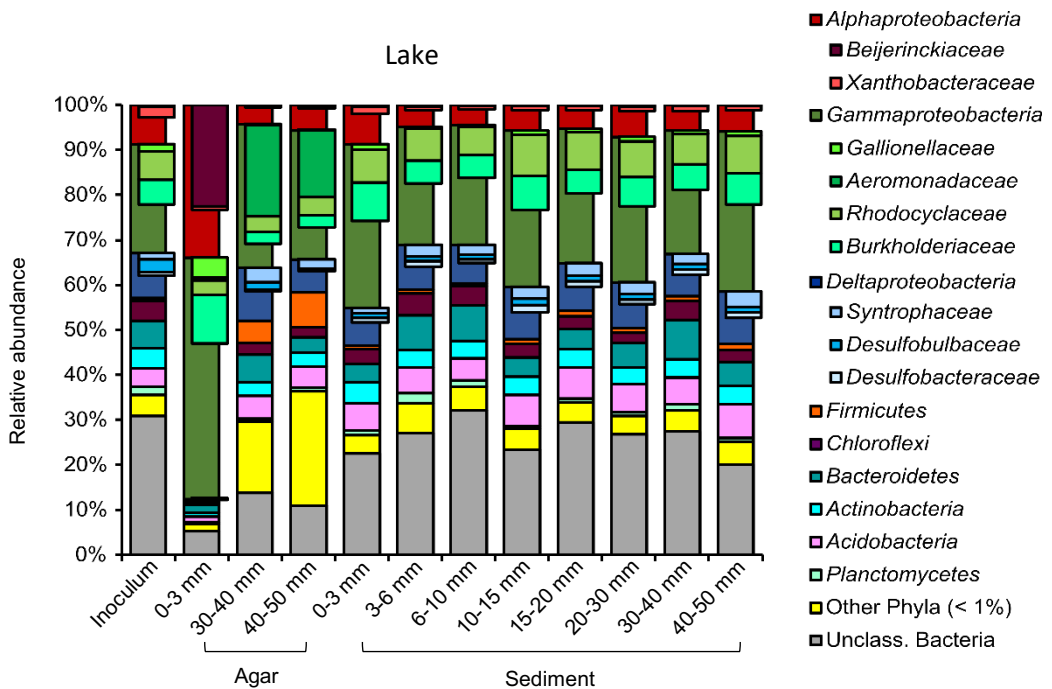


**Figure 16:** Community composition of lake sediment microcosms. 16S rRNA gene-based relative abundance of dominant bacterial groups (relative abundance >1%) observed in gradient incubations of lake Alatsee sediment. Divided into inoculum, and depth transects of both agar pillar and sediment after 4 weeks of incubation.

The intrinsic microbiota of the investigated aquifer sediments (see Figure 17) was mainly characterized by *Gammaproteobacteria* (28%), *Deltaproteobacteria* (15%) and *Epsilonproteobacteria* (6%), comparable also to previous work at the site (Pilloni et al., 2019). After 28 days of incubation, the agar pillar was highly dominated by *Gammaproteobacteria*, with *Burkholderiaceae* and *Rhodocyclaceae* prominent (up to 63%) in the oxic zone (down to 10 mm) while *Aeromonadaceae* markedly increased in abundance over depth in deeper anoxic layers (up to 66% at 20-25 mm). A notable population of *Desulfobacteraceae* (15%) and *Clostridiaceae* (19%) was detectable in the agar pillar right below the oxic/anoxic interface (10 mm), but members of the *Desulfobulbaceae* were not abundant. Upper sediment depths were again dominated by *Gammaproteobacteria*, however *Sulfuricellaceae* were especially enriched (up to 34%) down to 6 mm. Over depth, reads affiliated with the *Thiovulaceae* and *Desulfobulbaceae* became constantly more abundant (up to 19% and 11%, respectively). As opposed to the agar, *Firmicutes* were not abundant in deeper sediment samples (< 1%).

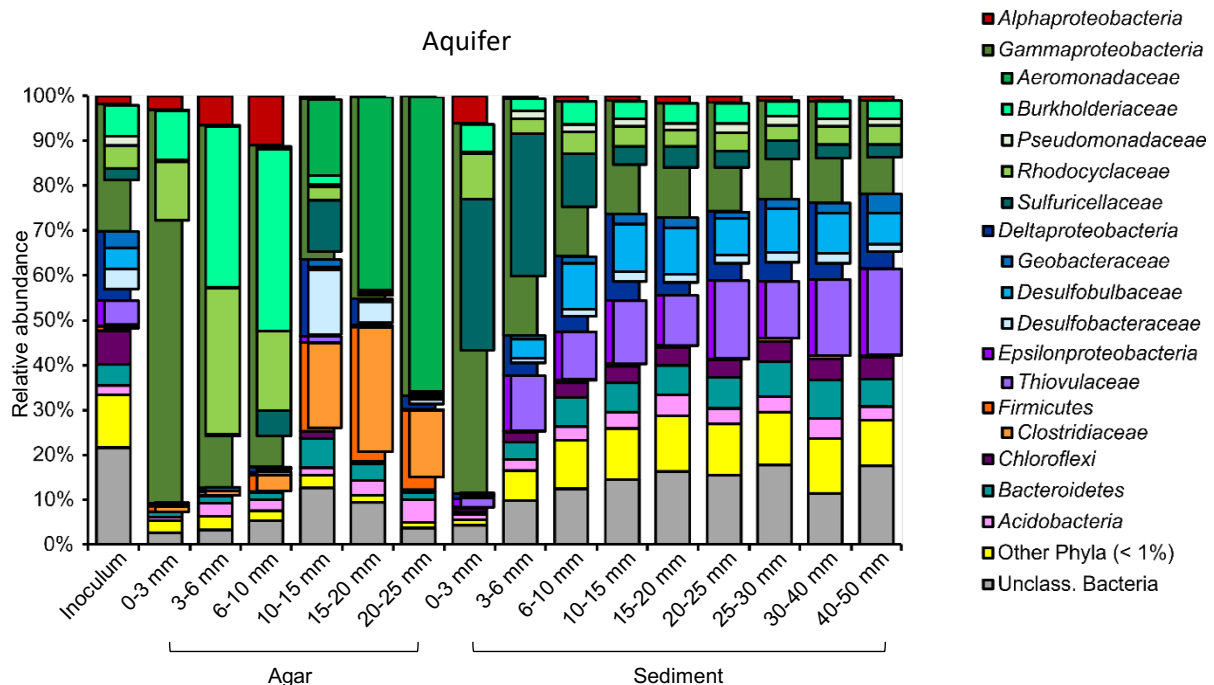


**Figure 17:** Community composition of aquifer sediment microcosms. 16S rRNA gene-based relative abundance of dominant bacterial groups (relative abundance >1%) observed in gradient incubations of aquifer samples. Divided into inoculum, and depth transects of both agar pillar and sediment after 4 weeks of incubation.

### 3.2.4. Phylogenetic placement of 16S rRNA amplicon sequences

The generated full-length amplicons allowed for a robust phylogenetic placement of the obtained CB 16S rRNA gene sequences. For streambed and lake Alatsee samples, 3 putative species-level clusters of freshwater CB sequences branched close to *Ca. Electronema palustris* (see Figure 18, group 1,2 and 3), while 2 putative species-level clusters branched closer to *Ca. Electronema nielsenii* and *Ca. Electronema aureum* (group 4 and 5). Sequences within these clusters showed maximum sequence similarities of ~94 – 95 % to either *Ca. E. palustris* or *Ca. E. nielsenii*, all but for group 5, which was <~99% similar to *Ca. E. nielsenii* (see Table 6). For aquifer sediment, one cluster of groundwater CB sequences branched with previously described groundwater CB, as sister group to *Desulfurivibrio* spp. (Müller *et al.*, 2016), while a second cluster found in sediment and agar was even more deeply branching (see Figure 18).

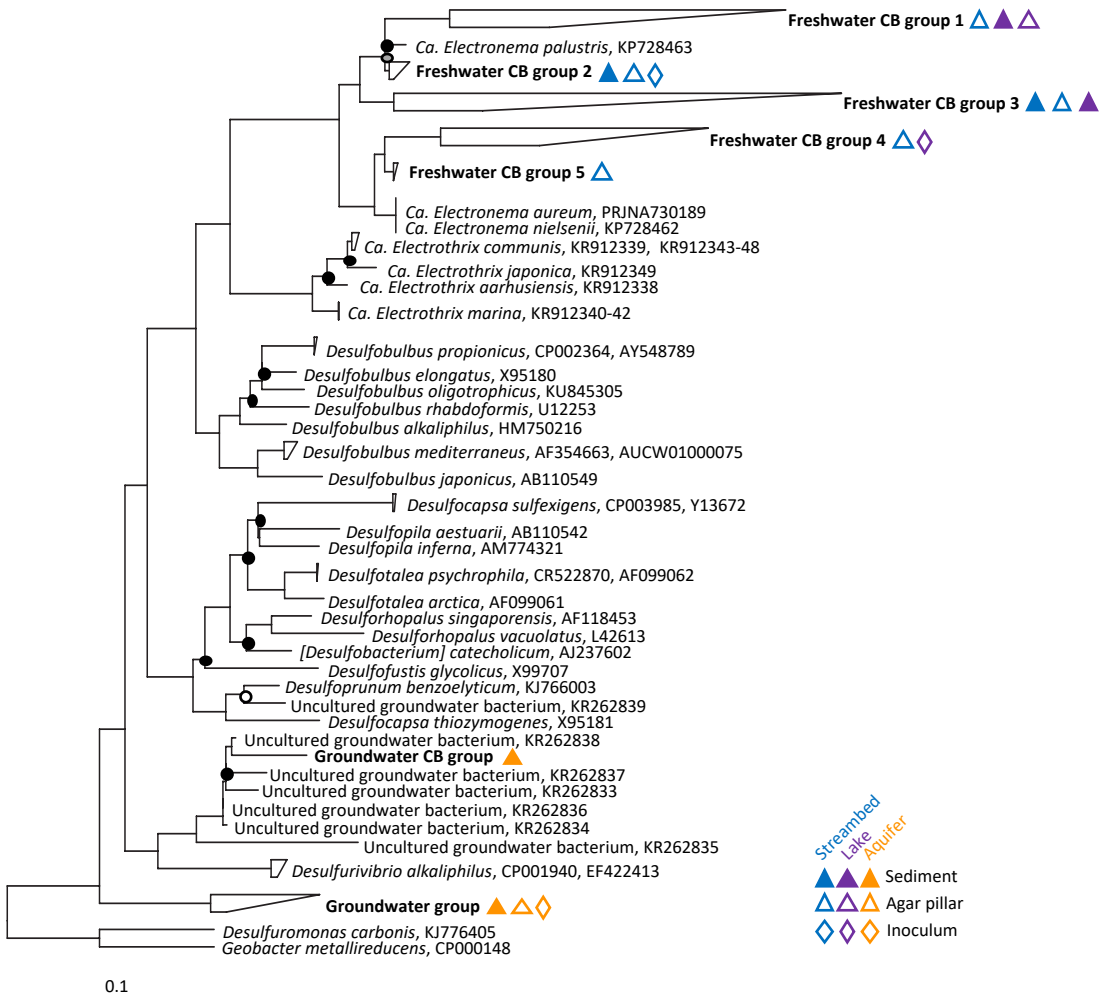


**Figure 18:** Phylogenetic placement of full-length 16S rRNA gene reads of presumed species-level cable bacteria groups reported in this study (in bold) within the *Desulfobulbaceae*. The accession numbers of selected sequence entries are given. The tree is rooted with outgroup sequences of *Geobacter metallireducens* and *Desulfuromonas carbonis*. Branching points without symbol indicate bootstrap values > 99. Black circles: bootstrap support > 90, grey circles: bootstrap support > 70 and open circles: bootstrap support > 55 (n = 1000). The scale bar shows 10 % distance.

**Table 6:** Pairwise 16S rRNA sequence similarity of freshwater cable bacteria

	<i>Ca. Electronema palustris</i>	<i>Ca. Electronema nielsenii</i>
Freshwater CB group 1	< 94.3 %	< 91.2 %
Freshwater CB group 2	< 99.6 %	< 95.5 %
Freshwater CB group 3	< 95.1 %	< 92.9 %
Freshwater CB group 4	< 90.6 %	< 93.7 %
Freshwater CB group 5	< 95.1 %	< 99.1 %

### 3.3. Cable bacteria in the aquatic sediments of the Fichtelgebirge

The Fichtelgebirge in northern Bavaria, Germany is a mountainous region known for spruce forests and as a former mining area. Several sediments from yet un-investigated acidic lakes and rivers were incubated in microcosms including a central embedded agar pillar to enrich for cable bacteria. Incubations were accompanied by microsensor profiling, imaging as well as community sequencing over depth and between agar pillar and surrounding sediment in comparison.

#### 3.3.1. Biogeochemistry of columns from the Fichtelgebirge

Microprofiling in search for hints of LDET was done over time in microcosm setups, both in sediment as well as in the agar pillar. Profiles over depth were taken from oxygen, pH and sulphide, while EP was not measured. In general, the pH was more acidic than in microcosms from previously studied sampling sites while *in situ* sulphide concentrations were low. Depth profiles of sediments differed slightly from those taken within the agar pillar. Oxygen could diffuse deeper into the agar than into the sediment with a steeper oxygen gradient observed in sediments. Over all columns, oxygen penetration depth was greater in agar than in sediment by 1-2 mm with low oxygen concentrations below 50 µM. The development of an oxic sediment layer could be observed instantly after column preparation and placement within freshwater tanks. Changes over time were also documented by taking images of the incubation setup (see Appendix 1, Figure 39, exemplary for River Eger columns). Sulphide was less detectable within the agar pillar, while the pH profiles were very similar between agar and sediment.

Microcosms from Lake Fichtelsee (see Figure 19) showed the highest  $\Sigma\text{H}_2\text{S}$  concentrations within the first week of incubation (4-4.5 µM from 10 to 32 mm), which dropped to <0.1 µM in week six, when the onset of the sulfidic zone was shifted to 25 mm depth, both in agar and sediment. This suggests that a suboxic zone (~5 mm to 18 mm) developed over incubation time and hints towards ongoing LDET. The pH remained similar, comparing both time points and was relatively acidic (5.5 below 10 mm in the first week, <5.5 below 15 mm in week six). After six weeks, a pH peak at the oxic/anoxic surface layer could be detected, which is a clear hint towards LDET. O<sub>2</sub> could was depleted below 4 mm in sediments (week 1 and 6) and below 7 mm in agar.

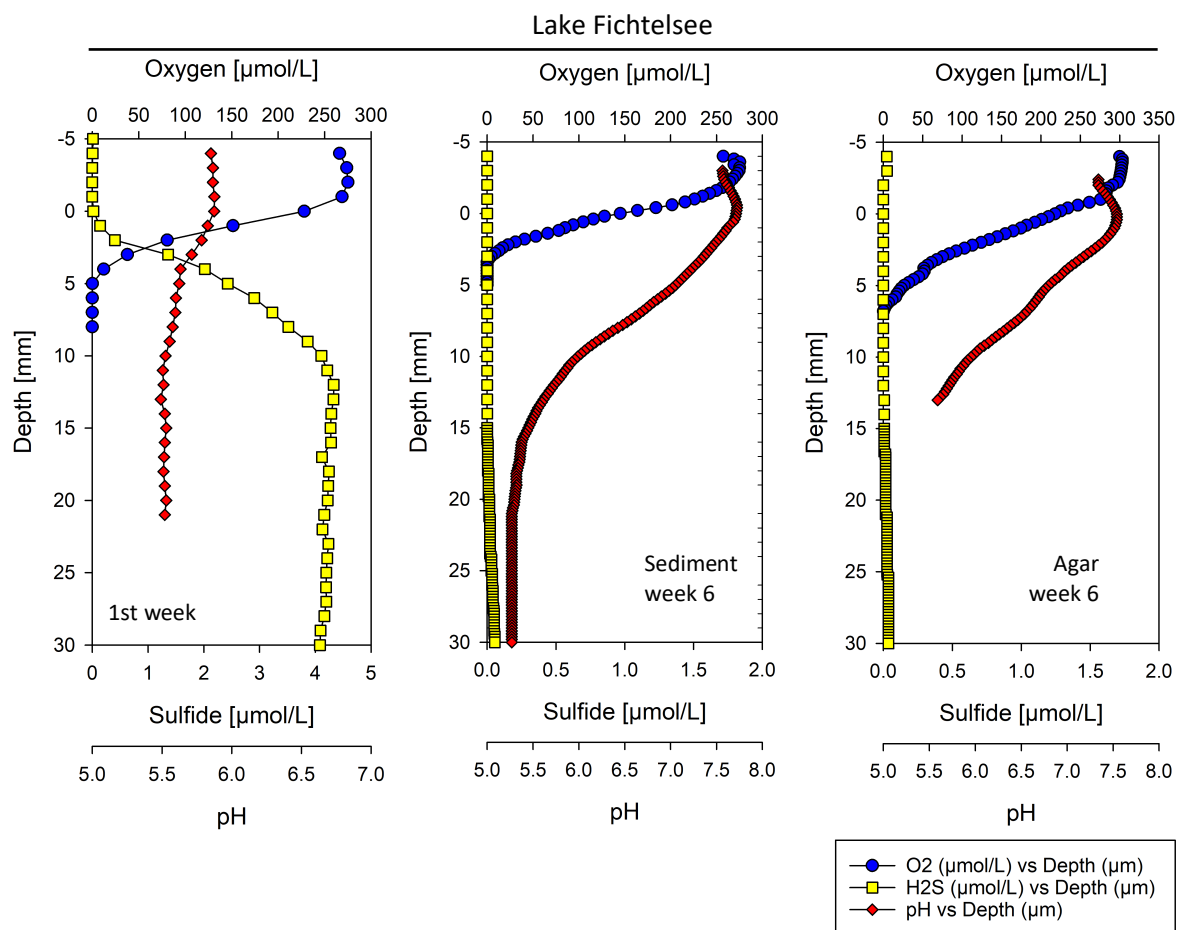


Figure 19: Geochemical depth profiles in column incubations of Lake Fichtelsee sediments. Left panel: sediment, 1<sup>st</sup> week; middle panel: agar pillar week 6; right panel: sediment week 6. Shown are means of triplicate profiles.

The initial onset of the sulfidic zone in Lake Weißenstädter See microcosms (see Figure 20) was at 5 mm depth ( $\sim 0.1 \mu\text{M}$ ). It shifted below 10 mm depth in sediment ( $\sum \text{H}_2\text{S}$  concentrations  $\sim 0.03 \mu\text{M}$ ) and below 20 mm depth in agar ( $\sim 0.01 \mu\text{M}$ ) in week six. A pH peak was visible in the first week at oxic/anoxic interface ( $\text{pH} > 8$ ) with pH dropping below ( $\text{pH} < 7$  below 10 mm). At the end of the incubation, the pH was more acidic ( $\text{pH} < 6$  below 10 mm). The onset of the anoxic zone was at 5 mm depth in the first week. Oxygen was depleted below 3 mm in sediment and below 5-6 mm in agar after six weeks.

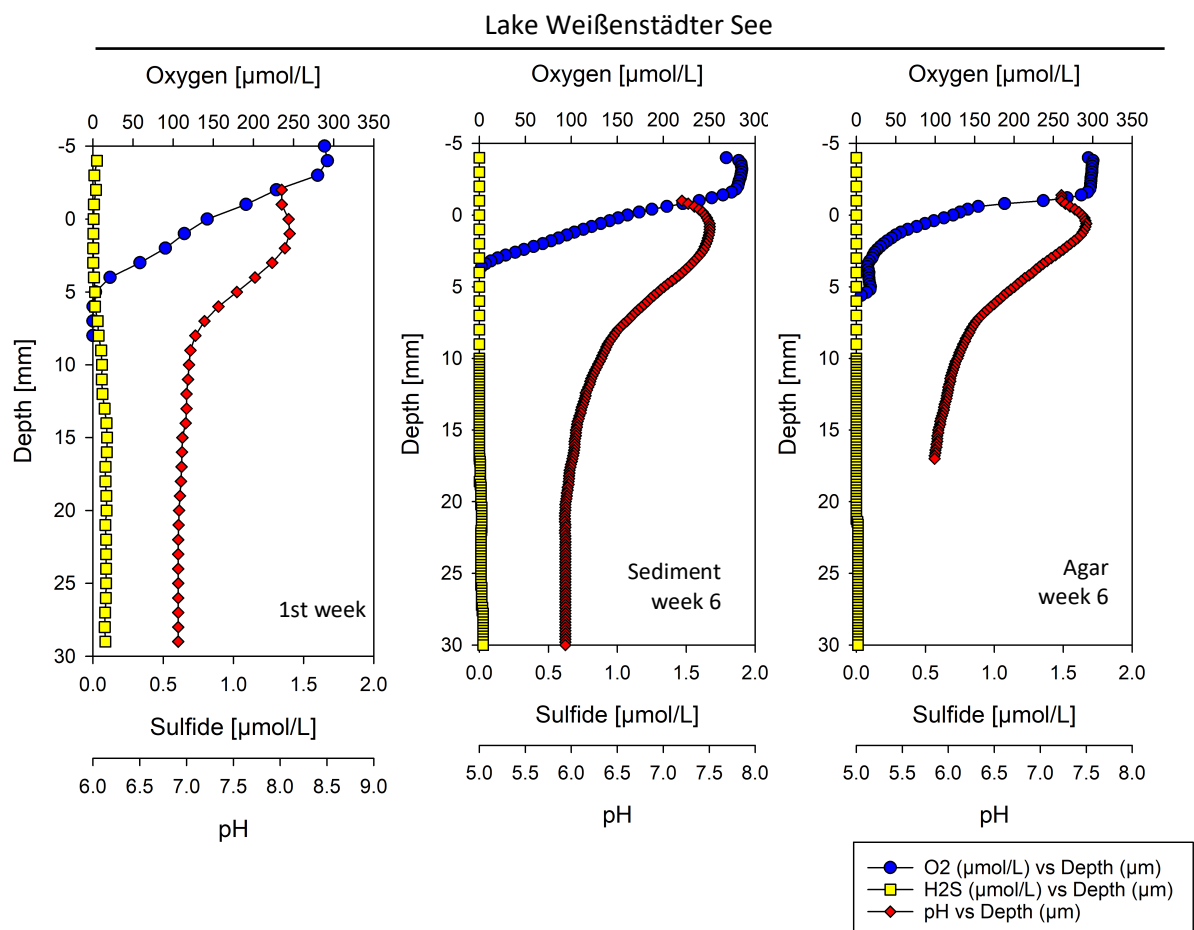


Figure 20: Geochemical depth profiles in column incubations of Lake Weißenstädter See sediments. Left panel: sediment, 1<sup>st</sup> week; middle panel: agar pillar week 6; right panel: sediment week 6. Shown are means of triplicate profiles.

In microcosms from River Eger (see Figure 21) initial  $\Sigma\text{H}_2\text{S}$  concentrations in the sediment were  $\sim 0.05 \mu\text{M}$  in the suboxic zone with the sulfidic zone starting below 30 mm depth ( $\Sigma\text{H}_2\text{S}$  concentrations  $> 1.5 \mu\text{M}$ ). After six weeks,  $\Sigma\text{H}_2\text{S}$  concentrations were below detection limit, both in sediment and agar. The pH profile initially showed a pH peak (pH  $\sim 6.75$ ) below the sediment surface and dropped to  $\sim 6.5$  below 20 mm depth. After incubation, the pH profile was  $\sim 6.75$  below the surface and decreased below to  $\sim 6.5$  below 20 mm depth, similar for agar and sediment. Oxygen initially penetrated until 5 mm depth, but after incubation, the onset of the anoxic zone was at 2 mm (sediment) or at 3 mm (agar).

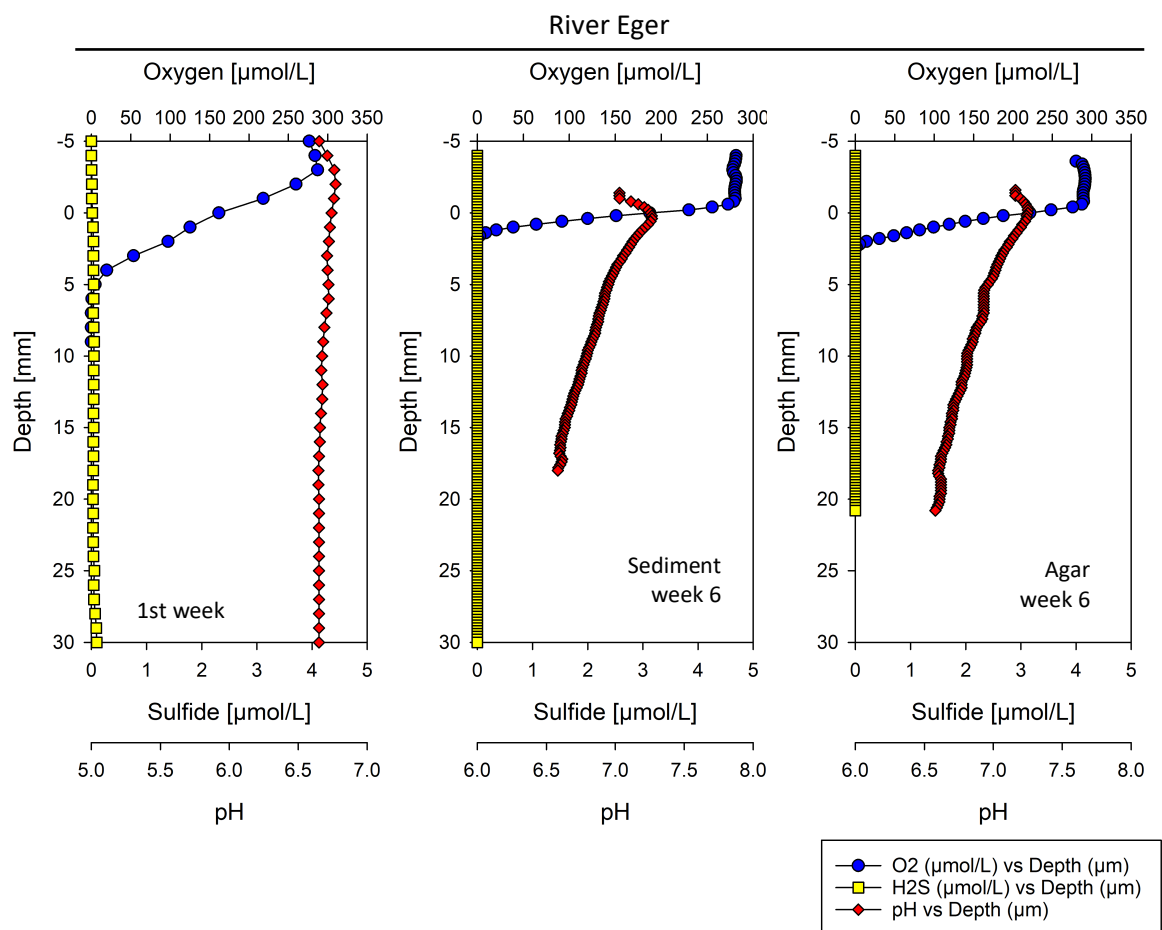


Figure 21: Geochemical depth profiles in column incubations of River Eger sediments. Left panel: sediment, 1<sup>st</sup> week; middle panel: agar pillar week 6; right panel: sediment week 6. Shown are means of triplicate profiles.

The initial sulfidic zone in the first week in microcosms from Stream Lehstenbach (see Figure 22) was below 10 mm depth ( $\Sigma\text{H}_2\text{S}$  concentrations  $\sim 0.3 \mu\text{M}$  below 20 mm). After incubation time, in week six, the sulfidic zone was shifted deeper (below 20 mm in sediment, below 30 mm in agar samples), although very low  $\Sigma\text{H}_2\text{S}$  concentrations were measured ( $\sim 0.01 \mu\text{M}$ ). The pH profile in the first week showed a pH peak at 7.3 below the surface and decreasing pH values below ( $\sim 6.4$  below 10 mm). The pH in anoxic sediment and agar was more acidic after six weeks of incubation, with a distinct pH peak at oxic/anoxic interface (pH=7.6) and decreasing continually within the anoxic zone to pH<6 below 15 mm depth. The pH profile in agar was similar.

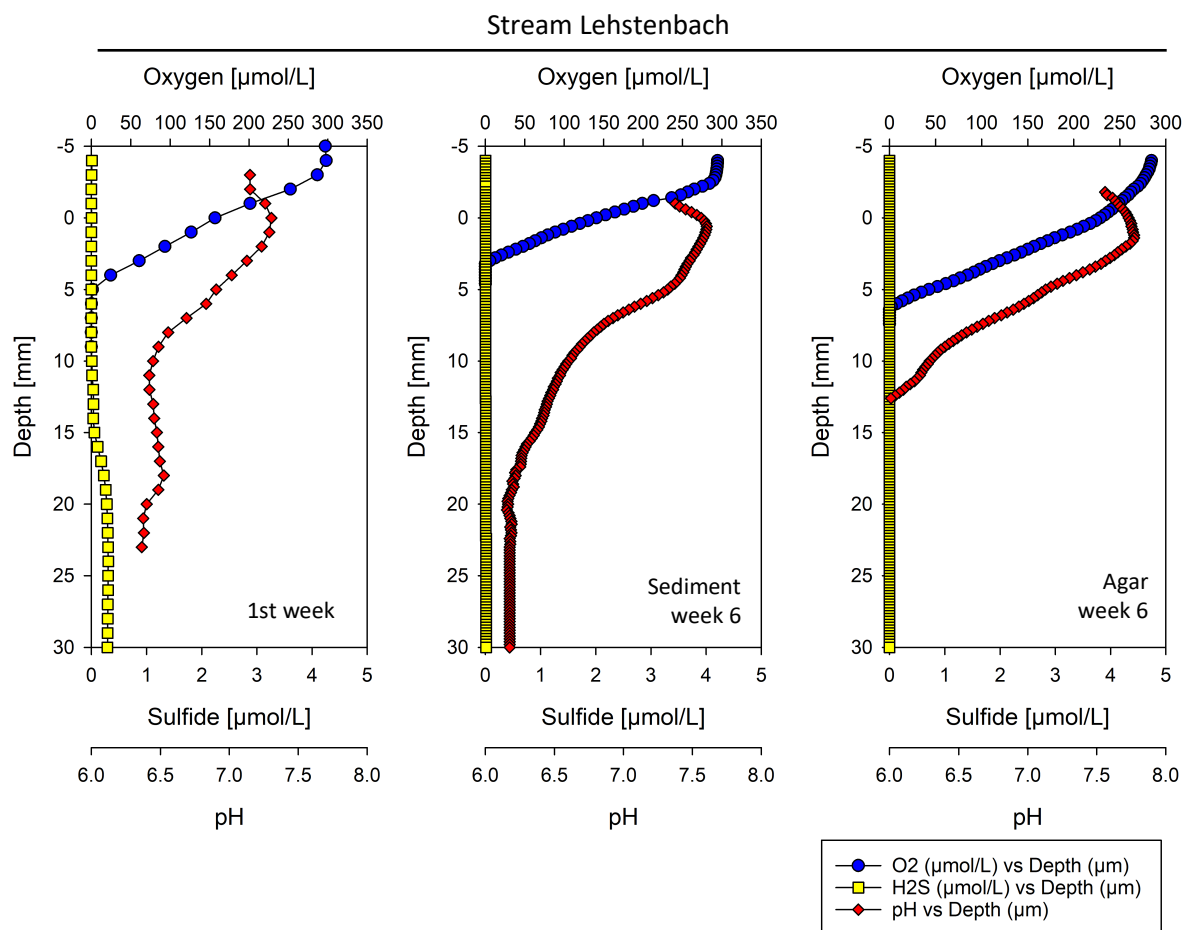


Figure 22: Geochemical depth profiles in column incubations of Stream Lehstenbach sediments. Left panel: sediment, 1<sup>st</sup> week; middle panel: agar pillar week 6; right panel: sediment week 6. Shown are means of triplicate profiles.

### 3.3.2. FISH and microscopy in Fichtelgebirge samples

Microscopy of sediment and agar pillar was done after at least 2 weeks of incubation so that cable bacteria filaments could develop. For cable bacteria detection, FISH was applied to samples and probe Dsb706-hybridized *Desulfobulbaceae* filaments were seen as proof for cable bacteria presence in the sample. Imaging was difficult as probe bleaching occurred rapidly. Dsb706-positive filaments sometimes were not intact with damaged outer membrane and filaments were in general shorter than 1 cm.

In microcosm samples from Lake Fichtelsee, microscopy of both agar and sediment samples revealed that filamentous bacteria were present, that stained positive with *Desulfobulbaceae*-specific probe Dsb706 (see Figure 23 A). Abundance of cable bacteria was greater in agar pillar samples, although

quantification was not possible, as occurrence was not homogeneous. The filaments were detected between 0-20 mm depth, with greater abundance between 5-10 mm.

In samples from River Eger microcosms, Dsb706 probe-positive filaments were visually confirmed for sediment samples only, as agar samples were often degraded at time of microscopy. Depths from 0-20 mm were checked for cable bacteria occurrence and they were found below 5 mm sediment depth (see Figure 23 B).

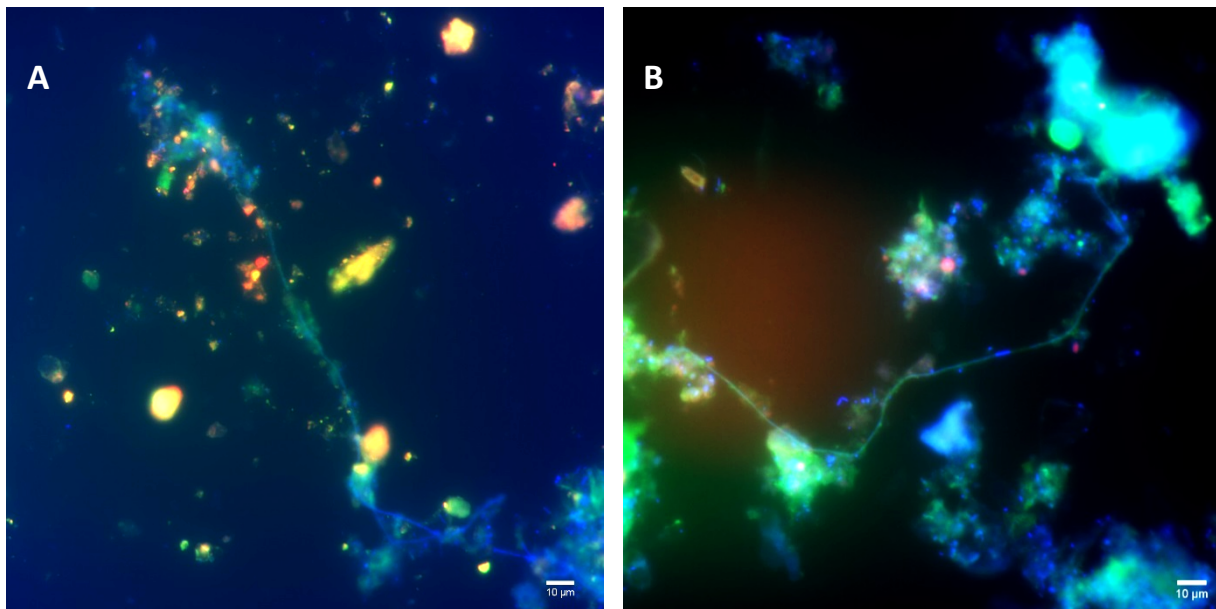


Figure 23: Fluorescence microscopy images from Fichtelgebirge gradient columns. The bar is 10  $\mu$ m. The images are artificial overlays of samples that were hybridized with probes Dsb706 (red) and EUB I-III (green) and counterstained with DAPI (cyan). A) A cable bacteria filament in an agar pillar sample from Fichtelsee gradient column at 0-10 mm depth. B) A cable bacteria filament in River Eger sediment samples from 5-10 mm depth.

In microcosms derived from both Lake Weißenstädter See as well as Stream Lehstenbach samples, no filaments that were hybridized with Dsb706 probe could be verified, neither in agar, nor in sediment samples.

### 3.3.3. 16S rRNA amplicon sequencing and community analysis in Fichtelgebirge samples

Illumina sequencing on an iSeq instrument was applied for all DNA extracts from the sampling sites in the Fichtelgebirge mountains, both sediment as well as agar. Community analysis from all sites showed that sequences from the *Desulfobulbaceae* family were enriched in agar samples. Although the relative abundance of 16S rRNA sequences is not quantitative, this hints at the agar pillar technique creating a selective niche for cable bacteria within *Desulfobulbaceae* family.

In microcosms from Lake Fichtelsee sediment (see Figure 24) the microbial community was dominated by *Proteobacteria*. The abundances of *Alphaproteobacteria* (mainly ~ 6-10 %) and *Verrumicrobia* (~ 6% in inoculum, ~ 4% in agar, ~ 6-8% in sediment) remained stable over time and depth both in agar as in sediment. *Gammaproteobacteria* population increased in oxic (55 % at 0-5 mm) and suboxic (80 % at 5-10 mm) agar layers compared to inoculum (15%). In anoxic agar layers below 15 mm, the abundance of *Gammaproteobacteria* decreased (~ 30%), as it did in sediment (~ 30% above 15 mm, ~ 13% below 15 mm). The main families within this phylum were *Rhodocyclaceae* and *Gallionellaceae* in agar, while *Burkholderiaceae* and *Rhodocyclaceae* were more abundant in sediment. *Deltaproteobacteria* were slightly enriched in agar below 20 mm depth (>11%) and sediment below 15 mm (>16%) compared to the inoculum (10%). *Desulfobulbaceae* were enriched in anoxic agar below 20 mm (>6%) compared to inoculum (<1%) and sediment (~ 1-3%). *Firmicutes* were only abundant in suboxic agar pillar (5% at 5-10 mm and 18% at 10-15 mm) while their abundance was negligible in inoculum (1%) and sediment (<2%). *Epsilonproteobacteria* were negligible in all depths except in suboxic agar (6%). *Chloroflexi* (with the main family *Anaerolineaceae*) were abundant in the inoculum (11%) and anoxic agar (6-8%), but not in oxic agar. In sediment, they occurred in oxic zones (5%) and in higher abundance also in anoxic zones (7-10%). This pattern was also observed for *Acidobacteria* (10% in inoculum, 10% in oxic agar, 2-5% in suboxic agar, 18% in anoxic agar, 13% in oxic sediment, 16-27% in anoxic sediment). *Bacteroidetes* abundance in sediment was similar to that in inoculum (~6-9%), while it was increased in oxic agar (15%) and at 10-15 mm depth (12%).

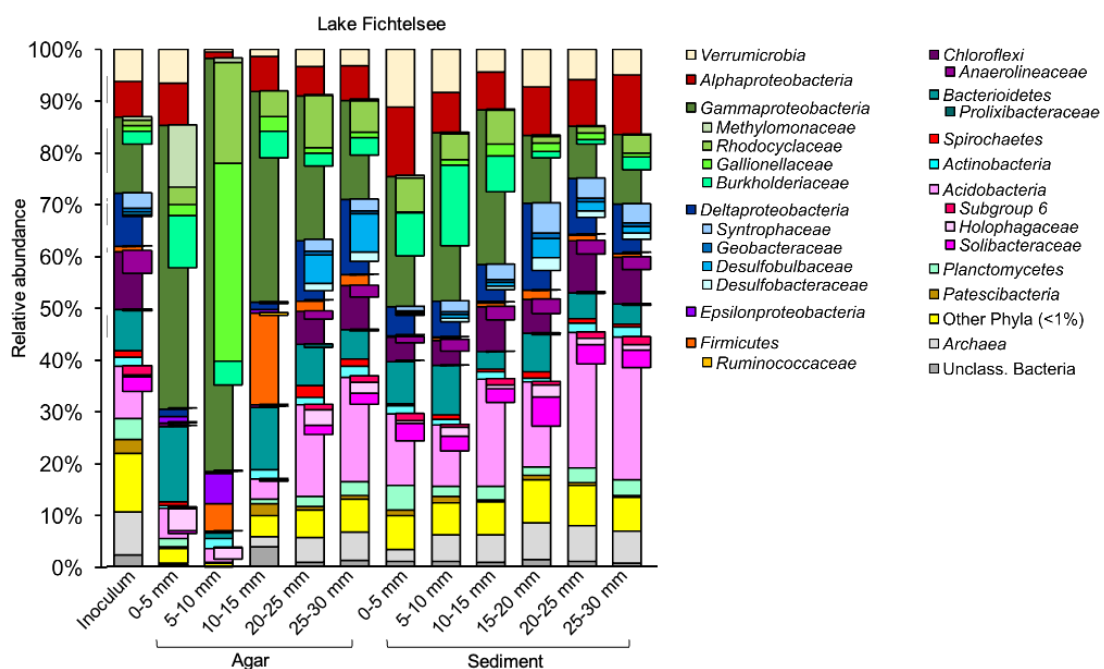


Figure 24: Microbial community composition in Lake Fichtelsee microcosms.

The microbial community in the agar pillar in microcosms from Lake Weißenstädter See (see Figure 25) was less diverse. Over all depths, *Firmicutes*, nearly completely from the *Ruminococcaceae* family dominated the agar pillar (57-76%), while they were less abundant in the sediment (2% in oxic, <6% in anoxic sediment). *Gammaproteobacteria* were more abundant in oxic environment and their abundance decreased over depth and they were more abundant in sediment than in agar (oxic agar 17%, anoxic agar 2% vs. oxic sediment 33%, anoxic sediment 5%). Important families were the *Rhodocycladaceae* and *Methylomonadaceae*. *Deltaproteobacteria* were similarly abundant (8-15%) amongst all samples except for deep agar below 25 mm. Interestingly, the *Desulfobulbaceae* family was most abundant in suboxic agar at 5-10 mm depth (5%), while they were negligible in sediment, where the *Syntrophaceae* family was the most abundant *Deltaproteobacteria* family (<6%). *Bacteroidetes* abundance was slightly increased in anoxic agar (<15%) vs. suboxic agar (6%), while it remained stable through sediment depths (~ 8%). *Chloroflexi* and *Acidobacteria* both were negligible in agar, while they increased in abundance over depth in sediment (*Chloroflexi* from 5% to 15%, *Acidobacteria* from 14% to 33%). *Verrumicrobia* and *Alphaproteobacteria* were abundant (7% and 8%, respectively) in oxic sediment and decreased in abundance in anoxic sediment, while they were negligible in agar. In agar, the total abundance of less-abundant phyla was <2%.

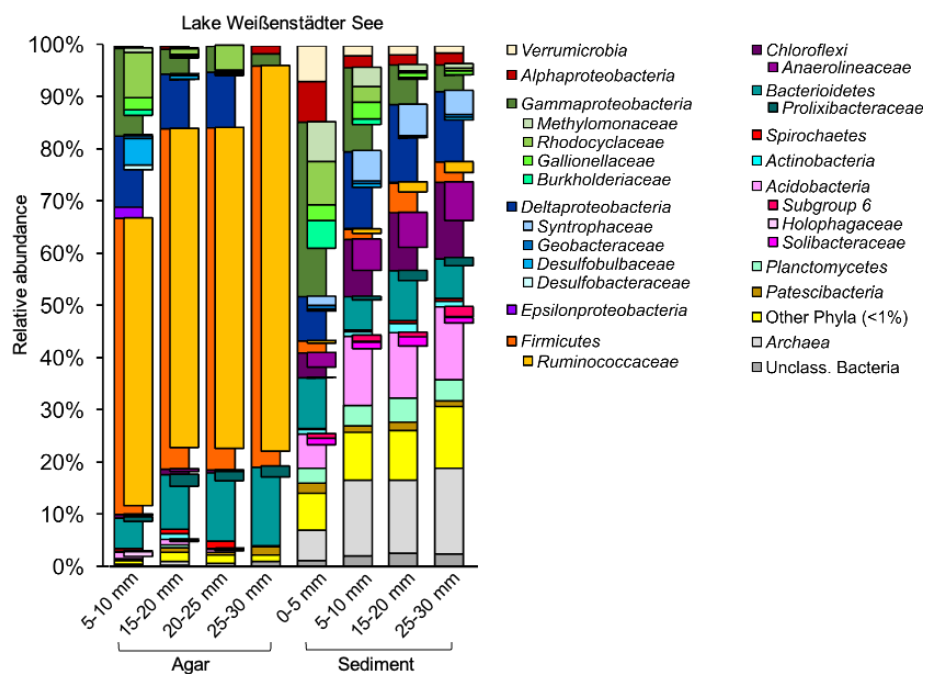


Figure 25: Microbial community composition in Lake Weißenstädter See microcosms.

The microbial community pattern in samples from River Eger (see Figure 26) showed that anoxic sediment community below 10 mm was very similar to the inoculum with the most abundant phyla being *Gammaproteobacteria* (11-15%), *Deltaproteobacteria* (10-13%), *Alphaproteobacteria* (2-5%), *Verrumicrobia* (~ 4%), *Chloroflexi* (~ 8%), *Bacteroidetes* (9-11%) and *Acidobacteria* (10-13%). Oxic sediment community composition differed, as *Gammaproteobacteria* abundance was increased (29%), while total abundance with more infrequent phyla (abundance < 1%) was decreased. The agar pillar was dominated by *Firmicutes* (33-48%), mainly by members of *Ruminococcaceae* family. *Gammaproteobacteria* abundance was important in suboxic agar at 5-10 mm (19%) and decreased over depth (<6%), while abundance of *Bacteroidetes* increased over depth (from 11% at 5-10 mm to 26 % below 25 mm). *Spirochaetes* were abundant in agar over all depths (4-8%), while being less abundant in inoculum and sediment (1-2%). Interestingly, the *Desulfobulbaceae* family was most abundant in suboxic agar (3%), while in sediment below 5 mm *Syntrophaceae* (~ 1%) and *Desulfobacteraceae* (~ 2%) were more abundant families of the *Deltaproteobacteria*. In agar, the total abundance of low-abundant phyla was reduced (3-7%) compared to inoculum and sediment (9-15%).

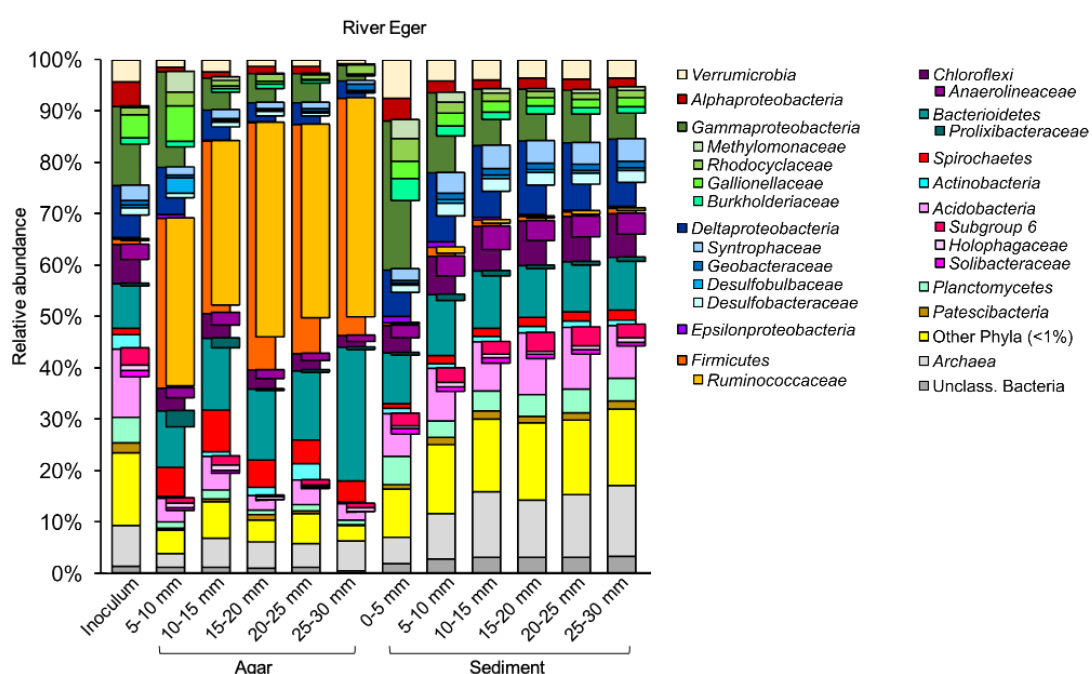


Figure 26: Microbial community composition in River Eger microcosms.

For microbial communities in Stream Lehstenbach (see Figure 27), the greatest differences could be observed between oxic and anoxic microbial community, both in agar, as well as in sediment. *Gammaproteobacteria* dominated the oxic and suboxic agar (53-57%) and were less abundant in

anoxic zones (7-9%), while in sediment their abundance was also greater in the oxic zone above 5 mm (24%) compared to anoxic sediment (<13%). In agar the most abundant families were *Gallionellaceae* and *Methylomonaceae*, while in sediment *Burkholderiaceae* were more abundant. *Verrumicrobia* were more abundant in sediment (16% in oxic zone, ~10% in anoxic layers) compared to agar (3% in oxic agar, ~ 7% in anoxic agar), while *Alphaproteobacteria* were comparable (~ 10% in oxic zone, ~ 4-7% in anoxic zone). *Chloroflexi* were only abundant under anoxic conditions, both in agar and sediment (4-6% both), in contrast to *Epsilonproteobacteria*, that were only abundant under oxic conditions and only in agar (2-6%). *Bacteroidetes* was the second most abundant phylum (agar: 10-16%, sediment: 10-21%) with the most abundant family *Prolibacteraceae* being more abundant under anoxic conditions. *Firmicutes* were only slightly enriched in anoxic agar (<3%) and were of negligible abundance in sediment, which was similar for *Spirochaetes* (<4%). *Acidobacteria* were ~ twice more abundant under anoxic conditions both in agar (oxic agar 4-6% vs. anoxic agar 11-12%) and in sediment (oxic 6% vs. anoxic 9-17%) with the most abundant families *Subgroup 6*, *Holophagaceae* and *Solibacteraceae*. *Deltaproteobacteria* were less abundant in oxic agar (4-5%) compared to oxic sediment (8%), but their abundance did not differ between anoxic agar (8-11%) and sediment (8-10%). *Desulfobulbaceae* abundance was greatest in agar at 10-15 mm depth (3%).

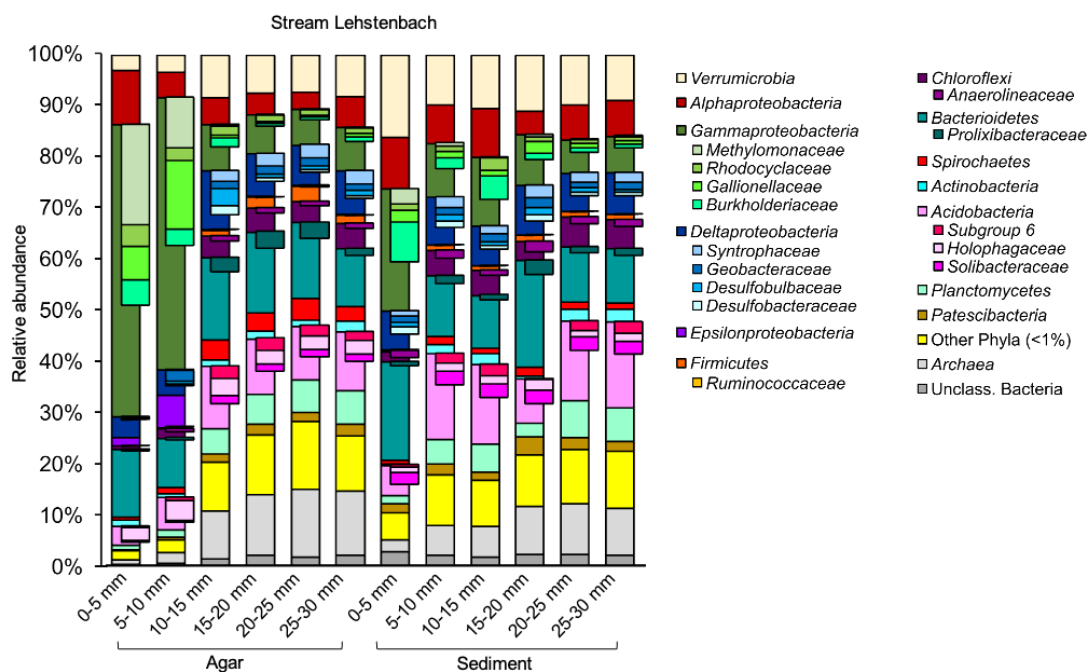
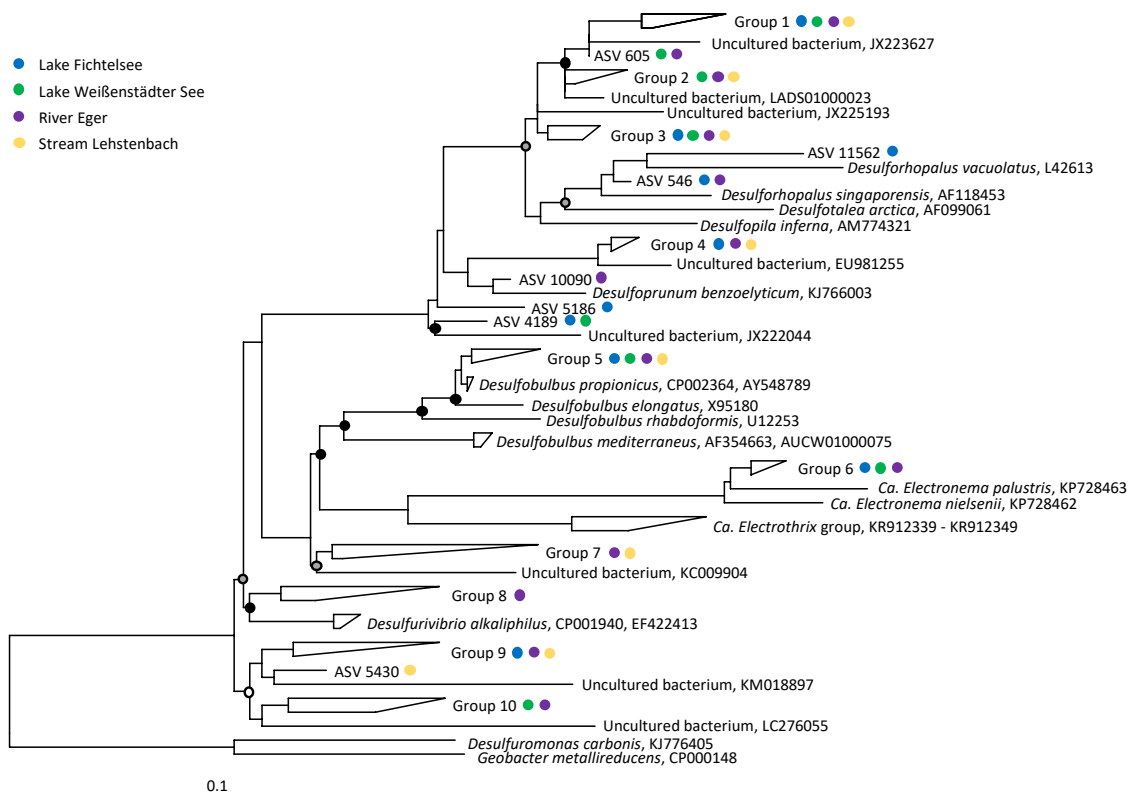


Figure 27: Microbial community composition in Stream Lehstenbach microcosms.

### 3.3.4. Phylogeny of Fichtelgebirge samples with ARB

The generated amplicons within the *Desulfobulbaceae* family were phylogenetically placed against the SILVA reference database. Many clustered with uncultured bacteria, but ASV 11562 and ASV 546 clustered with *Desulforhopalus* spp., while ASV 10090 clustered with *Desulfoprunum benzoelyticum*. Group 5 was affiliated with *Desulfobulbus propionicus* and group 8 with *Desulfurivibrio alkaliphilus*. Two ASVs, combined into group 6, branched within the freshwater CB closely to *Ca. Electronema palustris* (see Figure 28).



**Figure 28:** Phylogenetic placement of iSeq 16S rRNA amplicon reads within the *Desulfobulbaceae*. The accession numbers of sequence entries are given. Sampling location of ASVs and groups, consisting of multiple ASVs, are indicated by colour. The tree is rooted with outgroup sequences of *Geobacter metallireducens* and *Desulfuromonas carbonis*. Branching points without symbol indicate bootstrap values > 99. Black circles: bootstrap support > 94, grey circles: bootstrap support > 73 and open circles: bootstrap support > 48 ( $n = 1000$ ). The scale bar shows 10 % distance.

## 3.4. Testing the role of CB in anaerobic toluene degradation in lake sediments

### 3.4.1. Tracing of oxygen concentrations during microcosm incubation

The toluene-degrading microcosms were set-up to reflect environmental lake sediment conditions. Therefore, microcosm headspace as well as overlying water (see Figure 6) should remain oxic during

the full incubation period. To trace changes in oxygen concentrations in closed microcosms, sensor spots at relevant locations (HS and SN) were read from the outside.

Oxic conditions of headspace and supernatant during incubation for all treatments are depicted in Figure 29. For control microcosms, the oxygen content remained between 95-100% in the headspace and 80-90% in the supernatant. Microcosms containing unlabelled toluene had 94-98% oxygen in the headspace and 70-84% oxygen in the supernatant. Microcosms containing fully labelled toluene had 95-100% oxygen in the headspace and 70-77% oxygen in the supernatant. The microcosms with cable bacteria-free treatment with fully-labelled toluene and filters had 96-100% oxygen in the headspace and 74-88% oxygen in the supernatant. In all microcosms, headspace oxygen concentration remained with >94% above those of the supernatant.

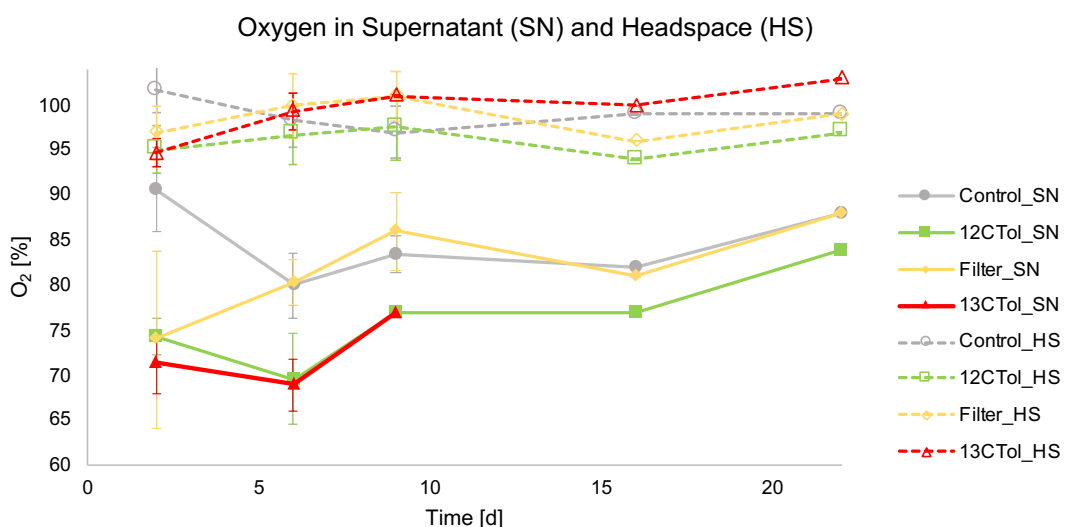


*Figure 29: Oxygen concentrations of microcosms during incubation. SN: supernatant, HS: headspace, grey: control without toluene, green: unlabelled toluene treatment, red: labelled toluene treatment, yellow: labelled toluene and cable bacteria-free treatment. Mean values with standard deviation are shown. Increasing oxygen concentrations were due to reduced number of replicates (for sacrificing) towards the end of the experiment.*

### 3.4.2. Production of CO<sub>2</sub> and <sup>13</sup>CO<sub>2</sub> during sediment incubation

Changes in CO<sub>2</sub> concentration in microcosm headspaces during incubation were measured by two different methods, gas chromatography (GC, see Appendix 1, Figure 40) and isotope-ratio mass spectrometer (IRMS, see Figure 30) for comparison. Both methods revealed a similar pattern, although absolute values were not the same. As IRMS was also used for <sup>13</sup>CO<sub>2</sub>-measurements, only IRMS values are described for comparability.

IRMS measurements indicated increasing CO<sub>2</sub> concentrations for control microcosms and <sup>12</sup>C-toluene-amended microcosms from 0.42% or 0.51% CO<sub>2</sub>, respectively, on day 1 to a maximum of 0.68%, and 0.93% CO<sub>2</sub> on day 6, followed by decreasing CO<sub>2</sub> concentrations to ~0.20% CO<sub>2</sub> after day 16 for control microcosms and to ~0.45% CO<sub>2</sub> for <sup>12</sup>C-toluene-amended microcosms. In contrast, both the <sup>13</sup>C-toluene-amended microcosms as well as the cable bacteria-free microcosms had maximum CO<sub>2</sub> concentrations of 0.37% and 0.22% on day 1 with slightly decreasing concentrations to ~0.20% CO<sub>2</sub> after day 13.

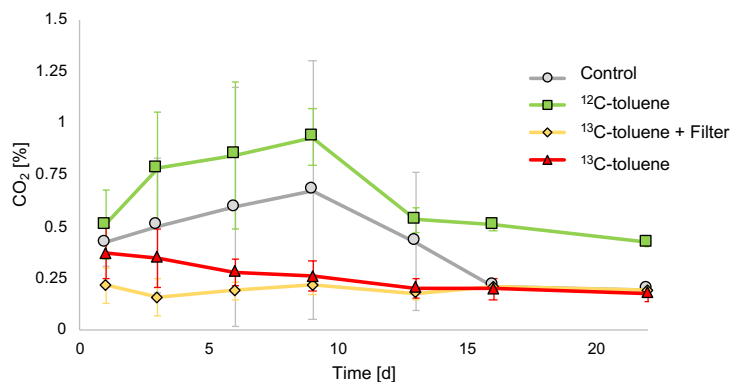


Figure 30: CO<sub>2</sub> concentrations in microcosm headspace. Measurements were performed by isotope-ratio mass spectrometer (IRMS). Error bars show standard deviation of measurements from at least 3 biological replicates (up to day 13).

The fraction of labelled carbon that ended up in headspace CO<sub>2</sub> is given as atom percent <sup>13</sup>CO<sub>2</sub> (see Figure 31) of total CO<sub>2</sub>. Compared to the fraction of <sup>13</sup>CO<sub>2</sub> in total headspace CO<sub>2</sub> given in volume percent <sup>13</sup>CO<sub>2</sub> (see Appendix 1, Figure 41). The trend in both graphs is similar, but only data for atom percent <sup>13</sup>CO<sub>2</sub> will be described in the following. Specifically, in headspaces from control as well as <sup>12</sup>C-toluene-amended microcosms atom percent <sup>13</sup>CO<sub>2</sub> stayed at ~1.09 for the duration of the experiment. In <sup>13</sup>C-toluene-amended microcosms, headspace atom percent <sup>13</sup>CO<sub>2</sub> increased from initial 1.14 on day 1 to a maximum of 23.70 (+/- 4.11) on day 6, and decreased afterwards to 6.45 (+/- 1.03) on day 22. In comparison, in <sup>13</sup>C-toluene-amended microcosms including filters, headspace atom percent <sup>13</sup>CO<sub>2</sub> increased from initial 1.13 on day 1 to a maximum of 8.35 (+/- 5.56) on day 6, upon which it decreased to 4.42 (+/- 0.07) on day 22. Comparing the two <sup>13</sup>C-toluene-amended microcosm groups, from day 6 onwards, microcosms with CB show significantly higher values of atom percent <sup>13</sup>CO<sub>2</sub> in headspace than in microcosms including filters (day 6: p=0.004, day 9: p=0.013, day 13: p=0.023).

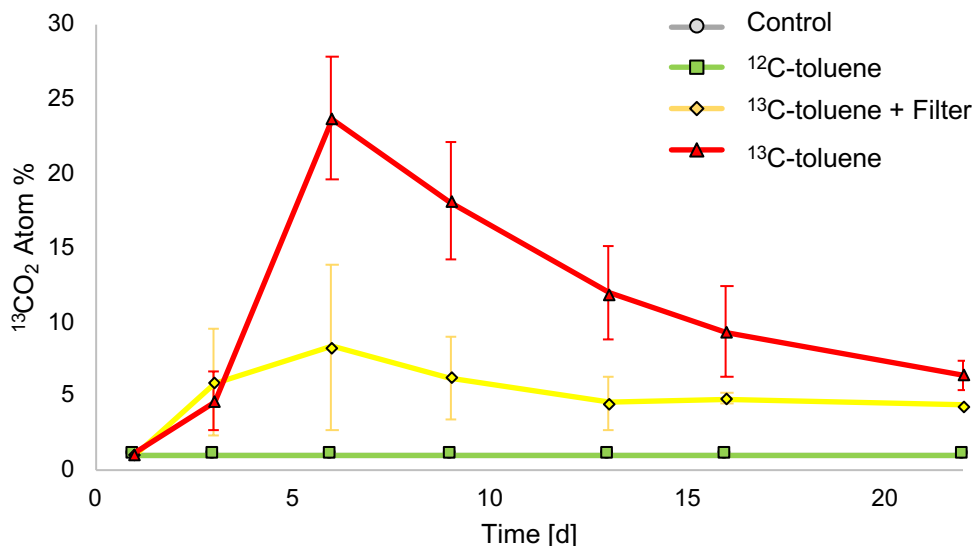


Figure 31: Atom %  $^{13}\text{CO}_2$  in microcosm headspace. Error bars show standard deviation of measurements from at least 3 biological replicates (up to day 13).

### 3.4.3. Biogeochemistry of toluene-degrading microcosms

In control microcosms (see Figure 32), the onset of the anoxic zone started at 6 mm depth (day 8) and moved up during incubation, to 5 mm depth on day 15 and 4 mm depth on day 29. The onset of the sulfidic zone was at 6 mm depth on day 8 (maximum  $> 50 \mu\text{M} \sum\text{H}_2\text{S}$  concentrations below 17 mm depth) and moved deeper during incubation, to 7 mm depth on day 15 ( $\sim 60 \mu\text{M} \sum\text{H}_2\text{S}$  concentrations below 12 mm depth) and 8 mm depth on day 29 (maximum  $\sim 80 \mu\text{M} \sum\text{H}_2\text{S}$  concentrations at 11 mm depth). Thus, the suboxic zone extended during incubation from 2 mm on day 15 to 4 mm on day 29. The pH on day 8 was 5.8 at the surface, decreased to a minimum of 5.1 at 7 mm depth and increased to  $\sim 5.4$  below 15 mm depth. On day 15, the surface pH was  $\sim 7.2$  and decreased below 7 mm depth to a minimum of  $\sim 4.9$  at 14 mm depth and increased afterwards to  $> 5.0$  below 15 mm depth. On day 29, the surface pH was  $\sim 5.5$  and decreased to a minimum of 4.6 at 3 mm depth and increased below 8 mm depth to  $\sim 5.5$ . Electric potential (EP) measurements revealed the onset of an EP below 2 mm depth on day 8, increasing to  $\sim 3$  and reaching a maximum of  $\sim 7.6$  at 13 mm depth. On day 15, an EP was detected beneath the surface which increased below with fluctuations between  $\sim 1.1$  and  $\sim 6.0$ . The EP on day 29 was detected  $\sim 1$  mm above surface and it increased to 2.7 at 6 mm depth and stayed relatively stable below.

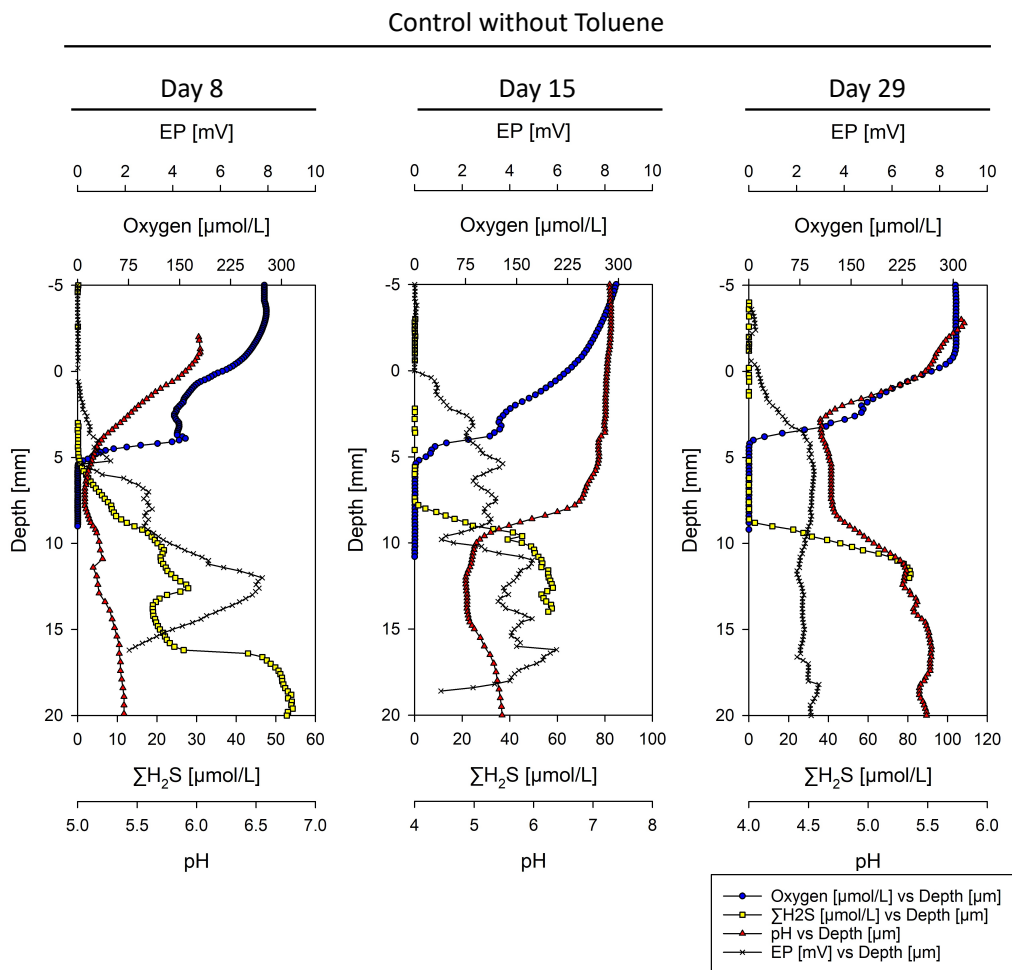


Figure 32: Geochemical depth profiles measured in control microcosm incubations. The left panel shows profiles from day 8, the middle panel from day 15 and the right panel from day 29.

In the microcosms amended with  $^{12}\text{C}$ -toluene (see Figure 33), the anoxic zone started below 3 mm depth on day 8, below 5 mm depth on day 15 and below 4 mm depth on day 29. The sulfidic zone began below 5 mm depth on day 8 ( $\Sigma\text{H}_2\text{S}$  concentrations) and 15 (reaching maximum  $>170 \mu\text{M}$   $\Sigma\text{H}_2\text{S}$  concentrations at 6 mm depth) and shifted deeper during incubation time to an onset at 7 mm depth on day 29 (maximum  $\Sigma\text{H}_2\text{S}$  concentrations of  $100 \mu\text{M}$  at 9 mm depth). Thus, the suboxic zone was 2 mm on day 8 and 3 mm on day 29. On day 8, surface pH was 6.3, decreased to a minimum of  $\sim 5.2$  at 7 mm depth and increased below 12 mm depth to  $\sim 5.5$ . On day 15, surface pH was  $\sim 5.5$  and decreased to a minimum of 4.9 at 3 mm depth, upon which it increased to  $>5.3$  below 6 mm depth. On day 29, the pH at the surface was 5.1, steadily decreased to a minimum of 4.8 at 6 mm depth, and increased below to  $>5.3$  below 11 mm depth. Measurable EPs were found on all days, starting below the surface and reaching maxima of 3.7 at 5 mm depth (8d), 5.4 at 5 mm depth (15d) and 3.5 at 6 mm depth (29d).

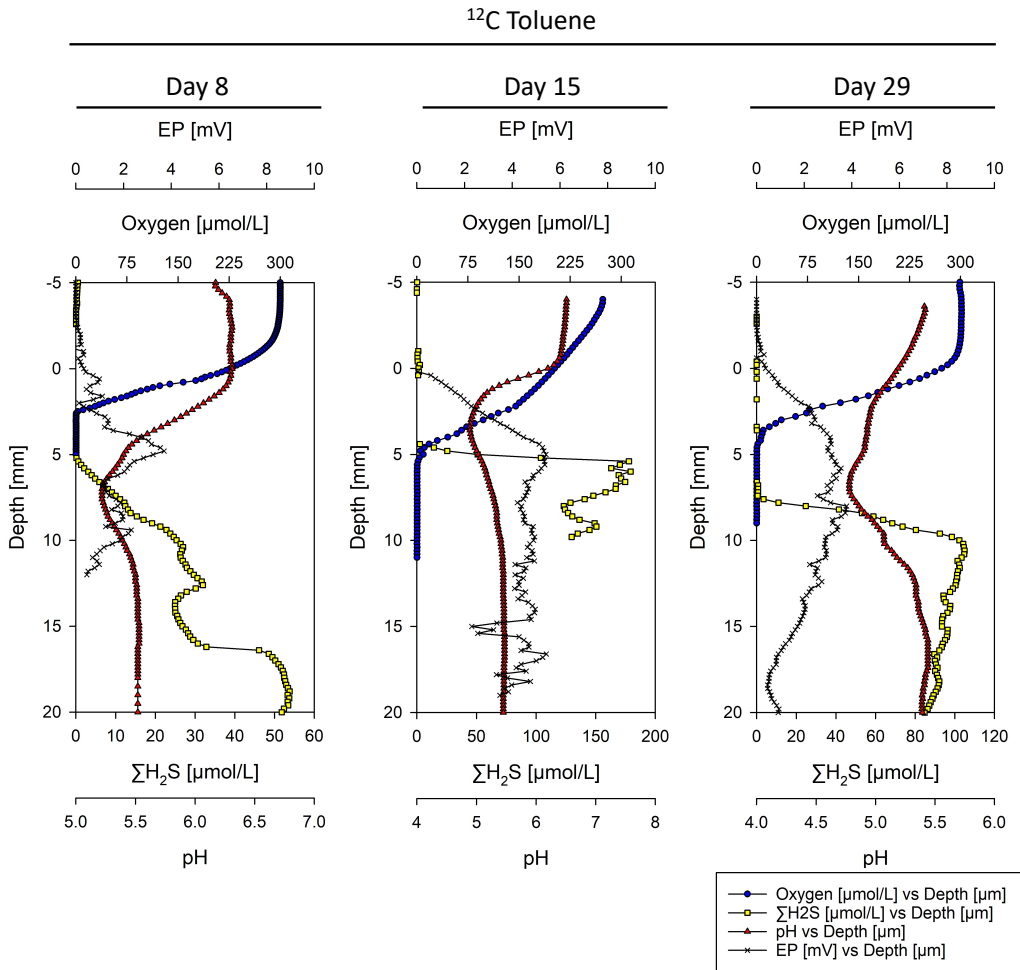


Figure 33: Geochemical depth profiles measured in microcosm incubations with  $^{12}\text{C}$ -toluene. The left panel shows profiles from day 8, the middle panel from day 15 and the right panel from day 29.

In the microcosms amended with  $^{13}\text{C}$ -toluene (see Figure 34) the onset of the anoxic zone was at 3 mm depth on day 8, below 5 mm depth on day 15 and below 4 mm depth on day 29. The sulfidic zone started below 3 mm depth on day 8 (reaching a maximum  $\Sigma\text{H}_2\text{S}$  concentration of 54  $\mu\text{M}$  at 17 mm depth) and shifted deeper to 7 mm depth on day 15 (strongly fluctuating, but reaching maximum  $\Sigma\text{H}_2\text{S}$  concentrations of  $> 150 \mu\text{M}$ ) and 8 mm depth on day 29 (maximum  $\Sigma\text{H}_2\text{S}$  concentrations of 115  $\mu\text{M}$  at 11 mm depth). Thus, the suboxic zone was 2 mm on day 15 and 4 mm on day 29. On day 8, the pH was 6.3 at surface, decreased to a minimum of 5.3 at 6 mm depth and increased to  $>5.5$  below 10 mm depth. On day 15, surface pH was  $\sim 5.6$  and the pH value decreased to a minimum of 5.0 at 4 mm depth, upon which it increased to  $\sim 5.3$  below 11 mm depth. On day 29, the pH was 5.0 at surface and it decreased to a minimum of 4.8. at 7 mm depth with an increase afterwards to  $\sim 5.5$  below 11 mm depth. EP onset was below 4 mm depth on day 8, with a maximum EP of 4.4 at 8 mm depth. On day 15, the EP was measurable below the surface, and it increased below, reaching a maximum of 5.7 at 7

mm depth, although it was strongly fluctuating. On day 29, a weak EP was measurable below 1 mm depth, reaching a maximum of 0.9 at 13 mm depth.

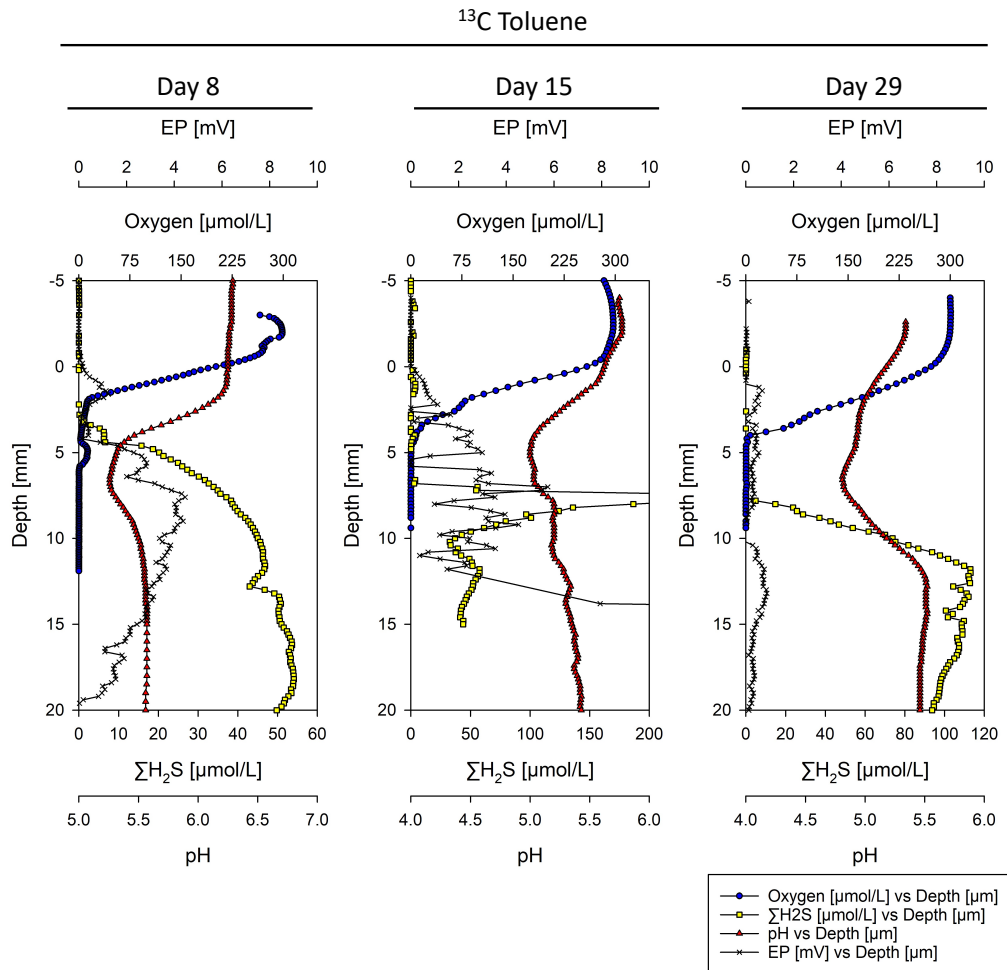


Figure 34: Geochemical depth profiles measured in microcosm incubations with  $^{13}\text{C}$ -toluene. The left panel shows profiles from day 8, the middle panel from day 15 and the right panel from day 29.

For the microcosms amended with  $^{13}\text{C}$ -toluene and including filter membranes (cable bacteria-free control), microprofiling was not possible. Initial conditions, such as  $\Sigma\text{H}_2\text{S}$  concentration and pH in porewater were expected to be the same as in the other microcosms including toluene, as all microcosms were prepared from the same slurry. Diffusion of dissolved substance in porewater through the filter membranes was assumed.

#### 3.4.4. Depth-resolved microbial communities

The microbial community development in the four different groups of microcosms was followed over time (inoculum = day 0, day 8, day 15, day 29) and over depth (0-5mm, 5-10mm, 10-15mm, 20-25mm, 25-30mm). For clarity and concision, the different groups will be called “control” for control

microcosms without toluene addition, “<sup>12</sup>C” for microcosms amended with <sup>12</sup>C -or unlabelled- toluene, “<sup>13</sup>C” for microcosms amended with <sup>13</sup>C -or labelled- toluene, and “<sup>13</sup>C+filt” for microcosms amended with <sup>13</sup>C -or labelled- toluene and including two filter membrane layers (at 5 and 10 mm depth) to prevent cable bacteria from developing.

In the inoculum (see Figure 35), the most abundant phylum was *Acidobacteria* (20-25%), with the main families *Holophagaceae* (~2.5%) and *Thermoanaerobaculaceae* (<1%). Members of *Bacteroidota* phylum were present (7-10%) with the family *Bacteroidetes vadimHA17* as most abundant (~3% total abundance). *Gammaproteobacteria* were present at 8-10% total abundance families, and here the most abundant families were *Gallionellaceae* and *Comamonadaceae* (~2% and ~1% total abundance, respectively). Members of the *Alphaproteobacteria* phylum were abundant (5-7%) with the main families *Xanthobacteraceae* (1-3% total abundance) and *Beijerinckiaceae* (1-2%). Members of *Desulfobacterota* phylum reached 7-8% abundance with *Geobacteraceae* family as the most abundant (2-3%). *Verrucomicrobiota* were present at 10-12% total abundance with *Pedosphaeraceae* and *Opitutaceae* being the most dominant families (~5% and ~4% total abundance, respectively). Members of phylum *Chloroflexi* (7-9%), with *Anaerolineaceae* (2%) as most prominent family were also present. The less abundant phyla were *Planctomycetes* (2-3%), *Actinobacteriota* (2-3%), *Spirochaetes* (~2%), *Firmicutes* (<1%), *Myxococcota* (2-3%) and *Patescibacteria* (<1%).

Over incubation time, community composition changed. Main differences within microcosm groups were visible between oxic upper sediment (0-5 mm depth), suboxic sediment (5-10 mm depth) and anoxic sediment (mostly below 10 mm depth). The microbial community in microcosms with toluene was composed differently than in toluene-free controls (see Figure 35). After 8 days of incubation, the most prominent change in the oxic sediment (5-10 mm depth) was the increase of members of the *Gammaproteobacteria* (~20% in control, ~22% in <sup>12</sup>C) in comparison to the inoculum. Here, the most abundant families were *Rhodocyclaceae* (~1-3% in each group), *Comamonadaceae* (~6% in control, ~4% in <sup>12</sup>C), *Burkholderiaceae* (~4% in control, ~3% in <sup>12</sup>C), *Gallionellaceae* (~1% in each group), while members of *Moraxellaceae* family were abundant only in toluene-amended microcosms (<0.1% in control, ~7% in <sup>12</sup>C). Other phyla were similarly abundant in incubations compared to inoculum, except for a decrease of *Acidobacteria* (to 15-22 % total abundance) and *Verrucomicrobiota* (to 7-9 % total abundance). Below, at 5-10 mm depth, the main change compared to experiment start, was also an increase of *Gammaproteobacteria* (~13% in both groups). While other *Gammaproteobacteria* families were similarly abundant in toluene-free controls and toluene-amended microcosms, *Moraxellaceae* were abundant (2% at 5-10mm, 4% at 10-15mm) only in toluene-amended microcosms below 5 mm

depth. Changes in microbial community compared to inoculum were neglectable in toluene-free controls below 10 mm depth, but only below 20 mm depth in toluene-amended microcosms.

After 15 days of incubation, the increase of *Gammaproteobacteria* abundance in the oxic sediment zone (0-5 mm) compared to experiment start became more prominent with ~40-43% in toluene-free control and toluene-amended microcosms. On a family level, present members belonged to *Rhodocyclaceae* (~4-5% in each group), *Comamonadaceae* (~9-10% in each group), *Burkholderiaceae* (6-9% in each group), *Gallionellaceae* (4-5% in each group). Members of *Moraxellaceae* family were again only abundant in toluene-amended microcosms (<1% in control, ~7% in <sup>12</sup>C). Members of *Alphaproteobacteria* were also more abundant than in the inoculum (7-10%). Members of all other phyla were similar or less abundant compared to inoculum. At 5-10 mm depth, the increase of *Gammaproteobacteria* abundance compared to experiment start was also visible, but was less prominent (~26-27% in each group). Here, members of *Moraxellaceae* were only abundant in toluene-amended microcosms. Below 10 mm depth, the microbial communities in all microcosms resembled the initial community profile.

At the end of incubation, at day 29, members of *Gammaproteobacteria* were more abundant at oxic sediment at 0-5 mm depth in toluene-amended microcosms compared to toluene-free control, but were the dominant group in both groups (~29% in control, ~40% in <sup>12</sup>C). On a family level, *Rhodocyclaceae* (~1% in control, ~6% in <sup>12</sup>C), *Comamonadaceae* (3% in control, 5-6% in <sup>12</sup>C), and *Burkholderiaceae* (3% in control, 6-7% in <sup>12</sup>C) were approximately twice as abundant in toluene-amended microcosms compared to toluene-free controls, while *Gallionellaceae* (7% in control, 4-5% in <sup>12</sup>C) were more abundant in toluene-free controls. *Moraxellaceae* were only abundant in toluene-amended microcosms (<1% in control, ~5% in <sup>12</sup>C). Members of *Alphaproteobacteria* were also more abundant than in the inoculum (10-11% in each group). Below 10 mm depth, the microbial communities in all microcosms resembled the initial community profile.

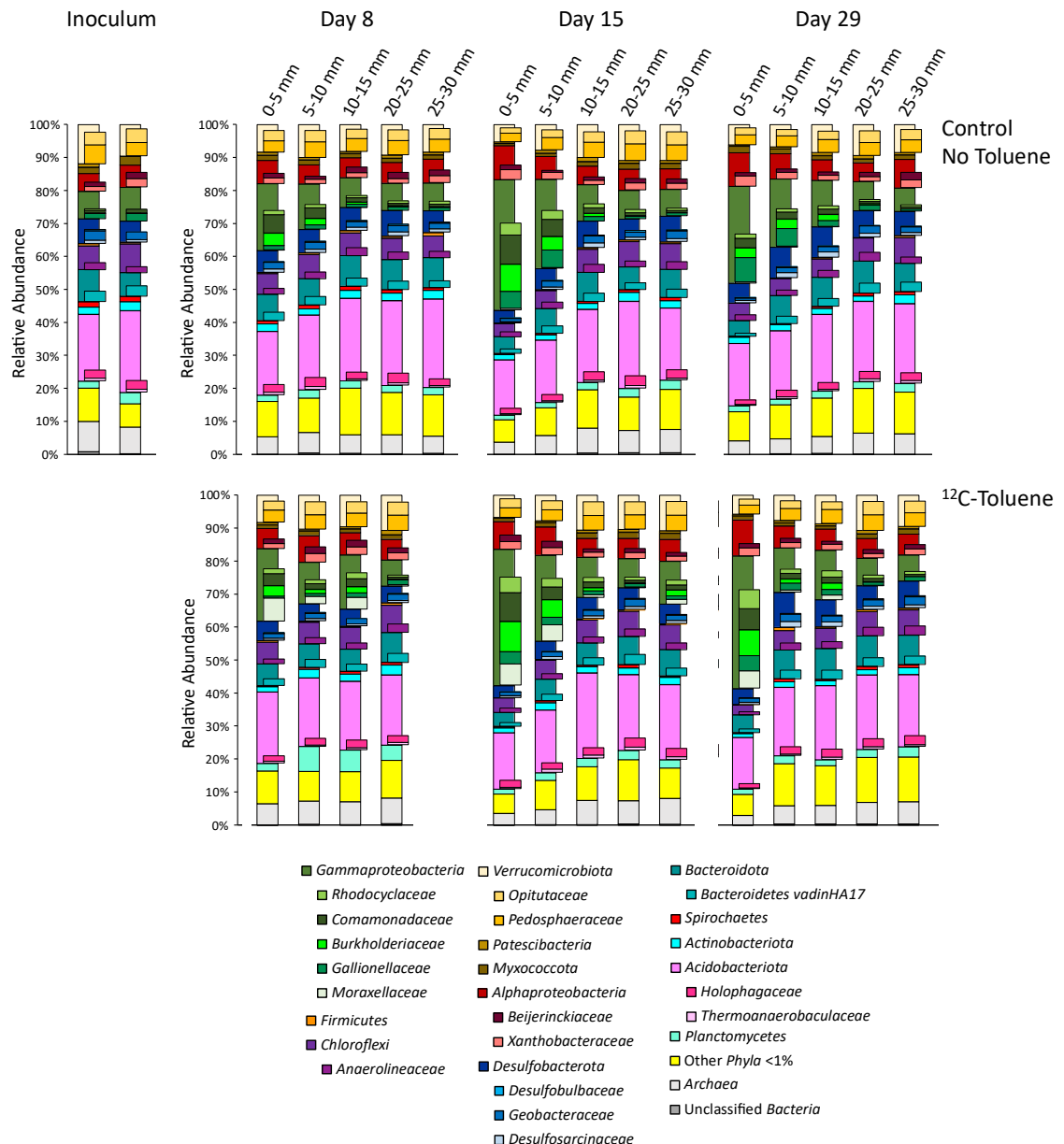


Figure 35: Community composition in inoculum and microcosms with and without toluene. 16S rRNA gene-based relative abundance of dominant bacterial groups (relative abundance >1%) observed in inoculum and microcosm incubations in toluene-free control and <sup>12</sup>C-toluene-amended group. Divided into depth transects after 8, 15 and 29 days of incubation.

Microbial community composition in <sup>13</sup>C-toluene-amended microcosms (see Figure 36) largely resembled that in <sup>12</sup>C-toluene-amended microcosms (described above, see Figure 35). However, while *Gammaproteobacteria* families, such as *Rhodocyclaceae*, *Comamonadaceae*, *Burkholderiaceae*, and *Moraxellaceae* were abundant above 5 mm depth in toluene-amended microcosms, they were present in abundance below 5 mm depth (depth of the upper filter) only in filter-free microcosms. These families belong to the lineages that were labelled during the <sup>13</sup>C-toluene experiment (also see Figure

37). Below the upper filter at 5 mm depth, filter-including microcosms showed a similar community composition as filter-free microcosms below 20 mm depth.

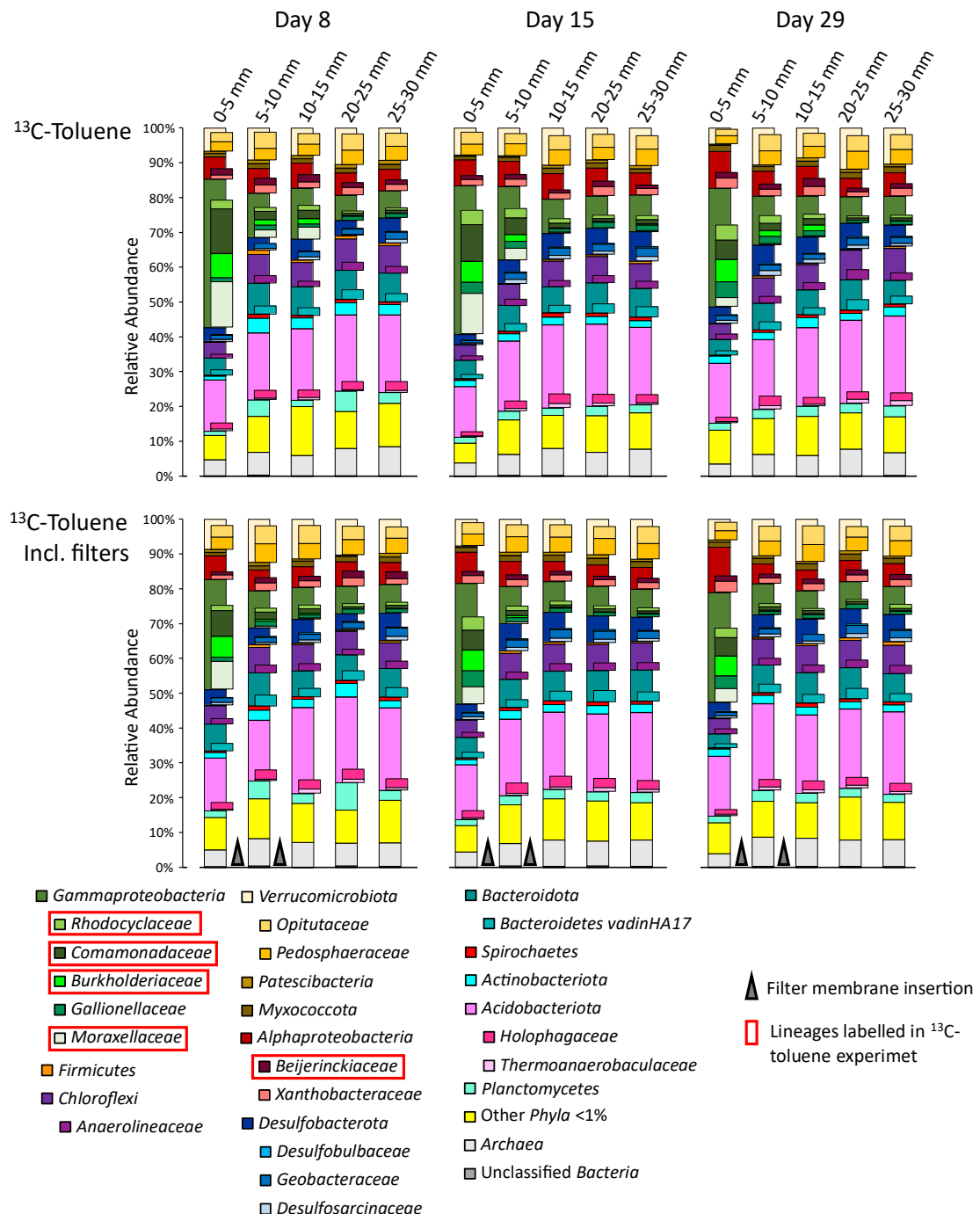


Figure 36: Community composition in  $^{13}\text{C}$ -toluene microcosms with and without filters. 16S rRNA gene-based relative abundance of dominant bacterial groups (relative abundance >1%) observed in microcosm incubations in filter-free (top panel) and filter-including (bottom panel) group. Divided into depth transects after 8, 15 and 29 days of incubation. Lineages that were labelled in the DNA-SIP experiment are marked in the legend with red frame.

### 3.4.5. $^{13}\text{C}$ -isotope-labelling of toluene degraders

DNA-SIP was done with DNA from toluene-amended microcosms (referred to as:  $^{12}\text{C}$ =unlabelled,  $^{13}\text{C}$ =labelled,  $^{13}\text{C+filt}$ = $^{13}\text{C}$ -labelled, including a filter to prevent CB-growth), sampled from two time points during the experiment: day 8 and day 15, and two depths: 5-10 mm depth (which became the suboxic zone by day 15) and 20-25 mm depth (anoxic). Density-gradients (see Appendix 1, Table 9) were comparable between all experiments, therefore microbial community compositions are shown for fractions. For unlabelled  $^{12}\text{C}$ -toluene-amended microcosms, 16S rRNA amplicons for “heavy” fractions, as which fraction 7 and lower were considered (vs. “light” fractions 8 and higher), were only available for DNA sampled from day 15 at 5-10 mm depth. From other depths and from day 8, 16S rRNA amplicons did not contain enough DNA for subsequent sequencing. For comparison, changes over density of SIP fractions in relative abundance of 16S rRNA amplicon reads of selected families are shown (Appendix 1, see Figure 42 for 5-10 mm depth, see Figure 43 for 20-25 mm depth), as well as comparative enrichment for day 15 5-10 mm (see Appendix 1, Table 10).

On day 8 at 5-10 mm depth, the microbial community in the “light” fractions 8 and 9 (values given as  $\chi_{\text{Fraction8}}/\chi_{\text{Fraction9}}$ ) resembled each other and the pooled profile (taken from before fractionation). In more detail, the most dominant phyla in “light” fractions were *Acidobacteriota* (~24/25% in  $^{12}\text{C}$ , ~28/16% in  $^{13}\text{C}$ , ~26/22% in  $^{13}\text{C+filt}$ ), *Actinobacteriota* (only fraction 8: ~7% in  $^{12}\text{C}$ , ~4% in  $^{13}\text{C}$ , ~6% in  $^{13}\text{C+filt}$ ), *Chloroflexi* (~9/6% in  $^{12}\text{C}$ , ~8/7% in  $^{13}\text{C}$ , ~9/6% in  $^{13}\text{C+filt}$ ), *Desulfobacterota* (~3/8% in  $^{12}\text{C}$ , ~5/13% in  $^{13}\text{C}$ , ~2/9% in  $^{13}\text{C+filt}$ ), *Gammaproteobacteria* (~18/17% in  $^{12}\text{C}$ , ~15/11% in  $^{13}\text{C}$ , ~13/12% in  $^{13}\text{C+filt}$ ), *Alphaproteobacteria* (~14/7% in  $^{12}\text{C}$ , ~10/3% in  $^{13}\text{C}$ , ~11/6% in  $^{13}\text{C+filt}$ ) and *Verrucomicrobiota* (~6/11% in  $^{12}\text{C}$ , ~9/10% in  $^{13}\text{C}$ , ~8/13% in  $^{13}\text{C+filt}$ ). On a family level, namely members of *Beijerinckiaceae* (~4/2% in  $^{12}\text{C}$ , ~2/1% in  $^{13}\text{C}$ , ~2/1% in  $^{13}\text{C+filt}$ ), *Xanthobacteraceae* (~4/3% in  $^{12}\text{C}$ , ~3/1% in  $^{13}\text{C}$ , ~4/3% in  $^{13}\text{C+filt}$ ) and *Burkholderiaceae* (~5/2% in  $^{12}\text{C}$ , ~3/0.5% in  $^{13}\text{C}$ , ~2/0.5% in  $^{13}\text{C+filt}$ ) were abundant. Members of *Desulfobulbaceae* family were more abundant in microcosms without filter compared to microcosms including filters (~0.1/0.2% in  $^{12}\text{C}$ , ~0.2/0.5% in  $^{13}\text{C}$ , 0/0% in  $^{13}\text{C+filt}$ ). In the “heavy” fraction 6 (no amplicons from  $^{12}\text{C}$  group), the community composition differed compared to “light” fractions. Here, *Gammaproteobacteria* (~80% in  $^{13}\text{C}$ , ~63% in  $^{13}\text{C+filt}$ ) and *Alphaproteobacteria* (~8% in  $^{13}\text{C}$ , ~7% in  $^{13}\text{C+filt}$ ) were dominant. The most abundant families all belonged to the *Gammaproteobacteria*, namely *Moraxellaceae* (~50% in  $^{13}\text{C}$ , ~43% in  $^{13}\text{C+filt}$ ), *Burkholderiaceae* (~11% in  $^{13}\text{C}$ , ~1% in  $^{13}\text{C+filt}$ ), *Comamonadaceae* (~11% in  $^{13}\text{C}$ , ~11% in  $^{13}\text{C+filt}$ ), and *Rhodocyclaceae* (~3% in  $^{13}\text{C}$ , ~4% in  $^{13}\text{C+filt}$ ). While members of other phyla had below or ~1% abundance in fraction 6 of  $^{13}\text{C}$  microcosms, *Verrucomicrobiota* (~0.9% in  $^{13}\text{C}$ , ~3% in  $^{13}\text{C+filt}$ ), *Chloroflexi* (~1% in  $^{13}\text{C}$ , ~3% in  $^{13}\text{C+filt}$ )

and *Acidobacteriota* (~4% in  $^{13}\text{C}$ , ~9% in  $^{13}\text{C+filt}$ ) were present at higher abundances in  $^{13}\text{C}$ -toluene-amended microcosms including filters.

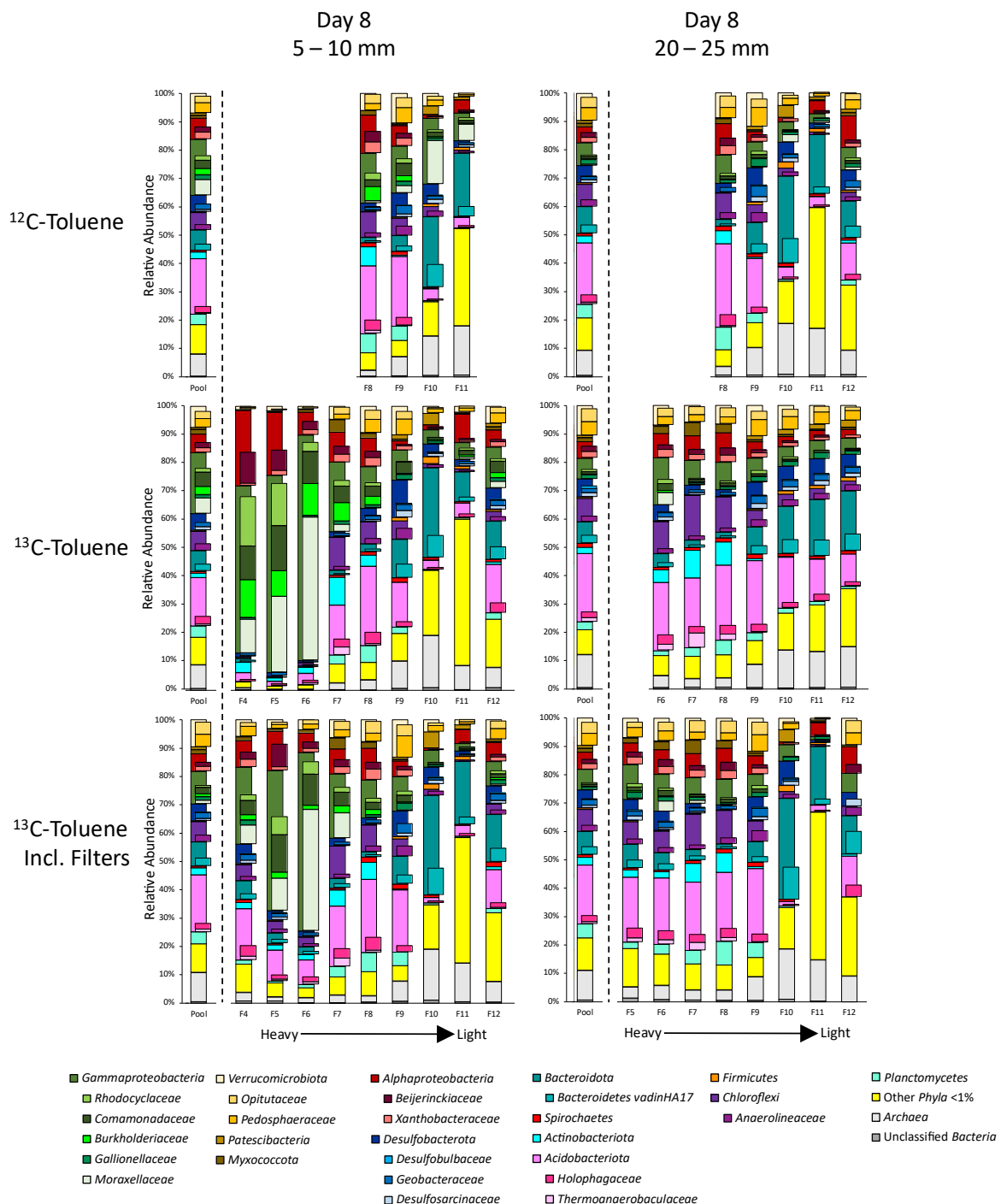


Figure 37: Community composition in fractions of SIP experiment sampled on day 8. 16S rRNA gene-based relative abundance of dominant bacterial groups (relative abundance  $>1\%$ ) observed in microcosm incubations in  $^{12}\text{C}$ -toluene and  $^{13}\text{C}$ -toluene-amended groups (with and without filters) at 5–10 mm depth (left) and 20–25 mm depth (right). Divided into pool (=before fractionation) and fractions (F) from heavy to light.

On day 8 at 20-25 mm depth, the microbial community composition in all “light” fractions (values given as  $x_{\text{Fraction8}}/x_{\text{Fraction9}}$ ) resembled each other and the pooled profile (taken from before fractionation). Abundant phyla were *Acidobacteriota* (~29/19% in  $^{12}\text{C}$ , ~25/26% in  $^{13}\text{C}$ , ~24/26% in  $^{13}\text{C+filt}$ ), *Actinobacteriota* (only fraction 8: ~5% in  $^{12}\text{C}$ , ~8% in  $^{13}\text{C}$ , ~7% in  $^{13}\text{C+filt}$ ), *Chloroflexi* (~9/6% in  $^{12}\text{C}$ , ~13/6% in  $^{13}\text{C}$ , ~12/7% in  $^{13}\text{C+filt}$ ), *Desulfobacterota* (~3/12% in  $^{12}\text{C}$ , ~2/9% in  $^{13}\text{C}$ , ~2/8% in  $^{13}\text{C+filt}$ ), *Gammaproteobacteria* (~10/9% in  $^{12}\text{C}$ , ~10/9% in  $^{13}\text{C}$ , ~9/8% in  $^{13}\text{C+filt}$ ), *Alphaproteobacteria* (~11/4% in  $^{12}\text{C}$ , ~10/6% in  $^{13}\text{C}$ , ~11/7% in  $^{13}\text{C+filt}$ ) and *Verrucomicrobiota* (~9/12% in  $^{12}\text{C}$ , ~7/11% in  $^{13}\text{C}$ , ~8/12% in  $^{13}\text{C+filt}$ ). Community profiles of “heavy” fraction 6 largely resembled the described profiles for “light” fractions, with the exception that *Gammaproteobacteria* (~17% in  $^{13}\text{C}$ , ~13% in  $^{13}\text{C+filt}$ ), namely members of *Moraxellaceae* (~4% in  $^{13}\text{C}$ , ~4% in  $^{13}\text{C+filt}$ ) and *Comamonadaceae* (~2% in  $^{13}\text{C}$ , ~1% in  $^{13}\text{C+filt}$ ) families were more abundant.

On day 15 at 5-10 mm depth, the microbial community in the “light” fractions 8 and 9 (values given as  $x_{\text{Fraction8}}/x_{\text{Fraction9}}$ ) resembled each other and the pooled profile (taken from before fractionation). More specifically, the most dominant phyla in “light” fractions were *Acidobacteriota* (~26/16% in  $^{12}\text{C}$ , ~23/29% in  $^{13}\text{C}$ , ~24/28% in  $^{13}\text{C+filt}$ ), *Actinobacteriota* (only fraction 8: ~4% in  $^{12}\text{C}$ , ~7% in  $^{13}\text{C}$ , ~9% in  $^{13}\text{C+filt}$ ), *Chloroflexi* (~7/6% in  $^{12}\text{C}$ , ~13/6% in  $^{13}\text{C}$ , ~13/7% in  $^{13}\text{C+filt}$ ), *Desulfobacterota* (~3/13% in  $^{12}\text{C}$ , ~3/9% in  $^{13}\text{C}$ , ~2/9% in  $^{13}\text{C+filt}$ ), *Gammaproteobacteria* (~22/21% in  $^{12}\text{C}$ , ~16/12% in  $^{13}\text{C}$ , ~16/11% in  $^{13}\text{C+filt}$ ), *Alphaproteobacteria* (~14/4% in  $^{12}\text{C}$ , ~11/8% in  $^{13}\text{C}$ , ~13/6% in  $^{13}\text{C+filt}$ ) and *Verrucomicrobiota* (~9/10% in  $^{12}\text{C}$ , ~6/11% in  $^{13}\text{C}$ , ~6/13% in  $^{13}\text{C+filt}$ ). On a family level, namely members of *Beijerinckiaceae* (~3/<1% in  $^{12}\text{C}$ , ~3/2% in  $^{13}\text{C}$ , ~2/1% in  $^{13}\text{C+filt}$ ) and *Xanthobacteraceae* (~3/1% in  $^{12}\text{C}$ , ~3/2% in  $^{13}\text{C}$ , ~3/2% in  $^{13}\text{C+filt}$ ) within *Alphaproteobacteria*, *Geobacteraceae* (~1/4% in  $^{12}\text{C}$ , ~1/3% in  $^{13}\text{C}$ , ~1/4% in  $^{13}\text{C+filt}$ ) within *Desulfobacterota* and *Moraxellaceae* (~1/4% in  $^{12}\text{C}$ , 0.2/0.1% in  $^{13}\text{C}$ , <1% in  $^{13}\text{C+filt}$ ), *Burkholderiaceae* (~7/1% in  $^{12}\text{C}$ , 2/1% in  $^{13}\text{C}$ , ~2/1% in  $^{13}\text{C+filt}$ ) and *Comamonadaceae* (~3/5% in  $^{12}\text{C}$ , 3/3% in  $^{13}\text{C}$ , ~2/2% in  $^{13}\text{C+filt}$ ) within *Gammaproteobacteria* were abundant. In the “heavy” fraction 6, the community composition differed compared to “light” fractions. Here, *Gammaproteobacteria* (~31% in  $^{12}\text{C}$ , ~72% in  $^{13}\text{C}$ , ~70% in  $^{13}\text{C+filt}$ ) and *Alphaproteobacteria* (~9% in  $^{12}\text{C}$ , ~10% in  $^{13}\text{C}$ , ~10% in  $^{13}\text{C+filt}$ ) were dominant, especially in  $^{13}\text{C}$ -toluene-amended microcosms (without filters). Members of other phyla were present at higher abundances in  $^{12}\text{C}$ -toluene-amended and  $^{13}\text{C+filt}$  microcosms, namely *Desulfobacterota* (~5% in  $^{12}\text{C}$ , ~2% in  $^{13}\text{C}$ , ~2% in  $^{13}\text{C+filt}$ ), *Verrucomicrobiota* (~4% in  $^{12}\text{C}$ , ~3% in  $^{13}\text{C}$ , ~3% in  $^{13}\text{C+filt}$ ), *Chloroflexi* (~7% in  $^{12}\text{C}$ , ~2% in  $^{13}\text{C}$ , ~2% in  $^{13}\text{C+filt}$ ) and *Acidobacteriota* (~22% in  $^{12}\text{C}$ , ~4% in  $^{13}\text{C}$ , ~9% in  $^{13}\text{C+filt}$ ) were present at higher abundances in microcosms including filters. The most abundant families all belonged to the *Gammaproteobacteria*, namely *Moraxellaceae* (~2% in  $^{12}\text{C}$ , ~29% in  $^{13}\text{C}$ , ~18% in  $^{13}\text{C+filt}$ ), *Burkholderiaceae* (~9% in  $^{12}\text{C}$ , ~6% in  $^{13}\text{C}$ , ~4% in  $^{13}\text{C+filt}$ ), *Comamonadaceae* (~7% in  $^{12}\text{C}$ , ~17% in  $^{13}\text{C}$ ,

~12% in  $^{13}\text{C}$ +filt), and *Rhodocyclaceae* (~2% in  $^{12}\text{C}$ , ~17% in  $^{13}\text{C}$ , ~26% in  $^{13}\text{C}$ +filt). For day 15 at 5-10 mm depth, comparative enrichment was calculated (see Appendix 1, Table 10).

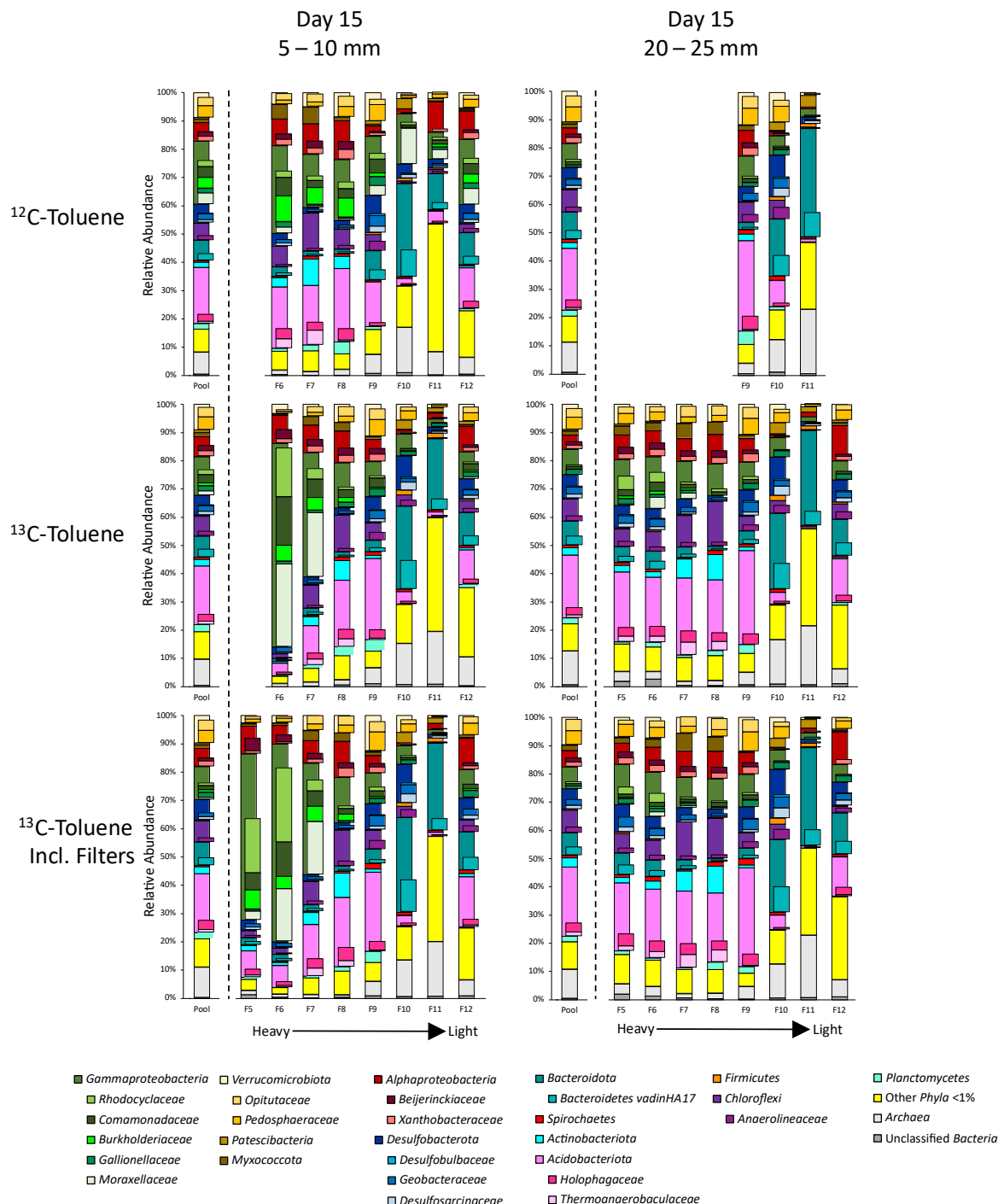


Figure 38 Community composition in fractions of SIP experiment sampled on day 15. 16S rRNA gene-based relative abundance of dominant bacterial groups (relative abundance >1%) observed in microcosm incubations in  $^{12}\text{C}$ -toluene and  $^{13}\text{C}$ -toluene-amended groups (with and without filters) at 5-10 mm depth (left) and 20-25 mm depth (right). Divided into pool (=before fractionation) and fractions (F) from heavy to light.

On day 15 at 20-25 mm depth, the microbial community in the “light” fractions 8 and 9 (values given as  $x_{\text{Fraction8}}/x_{\text{Fraction9}}$ , for  $^{12}\text{C}$ -toluene-amended microcosms only values for fraction 9 available) were similar to each other and the pooled profile (taken from before fractionation). More precisely, abundant phyla were *Acidobacteriota* (~32% in  $^{12}\text{C}$ , ~25/33% in  $^{13}\text{C}$ , ~24/35% in  $^{13}\text{C+filt}$ ), *Actinobacteriota* (~2% in  $^{12}\text{C}$ , ~9/1% in  $^{13}\text{C}$ , ~10/1% in  $^{13}\text{C+filt}$ ), *Chloroflexi* (~7% in  $^{12}\text{C}$ , ~16/5% in  $^{13}\text{C}$ , ~14/6% in  $^{13}\text{C+filt}$ ), *Desulfobacterota* (~5% in  $^{12}\text{C}$ , ~2/9% in  $^{13}\text{C}$ , ~3/9% in  $^{13}\text{C+filt}$ ), *Gammaproteobacteria* (~11% in  $^{12}\text{C}$ , ~11/9% in  $^{13}\text{C}$ , ~11/12% in  $^{13}\text{C+filt}$ ), *Alphaproteobacteria* (~9% in  $^{12}\text{C}$ , ~10/8% in  $^{13}\text{C}$ , ~10/8% in  $^{13}\text{C+filt}$ ) and *Verrucomicrobiota* (~12% in  $^{12}\text{C}$ , ~6/11% in  $^{13}\text{C}$ , ~7/12% in  $^{13}\text{C+filt}$ ). Community profiles of “heavy” fraction 6 largely resembled the described profiles for “light” fractions, with the exception that *Gammaproteobacteria* (~17% in  $^{13}\text{C}$ , ~13% in  $^{13}\text{C+filt}$ ), namely members of *Moraxellaceae* (~4% in  $^{13}\text{C}$ , ~2% in  $^{13}\text{C+filt}$ ), *Comamonadaceae* (~3% in  $^{13}\text{C}$ , ~1% in  $^{13}\text{C+filt}$ ), and *Rhodocyclaceae* (~3% in  $^{13}\text{C}$ , ~3% in  $^{13}\text{C+filt}$ ) families were more abundant, while members of *Acidobacteriota* (~23% in  $^{13}\text{C}$ , ~24% in  $^{13}\text{C+filt}$ ), *Actinobacteriota* (~2% in  $^{13}\text{C}$ , ~3% in  $^{13}\text{C+filt}$ ) and *Chloroflexi* (~7% in  $^{13}\text{C}$ , ~7% in  $^{13}\text{C+filt}$ ) were slightly less abundant.

## 4. Discussion

### 4.1. Tracing LDET and cable bacteria in freshwater sediments by gradient columns

Here, we introduce a novel enrichment strategy for CB, in form of a central agar pillar embedded within laboratory sediment gradient columns. Complemented by microsensor measurements and full-length 16S rRNA gene amplicon sequencing, we demonstrate the presence of LDET and diverse, potentially novel species-level populations of CB in the investigated freshwater sediments. These findings are therefore regarding objective 1 and 2.

#### 4.1.1. Establishing agar pillars with water-inundated soil columns

The pre-experiments were done in order to try the workflow with easy-to-obscure sampling material. Biogeochemical profiles showed decrease of  $\Sigma\text{H}_2\text{S}$  concentrations over time in the soil, while oxygen could diffuse deeper into the agar pillar than into the surrounding soil. The pH decrease from top downwards was below 1 unit. The depth-resolved community profiles revealed similarities between soil and agar pillar. Differences were observed for the upmost oxic zone of the agar pillar, which was dominated by members of the *Burkholderiaceae*, a typical soil bacterium. Among these, obligate aerobes are known, as well as anaerobes (Coenye, 2014). Predominant in deeper anoxic layers of agar are typical fermenters, such as members of the *Ruminococcaceae* family, while *Delta*proteobacteria are mostly absent from agar and more abundant in surrounding soil. For soil microcosms, the microbiome of an inserted agar pillar resembled mostly the surrounding soil microbiome, but was shifted towards *Gammaproteobacteria* in the extended oxic layer and towards *Firmicutes* in anoxic layers. Over depth, the community changes were negligible for soil, possibly due to unaltered conditions in the biogeochemical profile.

#### 4.1.2. Biogeochemistry and LDET in freshwater sediments

The results of our study demonstrate the potential for electrogenic processes and the presence of CB for a range of different freshwater habitats. The development of CB filaments within homogenized sediments in our study is comparable to time frames previously reported from marine sediment (Schauer *et al.*, 2014). Most distinctively, we observed biogeochemical patterns of LDET in the investigated streambed and lake sediments. Both sediments showed characteristic counter-gradients of oxygen and sulphide separated by a pronounced suboxic zone after incubation, along with a marked rise in EP over depth (Figure 11 and Figure 12). The EP increase of 10-15 mV in streambed columns (sediment and agar) and of up to 30 mV in Alatsee columns (sediment and agar) after 28 days of

incubation was in a similar range as previously reported for creek sediments with active freshwater CB (Risgaard-Petersen *et al.*, 2015).

CB can be quite abundant in organic-rich marine sediments, where they spatially separate redox half reactions by acting as living electron-conducting cables between the sulfidic and oxic zones (Nielsen *et al.*, 2010; Pfeffer *et al.*, 2012). Freshwater sediments are generally characterized by not only lower salt, but also much lower sulphide concentrations. The prompt detectability of LDET fuelled by sulphide oxidation in the sediments (albeit FeS-amended) investigated here, could indicate a continuous and rapid recycling of different sulphur species at low concentrations *in-situ*. Such “cryptic sulphur cycling” (Holmkvist *et al.*, 2011) has been described for marine habitats and may play an important, possibly underestimated role also in freshwater habitats (Pester *et al.*, 2012), especially in the presence of CB (Sandfeld *et al.*, 2020).

In the investigated streambed sediments, an electrogenic microbial community clearly developed over incubation, even more pronounced within the agar pillar. While the relative abundance of *Desulfobulbaceae* in sediment after incubation was comparable to their initial abundance (0.7-0.9%), a notable enrichment of *Desulfobulbaceae* (up to 8% of total 16S reads) was detected right below the oxic surface (at 3-6 mm depth) in the agar pillar. Within these *Desulfobulbaceae* reads, a smaller fraction of reads affiliated with *Ca. Electronema* (~0.2% total abundance) was also significantly enriched (~10-fold) within the agar pillar, compared to the surrounding sediment. For the investigated streambed sediments, the agar pillar was thus proven as a selective niche for CB enrichment, possibly serving as a viable strategy for the further cultivation and isolation of CB from these and other sediment inocula.

Lake Alatsee is a stratified lake with a sulphide-rich monimolimnion and dense seasonal populations of phototrophic sulphur-oxidizing bacteria (Oikonomou *et al.*, 2015). Our gradient column data indicates that also chemolithoautotrophic sulphur-oxidation via e-SOX can occur in Lake Alatsee sediments. Consistent with its sulfidic nature (Fritz *et al.*, 2012), we observed a high initial abundance of *Desulfobulbaceae* (~2.7%) in fresh Alatsee sediments. After column incubation, *Desulfobulbaceae* showed an average abundance of ~1.2% in sediments without any notable pattern of depth distribution. Unfortunately, several important depth sections of the agar pillar (3-30 mm) were lost during sampling due to disintegration of the agar. Still, based on the increase in EP, which was highest amongst all samples investigated, we presume that e-SOX and the responsible CB populations must have been highly active in the Alatsee agar pillars.

By contrast, incubations of contaminated aquifer sediments showed a very distinct microbial community pattern. The EP was lower and apparent only found within sediments (up to 6 mV), but not within the agar pillar. This observation coincided with the absence of any *Desulfobulbaceae* from the agar pillar, while they were most abundant (~10% in average) below a depth of 6 mm in these sediments compared to the surface sediment samples. This further adds to the need for a more careful differentiation between groundwater and surface freshwater CB, as discussed below.

#### 4.1.3. Selective niche of the agar pillar

The findings of our study demonstrate that the “agar pillar” approach is a viable strategy to enrich for CB from the investigated freshwater sediments. Microbial colonization of the initially sterile agar pillar must have occurred laterally from the homogenized sediments. We assumed the gel-like agar to promote the growth of CB filaments and their movement into and within the agar medium. The previously reported gliding motility of CB filaments (Bjerg *et al.*, 2016) might be more viable in the agar pillar compared to more particle-rich sediments. Over incubation time, the agar pillars equilibrated with the surrounding pore water chemistry, as supported by mostly consistent microprofiles of H<sub>2</sub>S, pH and EP after column setup (Figure 11, Figure 12, Figure 13). However, oxygen penetrated several mm deeper within the agar. Growing within the agar pillar could thus offer CB filaments the advantage of populating a more extensive zone with reduced oxygen availability over depth (5-8 mm in agar vs. 3-4 mm in lake and streambed sediment). Cathodic cells of CB filaments are proposed to use oxygen as electron sink alone, rather than conserving energy via aerobic respiration (Kjeldsen *et al.*, 2019). Consistent with the previous findings that cathodic cells within CB filaments are positioned at < 14 % air saturation (Scilipoti *et al.*, 2021), we only observed CB several mm below the oxic surface (>3 mm depth). In contrast to surface freshwater sediments, CB from groundwater sediments were not enriched in the selective niche of the agar pillar. Again, this substantiates the need to discern surface water and groundwater CB, likely exhibiting distinct physiologies and possibly also motility (Müller *et al.*, 2019).

#### 4.1.4. Phylogenetic placement of terrestrial cable bacteria

Within the two genus-level branches of CB separating the marine *Ca. Electrothrix* and the freshwater *Ca. Electronema* genera (Trojan *et al.*, 2016), sequences from Lake Alatsee and streambed sediments clearly clustered within the freshwater CB branch (Figure 18). However, 16S rRNA gene sequence identity to the proposed species *Ca. Electronema nielsenii* and *E. palustris* was below the 98.7% sequence identity threshold proposed for species-level differentiation (Stackebrandt and Ebers, 2006)

for freshwater CB groups 1, 3 and 5 (Figure 18, Table 6), and thus could represent new species-level taxonomic units of freshwater CB within the *Ca. Electronema* genus.

For the investigated aquifer sediments, the presence of filamentous *Desulfobulbaceae* was previously proven. Here, the generated 16S rRNA sequences revealed two distinct clusters, one as a sister group to *Desulfurivibrio alkaliphilus* affiliated with previous putative groundwater CB (Müller *et al.*, 2016), and one even more basal within the *Desulfobulbaceae*. The similarity of the generated full-length 16S rRNA sequences of the groundwater CB group (Figure 18) to that of other CB was less than 88 %. Moreover, while groundwater CB were present in our sediment columns, they were not enriched in the agar pillar. This further supports the notion that the ecophysiology of groundwater CB may be distinct from CB found in surface water sediments. Groundwater CB have been suggested to gain energy via sulphur disproportionation and can also grow independently of redox gradients (Müller *et al.*, 2019). Thus, the selective niche of the agar pillar may not be equally suited for the enrichment of such subsurface CB populations. Still, as an EP increase and filamentous *Desulfobulbaceae* were apparent in aquifer sediments in our columns over time, this work substantiates that also groundwater CB might actually be capable of LDET.

#### 4.1.5. Cable bacteria- and redox gradient-associated microbiomes

In column sediments and especially also in the agar pillars, the *Desulfobulbaceae* detected in our study were accompanied by distinctive associated microbiomes. It is hypothesized that other microbes can access CB filaments as an electron sinks under electron acceptor limitation (Vasquez-Cardenas *et al.*, 2015). However, specific interactions such as direct interspecies electron transfer (DIET) between CB and other microbes, have not yet been proven. The observed enrichment of CB together with putative fermenters and other, sulphide-adapted microbes leads us to assume that the agar pillar offers conditions that promotes such interactions between those groups of microorganisms. Members of the phylum *Firmicutes*, including *Ruminococcaceae* (especially for streambed sediments) and other *Clostridiaceae* (for aquifer sediments) were enriched in agar pillar samples compared to the surrounding sediment. For streambed sediments, enriched taxa also included members of the *Bacteroidetes* and *Spirochaetes*, many also typical fermenters (Güllert *et al.*, 2016). Members of the *Aeromonadaceae*, which are typically non-fermentative, were most abundant for the Alatsee anoxic agar pillar, and have been shown to capable of extracellular electron transfer (Conley *et al.*, 2018).

Although electron transfer from other microbes to CB has not been experimentally proven so far, it may be a viable strategy for electroactive bacteria to access CB filaments as an electron sink. Fermenters may energetically benefit from the presence of a conductive, electron-accepting structure.

For example, the need for an electron sink to overcome unbalanced fermentations can be realized in electro-fermentations by utilizing an electrode (Moscoviz *et al.*, 2016; Vassilev *et al.*, 2021). In anaerobic digestion systems (Guo *et al.*, 2020), growth in co-culture of *Clostridium acetobutylicum* and *Desulfovibrio vulgaris* has been described to involve biological nanotubes (Benomar *et al.*, 2015), recently also for *Clostridia* and CB in polluted river sediments (Liu *et al.*, 2021). Similarly, a recent study with polluted marine sediments (Marzocchi *et al.*, 2020) showed that CB filaments can enhance hydrocarbon degradation, potentially serving as living electrodes for pollutant degraders. Our study extends this perspective also for fermenters and CB in surface water sediments.

## 4.2. Cable bacteria from acidic mining-impacted freshwater sediments of the Fichtelgebirge

In this part of my thesis, I aimed to further evaluate the novel “agar pillar” cultivation method for targeted enrichment of cable bacteria, with regard to objective 1, and to track the distribution of cable bacteria in diverse freshwater environments of the Fichtelgebirge, with regard to objective 2. So far, cable bacteria presence was not documented in acidic lakes, and neither in sediments from a former mining region.

### 4.2.1. The “Agar Pillar” approach in acidic freshwater sediments

The outcomes of the study demonstrate that the “agar pillar” approach can be a feasible and comparatively quick strategy to enrich for CB from surface water sediments. The documented stable CB enrichment culture is more laborious and time-consuming to create (Thorup *et al.*, 2021). The agar pillar technique was already validated previously (see above 4.1.), but here, more acidic sediments could be added to the range of applications, also confirming CB presence for acidic sediments from a former mining region. However, I noted, that these more acidic sediments tended to aid in natural disintegration of the agar. Agar consists of complex polysaccharides, primarily agarose, and its physicochemical properties can be influenced by acidity, with a decrease of pH resulting in weaker gel strength (Lahaye and Rochas, 1991).

### 4.2.2. Phylogenetic placement of *Desulfobulbaceae* from mining-impacted freshwater

Reads affiliated within the *Desulfobulbaceae* showed affiliations with *Desulforhopalus* spp., *Desulforunum* spp., *Desulfobulbus* spp. and *Desulfurivibrio* spp. The groundwater CB typically are closely affiliated with *Desulfurivibrio* spp. (Müller *et al.*, 2016). 16S rRNA amplicon reads affiliated with

the described freshwater CB species *Ca. Electronema palustris* (Trojan *et al.*, 2016) were found in the samples from Lake Fichtelsee, Lake Weißenstädter See and River Eger, but not Stream Lehstenbach.

#### 4.2.3. Biogeochemistry and LDET in Acidic Mining-Impacted Freshwater Systems

In contrast to sulphide-rich marine sediments, freshwater sediments are generally characterized by much lower sulphide concentrations *in situ*. This was also the case for the freshwater sediment samples investigated in this study. However, cryptic sulphur cycling (Canfield *et al.*, 2010) would be invisible in *in situ* porewater sulphur chemistry, but nonetheless be an integral process in freshwater environment (Pester *et al.*, 2012). In all four investigated samples, hints for LDET in the biogeochemical sediment profiles were observed, namely the pH peak, the downshift of the sulfidic zone with simultaneous development of a suboxic zone and acidification of anoxic sediment over time. The presence of CB indeed enhances cryptic sulphur cycling in freshwater sediments (Sandfeld *et al.*, 2020), as sulphide oxidation by CB produces sulphate, which in turn stimulates sulphate reducing microorganisms within these sulphate-limited environments, who then produce sulphide, thus completing the cycle. In the microbial community, the relative abundance of the microbes participating in this active cryptic sulphur cycle is often low (Pester *et al.*, 2012), but they have great impact on the ecosystem. Known sulphate reducers, that are also present in the here investigated samples investigation, are phylogenetically affiliated with the *Deltaproteobacteria*, with families *Desulfobulbaceae*, *Desulfobacteraceae*, and *Syntrophaceae*, as well as to the phylum *Firmicutes* (Castro *et al.*, 2000; Watanabe *et al.*, 2016). Tracking the cryptic sulphur cycle was not the scope of this study, but I propose that CB, together with sulphate reducing microbes as their counterpart, found at the sites in this study, are important players in sulphur cycling in (acidic) surface waters in the Fichtelgebirge region.

In the investigated mining-impacted mineral-rich sediment samples, the acidification of the suboxic and anoxic zones might contribute to mobilization of cations in the porewater, similarly as described previously (Geerlings *et al.*, 2019). Especially in iron-rich lake Fichtelsee, ferrous iron ( $\text{Fe}^{2+}$ ) could diffuse both up- and downwards. Upon reaching the oxic zone,  $\text{Fe}^{2+}$ -reoxidation would occur (abiotically or biotically), resulting in iron oxide crust formation, as observed during incubations in this study and as documented previously for electrogenic sediments (Risgaard-Petersen *et al.*, 2012; Seitaj *et al.*, 2015). I suggest therefore, that CB also contribute to iron cycling via e-SOx in these mineral-rich freshwater sediments, similar to previous findings for marine CB (Sulu-Gambari *et al.*, 2016; Geerlings *et al.*, 2019).

In more eutrophic Lake Weißenstädter See, sulphur cycling CB might also have an impact on carbon cycling via anaerobic carbon mineralization (Pester *et al.*, 2012; Sandfeld *et al.*, 2020), or on

phosphorous cycling (Holmer and Storkholm, 2001). However, as sulphur cycling in freshwater sediments has previously been considered minor, its impact on other element cycles is still poorly understood (Holmer and Storkholm, 2001; Wu *et al.*, 2019).

#### 4.2.4. Cable bacteria-associated microbiomes from mining-impacted freshwater systems

In column sediments, but especially also in agar pillars, the detected *Desulfobulbaceae* were accompanied by distinctive associated microbiomes. Direct interactions, such as direct interspecies electron transfer (DIET) between CB and other microbes have not yet been proven, but it is hypothesized that other microbes can access CB filament as an electron sink under electron acceptor limitation (Vasquez-Cardenas *et al.*, 2015). By e-SO<sub>x</sub>, CB create an electric field in the sediment, which affects the surrounding microbial community. Electroactive microorganisms have been studied mainly in context of biotechnology, but the fact that they can be found in diverse phyla suggests that this trait is wide-spread also in nature, and that microbes are common in various habitats (Koch and Harnisch, 2016; Logan *et al.*, 2019).

In Lake Fichtelsee, *Gammaproteobacteria* dominated the upper agar pillar. Aerobic ferrous iron-oxidizing *Gallionellaceae* (Hallbeck and Pedersen, 2014) were most abundant at microoxic conditions at 5-10 mm depth, which suggests that ferrous iron was mobilized due to acidic pH and diffusing upwards from deeper sediment layers. The suboxic agar as specific niche also enriched for fermenters, such as *Rhodocyclaceae* (Oren, 2014), and sulphide-oxidizers, such as *Thiovulaceae* (Waite *et al.*, 2017), the dominating family within *Epsilonproteobacteria*. The FISH-analysis showed that CB filaments were present within the microbial community. By LDET, the pH in the sediment depth-profile changed over incubation time. The acidic conditions within deeper agar and sediment were favourable to *Acidobacteria*, that were enriched in these zones. In Lake Weissenstädter See, which is more eutrophic by comparison (Klupp, 1995), the agar pillar was dominated by fermenters, mainly *Ruminococcaceae* (Esquivel-Elizondo *et al.*, 2017; Louis and Flint, 2017). Here, we found freshwater CB *Candidatus Electronema* sequences, suggesting a co-inhabitancy of CB with fermenters. In microcosms from River Eger, which is one of the inflows of Lake Weißenstädter See, we observed a similar microbial community pattern to that observed for Lake Weißenstädter See microcosms. Members of *Ruminococcaceae* were still dominant in all suboxic to anoxic depths of the agar pillar, but other taxa were more abundant. Reads affiliated with freshwater CB *Candidatus Electronema* sequences were found enriched in the agar pillar, co-enriched with the fermenter reads, such as *Ruminococcaceae* (Louis and Flint, 2017) or *Spirochaetes* (Dong *et al.*, 2018). We have no evidence for CB in microcosms from Stream Lehstenbach, as neither FISH nor sequencing data provided proof of their presence. Furthermore, although present in the agar pillar, we observed no strong enrichment of fermenters

compared to sediment, and the community profiles of agar pillar and surrounding sediment resemble each other.

Taken together, these findings suggest that the compartment of the agar pillar alone, without electroactive microorganisms inhabiting it, such as was the case for Stream Lehstenbach microcosms, the agar pillar does not enrich for fermenters. We hypothesize therefore, that the agar pillar enriches for electroactive organisms, which then attract fermenting organisms, corresponding with observations for microcosms from Lake Fichtelsee, Lake Weissenstädter See and River Eger. Without electroactive organisms, fermenters populate the agar pillar in similar relative abundance as the surrounding sediment. It was proposed previously, that microbes could be able to use CB filaments as an electron acceptor when other electron acceptors are scarce (Vasquez-Cardenas *et al.*, 2015). Indeed, for contaminant biodegradation in marine sediments (Marzocchi *et al.*, 2020) it was shown that CB acted as living electrodes, hinting at possible interactions between electrogenic CB and degraders. In biotechnological applications, anodic electro-fermentation is used to stabilize redox balance by means of an electrode as electron acceptor for microbes for respiration under anaerobic conditions (Vassilev *et al.*, 2021). Our results expand on the perception of interactions within electroactive microbiome for fermenters and CB in surface water sediments.

#### 4.3. Toluene degradation in a freshwater sediment microbial community affected by LDET

In this part of my thesis, I aimed to investigate the impact of long-distance electron transfer on biodegradation in toluene contaminated sediments and identify associated toluene degrading microorganisms, with regard to objective 3, associated to the hypothesis that presence of long-distance electron transfer in sediments enhances biodegradation of toluene.

##### 4.3.1. Biogeochemistry in Microcosms Amended with Toluene and Control

External optode measurements, guaranteeing oxygen concentration tracking within a closed system, proved that all microcosm headspaces, as well as supernatants, stayed oxic for incubation duration (see Figure 29). This was important, as oxygen is the most favourable electron acceptor, providing the highest electrochemical energy gain (Borch *et al.*, 2010) and is only available to microbes in the uppermost oxic sediment layer via downwards diffusion from the water column.

The results of the experiment demonstrate development of similar depth-resolved biogeochemical patterns in microcosms without toluene (control) and in microcosms with toluene-amendment ( $^{12}\text{C}$ -toluene and  $^{13}\text{C}$ -toluene). Biogeochemistry in  $^{13}\text{C}$ -toluene-amended microcosms including filters could not be measured, due to the insertion of filter membranes comparable to previously published experimental setups (Pfeffer *et al.*, 2012; Schauer *et al.*, 2014). The development of distinct biogeochemical patterns of LDET in the investigated microcosms is similar to time frames previously observed in marine sediment (Schauer *et al.*, 2014). Our homogenized microcosm sediments showed characteristic counter-gradients of oxygen and sulphide separated by a pronounced suboxic zone, which developed during incubation. A development of EP over depth was observed with maxima of ~6-8 mV on day 15 of incubation (see control: Figure 32,  $^{12}\text{C}$ : Figure 33,  $^{13}\text{C}$ : Figure 34), and was thus approximately reduced by factor two compared to previously reported river (Risgaard-Petersen *et al.*, 2015) and lake (Sandfeld *et al.*, 2020) sediment with active freshwater CB, and slightly higher than observed for groundwater CB (this work, see Figure 13). Toluene-amendment to microcosms seemed to have no effect on sediment biogeochemistry concerning sulphide and pH. For microcosms including filters, filter membrane-insertion prevented depth-resolved biogeochemical microprofiling of gradients, but as these filter membranes have neglectable effects on diffusional transport (Sayre, 1926), biogeochemical gradients are hypothesized to be characteristic of the utilized sediment, without visible patterns for LDET, as CB growth was hampered.

#### 4.3.2. CO<sub>2</sub>-Enrichment in Microcosms

The results show that total CO<sub>2</sub> in microcosms headspaces (see Figure 30) initially increased in control and  $^{12}\text{C}$ -toluene-amended microcosms, while staying at initial levels or decreasing slightly in microcosms amended with  $^{13}\text{C}$ -toluene (with and without filters). As we would expect a similar CO<sub>2</sub> production for at least  $^{12}\text{C}$ - and  $^{13}\text{C}$ -toluene-amended microcosms, we suggest variability between replicate microcosms as explanation for the observed discrepancy, which can be experienced in microcosm studies (Pagaling *et al.*, 2017). Indeed, one single replicate, respectively, in both groups behaved differently from the others, leading to large values for standard variation (up to 93% for control microcosms, up to 43% for  $^{12}\text{C}$ -toluene-amended microcosms). Another, though speculative, possibility could be chemical differences, such as additives, between the ordered  $^{12}\text{C}$ - and  $^{13}\text{C}$ -toluene, possibly due to manufacturing processes. These then might have led to slightly different behaviour regarding any (bio-)chemical reactions.

The results for atom percent  $^{13}\text{CO}_2$  (see Figure 31) were less prone to variability between replicate microcosms, as they were a fraction of total CO<sub>2</sub> in microcosm headspace. From day 6, microcosms with CB exhibited significantly higher  $^{13}\text{CO}_2$  enrichment (approximately factor 3) in headspace than in

microcosms with filters, suggesting more rapid biodegradation of toluene to CO<sub>2</sub>. So far, there are few studies investigating influence of CB on biodegradation of hydrocarbons. For marine CB, it was demonstrated that they accelerate biodegradation similarly to electrodes (Marzocchi *et al.*, 2020), specifically by up to 24-25%. For polycyclic aromatic hydrocarbon (PAH) contamination in a river sediment, it was demonstrated that elevated oxygen levels in overlying water enhance biodegradation, possibly due to stimulation of CB growth (Liu *et al.*, 2021). As methodology, type of sediment and contaminant differed to our study, the data are not fully comparable, but offer an orientation. Toluene degradation was reduced when filters were included, evident in reduced <sup>13</sup>CO<sub>2</sub>-production. We hypothesize that in filter-free microcosms, the toluene degrader community developed faster and to higher abundance, so that toluene degradation occurred more rapidly, as observed by steeper increase in headspace <sup>13</sup>CO<sub>2</sub> concentrations (see Figure 31, see Appendix 1 Figure 41). Filter-insertion into microcosms at oxic-anoxic depth is used as measure to prevent CB-growth (Pfeffer *et al.*, 2012; Schauer *et al.*, 2014), which influenced toluene biodegradation in our experiment. Although direct interspecies electron transfer (DIET) has not been directly proven for CB, it is hypothesized that interactions between species might take place (Vasquez-Cardenas *et al.*, 2015) and CB can contribute to electron acceptor availability for other microbes living within otherwise electron acceptor-depleted environment.

#### 4.3.3. Depth-Resolved Microbial Community Composition in Microcosms

In microcosms sediments, the detected microbiomes were distinct and developed over time, especially in the upmost sediment (0-5 and 5-10 mm depth). Not surprisingly, in presence of toluene, well-known anaerobic and aerobic toluene degraders (from oxic, hypoxic, or anoxic habitats), predominantly members of *Moraxellaceae* family (Genovese *et al.*, 2008), were more abundant than in toluene-free control microcosms compared to microcosms with toluene (both <sup>12</sup>C-toluene and <sup>13</sup>C-toluene). While toluene-amended microcosms without filter membrane insertions showed a toluene degrader enrichment predominantly in the upmost 10 mm of sediment (on day 8 and day 15), the toluene-amended microcosms with filter membranes at 5 and 10 mm depth showed a similar degrader abundance only in sediment above the upper filter membrane. As filter membranes affect diffusive transport only negligibly (Sayre, 1926), we assume that toluene availability was comparable to microcosms without filter insertions. A similar microbiome developed in microcosms with filters below 5 mm depth compared to microcosms without filters below 10 mm depth. This leads us to conclude that absence of e-SOx below 5 mm depth due to the filters resulted in electron acceptor limitation for potential toluene degraders, leading to no enrichment of potential toluene degraders in the microbiome.

#### 4.3.4. Toluene-Degrader Community Identified by DNA-SIP

As methodological considerations, it must be remarked that the interpretation of SIP data strongly relies on comparing sequencing results between microcosms amended with  $^{12}\text{C}$ - and  $^{13}\text{C}$ -substrate, and over parallel ranges of buoyant densities (Whiteley *et al.*, 2007). This was not fully possible for this study, as “heavy”  $^{12}\text{C}$ -DNA fractions often contained too low DNA concentrations for subsequent 16S rRNA amplicon generation for sequencing. This implies that the whole microbial community from  $^{12}\text{C}$ -toluene-amended microcosms is already represented within the “light”  $^{12}\text{C}$ -DNA fractions. In comparison, “heavy”  $^{13}\text{C}$ -DNA fractions contained enough DNA for subsequent amplification. Another indicator for successful separation of  $^{12}\text{C}$ - and  $^{13}\text{C}$ -DNA is the community pattern over  $^{12}\text{C}$ -DNA fractions from day 15 at 5-10 mm depth, showing distinct differences from parallel  $^{13}\text{C}$ -DNA fractions.

The sequencing results from the DNA-SIP fractions reveal that the label ( $^{13}\text{C}$ ), introduced by amending the microcosms with  $^{13}\text{C}_7$ -toluene, is distributed among members of the microbial community already on day 8 (see Figure 37), and on day 15 (see Figure 38). Microprofiling data suggested onset of the anoxic sediment below 3-5 mm depth. Sequencing of “heavy”  $^{13}\text{C}$ -DNA fractions revealed the degrader community, with members affiliated with known contaminant degrader families. *Acinetobacter* spp., known for aerobic toluene degradation, is affiliated with the found *Moraxellaceae* family (Watanabe *et al.*, 2008). The genus *Thauera*, affiliated with the *Rhodocyclaceae* family is known for denitrifying toluene degradation, both under aerobic and anaerobic conditions (Shinoda *et al.*, 2004; Oren, 2014) and nitrogen-fixing *Azoarcus* sp. described as anaerobic toluene degrader (Zhou *et al.*, 1995; Achong *et al.*, 2001).. Within *Burkholderiaceae* family, *Ralstonia pickettii* posseses the ability of aerobic toluene degradation under hypoxic conditions (Ryan *et al.*, 2007; Lünsmann *et al.*, 2016). Within *Rhodocyclaceae* family, the genus *Quatrionicoccus* has been identified as hypoxic toluene degrader (Táncsics *et al.*, 2018), the genus *Zoogloea* has been connected to oxic or microoxic petroleum hydrocarbon and benzene degradation, and the species *Georgfuchsia toluolica* is known both for aerobic and anaerobic toluene degradation (Jechalke *et al.*, 2013; Atashgahi *et al.*, 2021; Farkas *et al.*). *Malikia spinosa* is a prominent aerobic toluene degrader within *Comamonadaceae* (Révész *et al.*, 2020). Several families therefore include members that are able to degrade toluene aerobically, as well as anaerobically, and microorganisms assumed to be anaerobic may possess genes for aerobic toluene degradation (Atashgahi *et al.*, 2021). The results from the  $^{13}\text{C}$ -isotope labelling incubation experiment show *Gammaproteobacteria* families *Rhodocyclaceae*, *Comamonadaceae*, *Burkholderiaceae* and *Moraxellaceae* occurring in slightly higher abundances in filter-free microcosms compared to filter-including microcosms. Moreover, members of *Beijerinckiaceae* were present in “heavy”  $^{13}\text{C}$ -DNA fractions, a family that is affiliated also with crude oil degrading members (Wang *et al.*, 2016). Changes

within degrader community composition became visible comparing results from day 8 to day 15. At the later timepoint, the early degrader community composition in microcosms had shifted, which was likely also influenced by cross-feeding (DeRito *et al.*, 2005) within the microbial community. *Gammaproteobacteria* families were enriched in <sup>13</sup>C-toluene microcosms with and without filters, compared to unlabelled <sup>12</sup>C-toluene control, while electroactive members of *Geobacteraceae* family were only enriched in filter-free microcosms.

A comparison between filter-free and filter-including <sup>13</sup>C-toluene-amended microcosms revealed that the relative abundance of the known contaminant degraders was increased in filter-free incubations. We therefore assume that possible LDET contributes to more rapid degrader development compared to microcosm treatments, where CB-formation is hampered. This finding coincides with the strong increase in headspace <sup>13</sup>CO<sub>2</sub> by more than two-fold (see Figure 31), also suggesting more rapid toluene biodegradation in filter-free microcosms. We conclude therefore, that LDET, possible in filter-free microcosms, might contribute to toluene biodegradation. Members of *Desulfobulbaceae* were not abundant in “heavy” <sup>13</sup>C-DNA fractions, suggesting lack of labelling, and indicating that there was no direct involvement of CB in toluene degradation. This leads to the conclusion that the observed accelerated toluene biodegradation in filter-free microcosms might rather be indirectly affected by unhindered LDET, where possible CB filaments might act as catalyst. In this scenario, toluene biodegradation activity would not be conducted by CB directly, but CB might 1) either increase electron acceptor availability for degraders through rapid recycling via e-SOx (Sandfeld *et al.*, 2020), or 2) may even pose themselves as electron sink by providing electron-accepting structures to degraders (e.g. filaments/cables), or 3) both. Analogously, a recent study with crude oil-polluted marine sediments (Marzocchi *et al.*, 2020) showed that CB-presence accelerated contaminant degradation, similar to electrodes. For PAH-contaminated river sediment, presence of CB in combination with artificially oxygenating surface water resulted in more rapid contaminant degradation (Liu *et al.*, 2021).

Taken together, these findings expand on the perspective of contaminant degradation in sediments, revealing it to be a concerted effort of the whole microbial community, rather than the standalone accomplishment of single lineages. Especially cable bacteria can act as catalysts in contaminant removal by establishing more favourable geochemical conditions for the degrader community. So far, despite a few recent studies (Marzocchi *et al.*, 2020; Liu *et al.*, 2021), the role of cable bacteria in contaminant removal has been largely unrecognized and neglected. However, due to the capability of cable bacteria to shape sediment biogeochemistry (Nielsen and Risgaard-Petersen, 2015), as well as their presence in sediments around the world (see Table 1), they should be considered for possible future bioremediation applications.

## 5. Synopsis and outlook

This thesis elucidates the role of long-distance electron transfer by cable bacteria in freshwater sediments and contaminated aquifers by combining the findings of an interdisciplinary methodological approach. By investigating the ecology of cable bacteria in different freshwater sediments, the overarching goal of this study was to improve our understanding of the impact cable bacteria have on the biogeochemistry of their environment and associated microbial communities. The hypotheses set for the project were addressed with state-of-the-art molecular biology and biogeochemical methods as summarized in the following.

To facilitate the enrichment of the notoriously difficult-to-cultivate cable bacteria, I developed a novel cultivation method. A central agar pillar was embedded within sediment in microcosms to achieve equilibrium with surrounding sediment and provide a selective niche for cable bacteria. With respect to the first hypothesis, *Physicochemical properties of agar pillars, embedded in a sediment matrix, provide a selective niche for microorganisms relying on geochemical gradients and therefore present a viable cultivation approach for the enrichment of freshwater cable bacteria*, the primary finding of this thesis was that freshwater cable bacteria, but not groundwater cable bacteria, were significantly enriched in agar pillars compared to surrounding sediment matrix. A preferential colonization of the agar pillar is likely linked to shallower oxygen concentration gradients, with deeper penetration, as compared to the surrounding sediment, thus supporting the first hypothesis.

The combination of the novel agar pillar enrichment strategy with state-of-the-art biogeochemical and molecular biology methods allowed me to track the previously unrecognized distribution and diversity of cable bacteria in diverse freshwater environments, including a streambed sediment, a sulfidic lake sediment, a contaminated aquifer, a eutrophic lake sediment and acidic mining-impacted river and lake sediments. With respect to the second hypothesis, *Sediment origin and biogeochemistry control the occurrence and/or diversity of cable bacteria*, potentially novel freshwater Ca. *Electronema* lineages were found among the detected putative cable bacteria. Potential groundwater cable bacteria within the *Desulfobulbaceae* clustered closer to *Desulfurivibrio* spp., thus accentuating the necessity to distinguish between freshwater and groundwater cable bacteria. Further, cable bacteria were detected in almost all the investigated habitats, thereby extending their recognized distribution. My findings also highlight distribution patterns of cable bacteria that are strong indicators of their interactions with other functional microbial groups within microbial communities, such as fermenters and other complex carbon-degrading microorganisms. By electrogenic sulphide oxidation, cable bacteria might be a so far underestimated, but nonetheless vital component in cryptic sulphur cycling

in freshwater sediments. As these are characterized by low *in situ* sulphate concentrations, cable bacteria can contribute to recycling of this scarce resource. Thus, cable bacteria not only have a direct impact on sediment biogeochemistry, but also affect it indirectly through multifaceted interactions with other members of the microbial community. In summary, these findings support the second hypothesis.

An environmentally relevant example of such multifaceted interactions is the impact of cable bacteria activity on pollutant degradation. With an experimentally sophisticated  $^{13}\text{C}$ -isotope labelling-approach, including depth-resolved biogeochemical and molecular biological analyses, I demonstrated the potential role of LDET in contaminant degradation. With respect to the third hypothesis, *Presence of long-distance electron transfer in sediments enhances biodegradation of toluene*, my findings show that cable bacteria apparently may accelerate toluene degradation by more than two-fold. Transfer of the  $^{13}\text{C}$ -label within the microbial community suggested that toluene degradation was primarily mediated by known toluene degrading groups, such as *Rhodocyclaceae*, *Comamonadaceae*, *Burkholderiaceae* and *Moraxellaceae*. Further, the results indicated a transfer of the  $^{13}\text{C}$ -isotope label to microbial lineages that are not known for toluene degradation. There was no evidence for a direct involvement of cable bacteria in toluene degradation, as suggested by lack of detectable enrichment in heavy fractions. Rather, increased toluene degradation activity in microcosms with unhindered LDET was potentially caused by indirect involvement of cable bacteria, by either increasing electron acceptor availability via e-SO<sub>x</sub>, or by serving as electron-accepting structures for toluene degraders. The third hypothesis could thus be confirmed. This experiment also highlights the limitations of DNA-SIP-approaches to detect microbial catabolic activity – as only a transfer of the  $^{13}\text{C}$ -isotope label to microbial biomass is detectable, other methodologies are necessary to track the fate of metabolites, microbial interactions and their resulting biogeochemical impact.

Altogether, my findings within the scope of this thesis contribute to understanding ecology and diversity of freshwater cable bacteria by extending their known range of habitats, as well as by providing insights into potential new lineages. The novel agar pillar enrichment strategy could potentially serve as enrichment method not only for marine cable bacteria, but also other microbes that are dependent on redox gradients. The procedural advantages of cultivation within an agar matrix may be of general interest to microbial ecologists seeking a sediment-free enrichment strategy for environmental microorganisms, theoretically also allowing for single cell isolation. Further, the agar pillar would make investigations of cable bacteria activity more accessible for advanced OMIC's techniques, including characterization of the metabolome or the -proteome, that often fail in complex environmental matrices such as sediment or soil.

Moreover, I highlighted the strong influence cable bacteria have on their environments, by impacting biogeochemical processes and their associated microbial community, both of which additionally affect each other. The strong influence of long-distance electron transfer on toluene degradation is lacking in our current perspective of environmental pollutant degradation in freshwater environments. Although speculative, it is possible that cable bacteria, through their ability to stimulate microbial degraders, might present the missing link when contaminant degradation is more efficient than anticipated, e.g. via biogeochemical modelling approaches. Due to their worldwide distribution, it appears necessary to consider and integrate the activity of cable bacteria into such modelling approaches, especially those of contaminant degradation as the foundation for any potential bioremediation applications.

## 6. References

- Abbas, S.Z., Rafatullah, M., Khan, M.A., and Siddiqui, M.R. (2019) Bioremediation and electricity generation by using open and closed sediment microbial fuel cells. *Front Microbiol* **9**: 1–12.
- Abdel-Shafy, H.I. and Mansour, M.S.M. (2016) A review on polycyclic aromatic hydrocarbons: source, environmental impact, effect on human health and remediation. *Egypt J Pet* **25**: 107–123.
- Achong, G.R., Rodriguez, A.M., and Spormann, A.M. (2001) Benzylsuccinate synthase of *Azoarcus* sp. strain T: cloning, sequencing, transcriptional organization, and its role in anaerobic toluene and m-xylene mineralization. *J Bacteriol* **183**: 6763–6770.
- Al-Mailem, D.M., Sorkhoh, N.A., Al-Awadhi, H., Elias, M., and Radwan, S.S. (2010) Biodegradation of crude oil and pure hydrocarbons by extreme halophilic Archaea from hypersaline coasts of the Arabian Gulf. *Extrem Life Extreme Cond* **14**: 321–328.
- Amann, R.I., Binder, B.J., Olson, R.J., Chisholm, S.W., Devereux, R., and Stahl, D.A. (1990) Combination of 16S rRNA-targeted oligonucleotide probes with flow cytometry for analyzing mixed microbial populations. *Appl Environ Microbiol* **56**: 1919–1925.
- Anneser, B., Einsiedl, F., Meckenstock, R.U., Richters, L., Wisotzky, F., and Griebler, C. (2008) High-resolution monitoring of biogeochemical gradients in a tar oil-contaminated aquifer. *Appl Geochem* **23**: 1715–1730.
- Apprill, A., McNally, S., Parsons, R., and Weber, L. (2015) Minor revision to V4 region SSU rRNA 806R gene primer greatly increases detection of SAR11 bacterioplankton. *Aquat Microb Ecol* **75**: 129–137.
- Atashgahi, S., Oosterkamp, M.J., Peng, P., Frank, J., Kraft, B., Hornung, B., et al. (2021) Proteogenomic analysis of *Georgfuchsia toluolica* revealed unexpected concurrent aerobic and anaerobic toluene degradation. *Environ Microbiol Rep* **13**: 841–851.
- ATSDR and U.S. Department of Health & Human Services (2019) CERCLA priority list of hazardous substances by the Agency for Toxic Substances and Disease Registry (ATSDR) and the U.S. Division of Toxicology and Human Health Sciences.
- Benomar, S., Ranava, D., Cárdenas, M.L., Trably, E., Rafrafi, Y., Ducret, A., et al. (2015) Nutritional stress induces exchange of cell material and energetic coupling between bacterial species. *Nat Commun* **6**: 1–10.
- Berner, R.A. (1981) A new geochemical classification of sedimentary environments. *J Sediment Petrol* **51**: 359–365.

Berner, R.A. (2020) Early diagenesis: a theoretical approach, Princeton University Press.

Besnard, A.F. (1854) Die Mineralien Bayerns nach ihren Fundstätten: eine mineralogisch-topographische Skizze, Kollmann.

Beyer, J., Trannum, H.C., Bakke, T., Hodson, P.V., and Collier, T.K. (2016) Environmental effects of the Deepwater Horizon oil spill: a review. *Mar Pollut Bull* **110**: 28–51.

Biegert, T., Fuchs, G., and Heider, J. (1996) Evidence that anaerobic oxidation of toluene in the denitrifying bacterium *Thauera aromatica* is initiated by formation of benzylsuccinate from toluene and fumarate. *Eur J Biochem* **238**: 661–668.

Bjerg, J.T., Damgaard, L.R., Holm, S.A., Schramm, A., and Nielsen, L.P. (2016) Motility of electric cable bacteria. *Appl Environ Microbiol* **82**: 3816–3821.

Borch, T., Kretzschmar, R., Kappler, A., Cappellen, P.V., Ginder-Vogel, M., Voegelin, A., and Campbell, K. (2010) Biogeochemical redox processes and their impact on contaminant dynamics. *Environ Sci Technol* **44**: 15–23.

Brodersen, K.E., Nielsen, D.A., Ralph, P.J., and Kühl, M. (2015) Oxic microshield and local pH enhancement protects *Zostera muelleri* from sediment derived hydrogen sulphide. *New Phytol* **205**: 1264–1276.

Burdorf, L., Hidalgo-Martinez, S., Cook, P., and Meysman, F. (2016) Long-distance electron transport by cable bacteria in mangrove sediments. *Mar Ecol Prog Ser* **545**: 1–8.

Butler, J.E., Young, N.D., and Lovley, D.R. (2010) Evolution of electron transfer out of the cell: comparative genomics of six *Geobacter* genomes. *BMC Genomics* **11**: 1–12.

Callahan, B.J., McMurdie, P.J., Rosen, M.J., Han, A.W., Johnson, A.J.A., and Holmes, S.P. (2016) DADA2: high-resolution sample inference from illumina amplicon data. *Nat Methods* **13**: 581–583.

Callahan, B.J., Wong, J., Heiner, C., Oh, S., Theriot, C.M., Gulati, A.S., et al. (2019) High-throughput amplicon sequencing of the full-length 16S rRNA gene with single-nucleotide resolution. *Nucleic Acids Res* **47**: e103.

Canfield, D.E., Stewart, F.J., Thamdrup, B., De Brabandere, L., Dalsgaard, T., Delong, E.F., et al. (2010) A cryptic sulfur cycle in oxygen-minimum-zone waters off the Chilean coast. *Science* **330**: 1375–1378.

Castro, H.F., Williams, N.H., and Ogram, A. (2000) Phylogeny of sulfate-reducing bacteria. *FEMS Microbiol Ecol* **31**: 1–9.

Coenye, T. (2014) The family Burkholderiaceae. In *The Prokaryotes*. Rosenberg, E., DeLong, E.F., Lory, S., Stackebrandt, E., and Thompson, F. (eds). Berlin, Heidelberg: Springer Berlin Heidelberg, pp. 759–776.

Cohr, K.-H. and Stockholm, J. (1979) Toluene: a toxicologic review. *Scand J Work Environ Health* **5**: 71–90.

Committee on Bioavailability of Contaminants in Soils and Sediments (2003) Bioavailability of contaminants in soils and sediments: processes, tools, and applications, Washington, DC: The National Academies Press: National Research Council.

Conley, B.E., Intile, P.J., Bond, D.R., and Gralnick, J.A. (2018) Divergent Nrf family proteins and MtrCAB homologs facilitate extracellular electron transfer in *Aeromonas hydrophila*. *Appl Environ Microbiol* **84**: e02134-18.

Cornelissen, R., Bøggild, A., Thiruvallur Eachambadi, R., Koning, R.I., Kremer, A., Hidalgo-Martinez, S., et al. (2018) The cell envelope structure of cable bacteria. *Front Microbiol* **9**: 1–13.

Daims, H., Brühl, A., Amann, R., Schleifer, K.-H., and Wagner, M. (1999) The domain-specific probe EU338 is insufficient for the detection of all bacteria: development and evaluation of a more comprehensive probe set. *Syst Appl Microbiol* **22**: 434–444.

Dam, A.-S., Marshall, I.P.G., Risgaard-Petersen, N., Burdorf, L.D.W., and Marzocchi, U. (2021) Effect of salinity on cable bacteria species composition and diversity. *Environ Microbiol* **23**: 2605–2616.

Damgaard, L.R., Risgaard-Petersen, N., and Nielsen, L.P. (2014) Electric potential microelectrode for studies of electrobiogeophysics: electric potential microelectrode. *J Geophys Res Biogeosciences* **119**: 1906–1917.

Davison, W. (1993) Iron and manganese in lakes. *Earth-Sci Rev* **34**: 119–163.

DeRito, C.M., Pumphrey, G.M., and Madsen, E.L. (2005) Use of field-based stable isotope probing to identify adapted populations and track carbon flow through a phenol-degrading soil microbial community. *Appl Environ Microbiol* **71**: 7858–7865.

Devika, N. and Rastogi, A.K. (2018) Remediation techniques for BTEX contamination of groundwater—a review. *Int J Eng Res Technol* **3**: 1–6.

Dong, X., Greening, C., Brüls, T., Conrad, R., Guo, K., Blaskowski, S., et al. (2018) Fermentative Spirochaetes mediate necromass recycling in anoxic hydrocarbon-contaminated habitats. *ISME J* **12**: 2039–2050.

Eachambadi, R.T., Bonné, R., Cornelissen, R., Hidalgo-Martinez, S., Vangronsveld, J., Meysman, F.J.R., et al. (2020) An ordered and fail-safe electrical network in cable bacteria. *Adv Biosyst* **4**: 1–6.

Edgar, R.C., Haas, B.J., Clemente, J.C., Quince, C., and Knight, R. (2011) UCHIME improves sensitivity and speed of chimera detection. *Bioinformatics* **27**: 2194–2200.

Edwards, U., Rogall, T., Blöcker, H., Emde, M., and Böttger, E.C. (1989) Isolation and direct complete nucleotide determination of entire genes. Characterization of a gene coding for 16S ribosomal RNA. *Nucleic Acids Res* **17**: 7843–7853.

Esquivel-Elizondo, S., Ilhan, Z.E., Garcia-Peña, E.I., and Krajmalnik-Brown, R. (2017) Insights into butyrate production in a controlled fermentation system via gene predictions. *mSystems* **2**: e00051-17.

Evans, P.J., Mang, D.T., and Young, L.Y. (1991) Degradation of toluene and m-xylene and transformation of o-xylene by denitrifying enrichment cultures. *Appl Environ Microbiol* **57**: 450–454.

Farkas, M., Táncsics, A., Kriszt, B., Benedek, T., Tóth, E.M., Kéki, Z., et al. Zoogloea oleivorans sp. nov., a floc-forming, petroleum hydrocarbon-degrading bacterium isolated from biofilm. *Int J Syst Evol Microbiol* **65**: 274–279.

Favre, H.A. and Powell, W.H. (2013) Nomenclature of organic chemistry.

Fikenscher, G.W.A. (1807) Lehrbuch der Landesgeschichte des Fürstenthums Bayreuth, Raspe.

Fritz, G.B., Pfannkuchen, M., Struck, U., Hengherr, S., Strohmeier, S., and Brümmer, F. (2012) Characterizing an anoxic habitat: sulfur bacteria in a meromictic alpine lake. In *Anoxia: Evidence for Eukaryote Survival and Paleontological Strategies*. Cellular Origin, Life in Extreme Habitats and Astrobiology. Altenbach, A.V., Bernhard, J.M., and Seckbach, J. (eds). Dordrecht: Springer Netherlands, pp. 449–461.

Froelich, P.N., Klinkhammer, G.P., Bender, M.L., Luedtke, N.A., Heath, G.R., Cullen, D., et al. (1979) Early oxidation of organic matter in pelagic sediments of the eastern equatorial Atlantic: suboxic diagenesis. *Geochim Cosmochim Acta* **43**: 1075–1090.

Fuchs, G., Boll, M., and Heider, J. (2011) Microbial degradation of aromatic compounds — from one strategy to four. *Nat Rev Microbiol* **9**: 803–816.

Geerlings, N.M.J., Karman, C., Trashin, S., As, K.S., Kienhuis, M.V.M., Hidalgo-Martinez, S., et al. (2020) Division of labor and growth during electrical cooperation in multicellular cable bacteria. *Proc Natl Acad Sci* **117**: 5478–5485.

Geerlings, N.M.J., Zetsche, E.-M., Hidalgo-Martinez, S., Middelburg, J.J., and Meysman, F.J.R. (2019) Mineral formation induced by cable bacteria performing long-distance electron transport in marine sediments. *Biogeosciences* **16**: 811–829.

Genovese, M., Denaro, R., Cappello, S., Di Marco, G., La Spada, G., Giuliano, L., et al. (2008) Bioremediation of benzene, toluene, ethylbenzene, xylenes-contaminated soil: a biopile pilot experiment. *J Appl Microbiol* **105**: 1694–1702.

Griebler, C. and Lueders, T. (2009) Microbial biodiversity in groundwater ecosystems. *Freshw Biol* **54**: 649–677.

Gülensoy, N. and Alvarez, P.J.J. (1999) Diversity and correlation of specific aromatic hydrocarbon biodegradation capabilities. *Biodegradation* **10**: 331–340.

Güllert, S., Fischer, M.A., Turaev, D., Noebauer, B., Ilmberger, N., Wemheuer, B., et al. (2016) Deep metagenome and metatranscriptome analyses of microbial communities affiliated with an industrial biogas fermenter, a cow rumen, and elephant feces reveal major differences in carbohydrate hydrolysis strategies. *Biotechnol Biofuels* **9**: 1–20.

Guo, F. and Zhang, T. (2013) Biases during DNA extraction of activated sludge samples revealed by high throughput sequencing. *Appl Microbiol Biotechnol* **97**: 4607–4616.

Guo, X., Sun, C., Lin, R., Xia, A., Huang, Y., Zhu, X., et al. (2020) Effects of foam nickel supplementation on anaerobic digestion: direct interspecies electron transfer. *J Hazard Mater* **399**: 1–10.

Hallbeck, L. and Pedersen, K. (2014) The family Gallionellaceae. In *The Prokaryotes: Alphaproteobacteria and Betaproteobacteria*. Rosenberg, E., DeLong, E.F., Lory, S., Stackebrandt, E., and Thompson, F. (eds). Berlin, Heidelberg: Springer, pp. 853–858.

Heipieper, H.J. and Martínez, P.M. (2010) Toxicity of hydrocarbons to microorganisms. In *Handbook of Hydrocarbon and Lipid Microbiology*. Timmis, K.N. (ed). Berlin, Heidelberg: Springer, pp. 1563–1573.

Hermans, M., Lenstra, W.K., Hidalgo-Martinez, S., van Helmond, N.A.G.M., Witbaard, R., Meysman, F.J.R., et al. (2019) Abundance and biogeochemical impact of cable bacteria in Baltic Sea sediments. *Environ Sci Technol* **53**: 7494–7503.

Holmer, M. and Storkholm, P. (2001) Sulphate reduction and sulphur cycling in lake sediments: a review. *Freshw Biol* **46**: 431–451.

Holmkvist, L., Ferdelman, T.G., and Jørgensen, B.B. (2011) A cryptic sulfur cycle driven by iron in the methane zone of marine sediment (Aarhus Bay, Denmark). *Geochim Cosmochim Acta* **75**: 3581–3599.

Hong, Y., Wu, J., Wilson, S., and Song, B. (2019) Vertical stratification of sediment microbial communities along geochemical gradients of a subterranean estuary located at the Gloucester Beach of Virginia, United States. *Front Microbiol* **9**: 1–11.

Hunt, L.J., Duca, D., Dan, T., and Knopper, L.D. (2019) Petroleum hydrocarbon (PHC) uptake in plants: a literature review. *Environ Pollut* **245**: 472–484.

Jechalke, S., Franchini, A.G., Bastida, F., Bombach, P., Rosell, M., Seifert, J., et al. (2013) Analysis of structure, function, and activity of a benzene-degrading microbial community. *FEMS Microbiol Ecol* **85**: 14–26.

Jeroschewski, P., Steuckart, C., and Kühl, M. (1996) An amperometric microsensor for the determination of H<sub>2</sub>S in aquatic environments. *Anal Chem* **68**: 4351–4357.

Jiang, Z., Zhang, S., Klausen, L.H., Song, J., Li, Q., Wang, Z., et al. (2018) In vitro single-cell dissection revealing the interior structure of cable bacteria. *Proc Natl Acad Sci* **115**: 8517–8522.

Jindrová, E., Chocová, M., Demnerová, K., and Brenner, V. (2002) Bacterial aerobic degradation of benzene, toluene, ethylbenzene and xylene. *Folia Microbiol (Praha)* **47**: 83–93.

Jost, D., Haberer, C.M., Grathwohl, P., Winter, J., and Gallert, C. (2015) Oxygen transfer in a fluctuating capillary fringe: impact of microbial respiratory activity. *Vadose Zone J* **14**: 1–14.

Kessler, A.J., Wawryk, M., Marzocchi, U., Roberts, K.L., Wong, W.W., Risgaard-Petersen, N., et al. (2019) Cable bacteria promote DNRA through iron sulfide dissolution. *Limnol Oceanogr* **64**: 1228–1238.

Kirk, T.K. and Farrell, R.L. (1987) Enzymatic “combustion”: the microbial degradation of lignin. *Annu Rev Microbiol* **41**: 465–501.

Kjeldsen, K.U., Schreiber, L., Thorup, C.A., Boesen, T., Bjerg, J.T., Yang, T., et al. (2019) On the evolution and physiology of cable bacteria. *Proc Natl Acad Sci* **116**: 19116–19125.

Kleinsteuber, S., Schleinitz, K.M., and Vogt, C. (2012) Key players and team play: anaerobic microbial communities in hydrocarbon-contaminated aquifers. *Appl Microbiol Biotechnol* **94**: 851–873.

Klupp, R. (1995) Regulation von Weißfischbeständen in stehenden Gewässern, Laufen/Salzach: Bayerische Akademie für Naturschutz und Landschaftspflege (ANL).

Koch, C. and Harnisch, F. (2016) Is there a specific ecological niche for electroactive microorganisms? *ChemElectroChem* **3**: 1282–1295.

Koretsky, C.M., Haas, J.R., Miller, D., and Ndenga, N.T. (2006) Seasonal variations in pore water and sediment geochemistry of littoral lake sediments (Asylum Lake, MI, USA). *Geochim Trans* **7**: 1–26.

Korlach, J. (2013) Understanding accuracy in SMRT® sequencing.

Kristjansson, J.K., Schönheit, P., and Thauer, R.K. (1982) Different K<sub>s</sub> values for hydrogen of methanogenic bacteria and sulfate reducing bacteria: an explanation for the apparent inhibition of methanogenesis by sulfate. *Arch Microbiol* **131**: 278–282.

Kuever, J. (2014) The family Desulfobulbaceae. In *The Prokaryotes*. Rosenberg, E., DeLong, E.F., Lory, S., Stackebrandt, E., and Thompson, F. (eds). Berlin, Heidelberg: Springer Berlin Heidelberg, pp. 75–86.

Lahaye, M. and Rochas, C. (1991) Chemical structure and physico-chemical properties of agar. *Hydrobiologia* **221**: 137–148.

Lane, D.J. (1991) 16S/23S rRNA sequencing. In *E. Stackebrandt and M. Goodfellow (ed.), Nucleic acid techniques in bacterial systematics*. Chichester; New York: John Wiley & Sons, pp. 115–175.

Lane, N. and Martin, W. (2010) The energetics of genome complexity. *Nature* **467**: 929–934.

Larsen, S., Nielsen, L.P., and Schramm, A. (2015) Cable bacteria associated with long-distance electron transport in New England salt marsh sediment. *Environ Microbiol Rep* **7**: 175–179.

Leahy, J.G. and Colwell, R.R. (1990) Microbial degradation of hydrocarbons in the environment. *Microbiol Rev* **54**: 305–315.

Li, C., Reimers, C.E., and Alleau, Y. (2020) Inducing the attachment of cable bacteria on oxidizing electrodes. *Biogeosciences* **17**: 597–607.

Liu, F., Wang, Z., Wu, B., Bjerg, J.T., Hu, W., Guo, X., et al. (2021) Cable bacteria extend the impacts of elevated dissolved oxygen into anoxic sediments. *ISME J* **15**: 1551–1563.

Llobet-Brossa, E., Rosselló-Mora, R., and Amann, R. (1998) Microbial community composition of Wadden Sea sediments as revealed by fluorescence in situ hybridization. *Appl Environ Microbiol* **64**: 2691–2696.

Logan, B.E., Rossi, R., Ragab, A., and Saikaly, P.E. (2019) Electroactive microorganisms in bioelectrochemical systems. *Nat Rev Microbiol* **17**: 307–319.

- Louis, P. and Flint, H.J. (2017) Formation of propionate and butyrate by the human colonic microbiota. *Environ Microbiol* **19**: 29–41.
- Lovley, D.R., Baedecker, M.J., Lonergan, D.J., Cozzarelli, I.M., Phillips, E.J.P., and Siegel, D.I. (1989) Oxidation of aromatic contaminants coupled to microbial iron reduction. *Nature* **339**: 297–300.
- Loy, A., Lehner, A., Lee, N., Adamczyk, J., Meier, H., Ernst, J., et al. (2002) Oligonucleotide microarray for 16s rRNA gene-based detection of all recognized lineages of sulfate-reducing prokaryotes in the environment. *Appl Environ Microbiol* **68**: 5064–5081.
- Ludwig, W., Strunk, O., Westram, R., Richter, L., Meier, H., Yadhukumar, et al. (2004) ARB: a software environment for sequence data. *Nucleic Acids Res* **32**: 1363–1371.
- Lueders, T. (2017) The ecology of anaerobic degraders of BTEX hydrocarbons in aquifers. *FEMS Microbiol Ecol* **93**: 1–13.
- Lueders, T., Manefield, M., and Friedrich, M.W. (2004) Enhanced sensitivity of DNA- and rRNA-based stable isotope probing by fractionation and quantitative analysis of isopycnic centrifugation gradients. *Environ Microbiol* **6**: 73–78.
- Lünsmann, V., Kappelmeyer, U., Benndorf, R., Martínez-Lavanchy, P.M., Taubert, A., Adrian, L., et al. (2016) In situ protein-SIP highlights Burkholderiaceae as key players degrading toluene by para ring hydroxylation in a constructed wetland model. *Environ Microbiol* **18**: 1176–1186.
- Malkin, S.Y. and Meysman, F.J.R. (2015) Rapid redox signal transmission by “cable bacteria” beneath a photosynthetic biofilm. *Appl Environ Microbiol* **81**: 948–956.
- Malkin, S.Y., Rao, A.M., Seitaj, D., Vasquez-Cardenas, D., Zetsche, E.-M., Hidalgo-Martinez, S., et al. (2014) Natural occurrence of microbial sulphur oxidation by long-range electron transport in the seafloor. *ISME J* **8**: 1843–1854.
- Malkin, S.Y., Seitaj, D., Burdorf, L.D.W., Nieuwhof, S., Hidalgo-Martinez, S., Tramper, A., et al. (2017) Electrogenic sulfur oxidation by cable bacteria in bivalve reef sediments. *Front Mar Sci* **4**: 1–19.
- Martin, B.C., Bougoure, J., Ryan, M.H., Bennett, W.W., Colmer, T.D., Joyce, N.K., et al. (2019) Oxygen loss from seagrass roots coincides with colonisation of sulphide-oxidising cable bacteria and reduces sulphide stress. *ISME J* **13**: 707–719.
- Marzocchi, U., Bonaglia, S., Velde, S. van de, Hall, P.O.J., Schramm, A., Risgaard-Petersen, N., and Meysman, F.J.R. (2018) Transient bottom water oxygenation creates a niche for cable bacteria in long-term anoxic sediments of the Eastern Gotland Basin. *Environ Microbiol* **20**: 3031–3041.

- Marzocchi, U., Palma, E., Rossetti, S., Aulenta, F., and Scoma, A. (2020) Parallel artificial and biological electric circuits power petroleum decontamination: the case of snorkel and cable bacteria. *Water Res* **173**: 1–10.
- Marzocchi, U., Trojan, D., Larsen, S., Louise Meyer, R., Peter Revsbech, N., Schramm, A., et al. (2014) Electric coupling between distant nitrate reduction and sulfide oxidation in marine sediment. *ISME J* **8**: 1682–1690.
- Matturro, B., Cruz Viggi, C., Aulenta, F., and Rossetti, S. (2017) Cable bacteria and the bioelectrochemical snorkel: the natural and engineered facets playing a role in hydrocarbons degradation in marine sediments. *Front Microbiol* **8**: 1–13.
- McCarty, P.L. and Criddle, C.S. (2012) Chemical and biological processes: the need for mixing. In *Delivery and Mixing in the Subsurface: Processes and Design Principles for In Situ Remediation*. SERDP ESTCP Environmental Remediation Technology. Kitanidis, P.K. and McCarty, P.L. (eds). New York, NY: Springer, pp. 7–52.
- McMurdie, P.J. and Holmes, S. (2013) Phyloseq: an R package for reproducible interactive analysis and graphics of microbiome census data. *PLoS ONE* **8**: e61217.
- Meckenstock, R.U., Elsner, M., Griebler, C., Lueders, T., Stumpp, C., Aamand, J., et al. (2015) Biodegradation: updating the concepts of control for microbial cleanup in contaminated aquifers. *Environ Sci Technol* **49**: 7073–7081.
- Meier, H., Mertens, M., and Huwe, B. (2003) Phosphorbilanzierung von Fischteichen - der Einfluss der Teichwirtschaft auf die Wasserqualität des Weißenstädter Sees. *Fisch Teichwirt* **54**: 247–251.
- Meysman, F.J.R. (2018) Cable bacteria take a new breath using long-distance electricity. *Trends Microbiol* **26**: 411–422.
- Meysman, F.J.R., Cornelissen, R., Trashin, S., Bonné, R., Martinez, S.H., van der Veen, J., et al. (2019) A highly conductive fibre network enables centimetre-scale electron transport in multicellular cable bacteria. *Nat Commun* **10**: 1–8.
- Meysman, F.J.R., Risgaard-Petersen, N., Malkin, S.Y., and Nielsen, L.P. (2015) The geochemical fingerprint of microbial long-distance electron transport in the seafloor. *Geochim Cosmochim Acta* **152**: 122–142.
- Millero, F.J., Plese, T., and Fernandez, M. (1988) The dissociation of hydrogen sulfide in seawater. *Limnol Oceanogr* **33**: 269–274.
- Moscoviz, R., Toledo-Alarcón, J., Trably, E., and Bernet, N. (2016) Electro-fermentation: how to drive fermentation using electrochemical systems. *Trends Biotechnol* **34**: 856–865.

Mosher, J.J., Bowman, B., Bernberg, E.L., Shevchenko, O., Kan, J., Korlach, J., and Kaplan, L.A. (2014) Improved performance of the PacBio SMRT technology for 16S rDNA sequencing. *J Microbiol Methods* **104**: 59–60.

Moss, G.P., Smith, P. a. S., and Tavernier, D. (1995) Glossary of class names of organic compounds and reactivity intermediates based on structure (IUPAC recommendations 1995). *Pure Appl Chem* **67**: 1307–1375.

Müller, H., Bosch, J., Griebler, C., Damgaard, L.R., Nielsen, L.P., Lueders, T., and Meckenstock, R.U. (2016) Long-distance electron transfer by cable bacteria in aquifer sediments. *ISME J* **10**: 2010–2019.

Müller, H., Marozava, S., Probst, A.J., and Meckenstock, R.U. (2019) Groundwater cable bacteria conserve energy by sulfur disproportionation. *ISME J* **14**: 623–634.

Müller, H. and Meckenstock, R.U. (2017) Kabelbakterien ermöglichen neue geochemische Prozesse. *BIOspektrum* **23**: 388–390.

Muyzer, G., Teske, A., Wirsén, C.O., and Jannasch, H.W. (1995) Phylogenetic relationships of Thiomicrospira species and their identification in deep-sea hydrothermal vent samples by denaturing gradient gel electrophoresis of 16S rDNA fragments. *Arch Microbiol* **164**: 165–172.

Nielsen, L.P. (2016) Ecology: electrical cable bacteria save marine life. *Curr Biol* **26**: R32–R33.

Nielsen, L.P. and Risgaard-Petersen, N. (2015) Rethinking sediment biogeochemistry after the discovery of electric currents. *Annu Rev Mar Sci* **7**: 425–442.

Nielsen, L.P., Risgaard-Petersen, N., Fossing, H., Christensen, P.B., and Sayama, M. (2010) Electric currents couple spatially separated biogeochemical processes in marine sediment. *Nature* **463**: 1071–1074.

Njobuenwu, D.O., Amadi, S.A., and Ukpaka, P.C. (2005) Dissolution rate of BTEX contaminants in water. *Can J Chem Eng* **83**: 985–989.

Oikonomou, A., Filker, S., Breiner, H.-W., and Stoeck, T. (2015) Protistan diversity in a permanently stratified meromictic lake (Lake Alatsee, SW Germany). *Environ Microbiol* **17**: 2144–2157.

Oikonomou, A., Pachiadaki, M., and Stoeck, T. (2014) Protistan grazing in a meromictic freshwater lake with anoxic bottom water. *FEMS Microbiol Ecol* **87**: 691–703.

Oren, A. (2014) The family Rhodocyclaceae. In *The Prokaryotes: Alphaproteobacteria and Betaproteobacteria*. Rosenberg, E., DeLong, E.F., Lory, S., Stackebrandt, E., and Thompson, F. (eds). Berlin, Heidelberg: Springer, pp. 975–998.

Otte, J.M., Harter, J., Laufer, K., Blackwell, N., Straub, D., Kappler, A., and Kleindienst, S. (2018) The distribution of active iron-cycling bacteria in marine and freshwater sediments is decoupled from geochemical gradients. *Environ Microbiol* **20**: 2483–2499.

Pagaling, E., Vassileva, K., Mills, C.G., Bush, T., Blythe, R.A., Schwarz-Linek, J., et al. (2017) Assembly of microbial communities in replicate nutrient-cycling model ecosystems follows divergent trajectories, leading to alternate stable states. *Environ Microbiol* **19**: 3374–3386.

Parada, A.E., Needham, D.M., and Fuhrman, J.A. (2016) Every base matters: assessing small subunit rRNA primers for marine microbiomes with mock communities, time series and global field samples. *Environ Microbiol* **18**: 1403–1414.

Pernthaler, J., Glöckner, F.O., Schönhuber, W., and Amann, R. (2001) Fluorescence in situ hybridization with rRNA-targeted oligonucleotide probes. *30*: 207–210.

Pester, M., Knorr, K.-H., Friedrich, M., Wagner, M., and Loy, A. (2012) Sulfate-reducing microorganisms in wetlands – fameless actors in carbon cycling and climate change. *Front Microbiol* **3**: 1–19.

Pfeffer, C., Larsen, S., Song, J., Dong, M., Besenbacher, F., Meyer, R.L., et al. (2012) Filamentous bacteria transport electrons over centimetre distances. *Nature* **491**: 218–221.

Pilloni, G., Bayer, A., Ruth-Anneser, B., Fillinger, L., Engel, M., Griebler, C., and Lueders, T. (2019) Dynamics of hydrology and anaerobic hydrocarbon degrader communities in a tar-oil contaminated aquifer. *Microorganisms* **7**: 1–15.

Pilloni, G., von Netzer, F., Engel, M., and Lueders, T. (2011) Electron acceptor-dependent identification of key anaerobic toluene degraders at a tar-oil-contaminated aquifer by Pyro-SIP. *FEMS Microbiol Ecol* **78**: 165–175.

Pruesse, E., Quast, C., Knittel, K., Fuchs, B.M., Ludwig, W., Peplies, J., and Glöckner, F.O. (2007) SILVA: a comprehensive online resource for quality checked and aligned ribosomal RNA sequence data compatible with ARB. *Nucleic Acids Res* **35**: 7188–7196.

Quast, C., Pruesse, E., Yilmaz, P., Gerken, J., Schweer, T., Yarza, P., et al. (2013) The SILVA ribosomal RNA gene database project: improved data processing and web-based tools. *Nucleic Acids Res* **41**: D590–D596.

Rabus, R., Boll, M., Heider, J., Meckenstock, R.U., Buckel, W., Einsle, O., et al. (2016) Anaerobic microbial degradation of hydrocarbons: from enzymatic reactions to the environment. *Microb Physiol* **26**: 5–28.

Ramos-Padrón, E., Bordenave, S., Lin, S., Bhaskar, I.M., Dong, X., Sensen, C.W., et al. (2011) Carbon and sulfur cycling by microbial communities in a gypsum-treated oil sands tailings pond. *Environ Sci Technol* **45**: 439–446.

Rao, A., Risgaard-Petersen, N., and Neumeier, U. (2016) Electrogenic sulfur oxidation in a northern saltmarsh (St. Lawrence Estuary, Canada). *Can J Microbiol* **62**: 530–537.

Reed, W.E. and Kaplan, I.R. (1977) The chemistry of marine petroleum seeps. *J Geochem Explor* **7**: 255–293.

Révész, F., Farkas, M., Kriszt, B., Szoboszlay, S., Benedek, T., and Táncsics, A. (2020) Effect of oxygen limitation on the enrichment of bacteria degrading either benzene or toluene and the identification of *Malikia spinosa* (Comamonadaceae) as prominent aerobic benzene-, toluene-, and ethylbenzene-degrading bacterium: enrichment, isolation and whole-genome analysis. *Environ Sci Pollut Res* **27**: 31130–31142.

Revbech, N.P. (1989) An oxygen microsensor with a guard cathode. *Limnol Oceanogr* **34**: 474–478.

Revbech, N.P. and Jørgensen, B.B. (1986) Microelectrodes: their use in microbial ecology. In *Advances in Microbial Ecology*. Advances in Microbial Ecology. Marshall, K.C. (ed). Boston, MA: Springer US, pp. 293–352.

Risgaard-Petersen, N., Kristiansen, M., Frederiksen, R.B., Dittmer, A.L., Bjerg, J.T., Trojan, D., et al. (2015) Cable bacteria in freshwater sediments. *Appl Environ Microbiol* **81**: 6003–6011.

Risgaard-Petersen, N., Revil, A., Meister, P., and Nielsen, L.P. (2012) Sulfur, iron-, and calcium cycling associated with natural electric currents running through marine sediment. *Geochim Cosmochim Acta* **92**: 1–13.

Ryan, M. p., Pembroke, J. t., and Adley, C. c. (2007) *Ralstonia pickettii* in environmental biotechnology: potential and applications. *J Appl Microbiol* **103**: 754–764.

Sandfeld, T., Marzocchi, U., Petro, C., Schramm, A., and Risgaard-Petersen, N. (2020) Electrogenic sulfide oxidation mediated by cable bacteria stimulates sulfate reduction in freshwater sediments. *ISME J* **14**: 1233–1246.

Sayre, J.D. (1926) Physiology of stomata of *Rumex patientia*. *Ohio J Sci* **57**: 205–206.

Schauer, R., Risgaard-Petersen, N., Kjeldsen, K.U., Tataru Bjerg, J.J., Jørgensen, B.B., Schramm, A., and Nielsen, L.P. (2014) Succession of cable bacteria and electric currents in marine sediment. *ISME J* **8**: 1314–1322.

Schloss, P.D., Jenior, M.L., Koumpouras, C.C., Westcott, S.L., and Highlander, S.K. (2016) Sequencing 16S rRNA gene fragments using the PacBio SMRT DNA sequencing system. *PeerJ* **4**: e1869.

Schloss, P.D., Westcott, S.L., Ryabin, T., Hall, J.R., Hartmann, M., Hollister, E.B., et al. (2009) Introducing mothur: open-source, platform-independent, community-supported software for describing and comparing microbial communities. *Appl Environ Microbiol* **75**: 7537–7541.

Scholz, V.V., Martin, B.C., Meyer, R., Schramm, A., Fraser, M.W., Nielsen, L.P., et al. (2021) Cable bacteria at oxygen-releasing roots of aquatic plants: a widespread and diverse plant–microbe association. *New Phytol* **232**: 2138–2151.

Scholz, V.V., Meckenstock, R.U., Nielsen, L.P., and Risgaard-Petersen, N. (2020) Cable bacteria reduce methane emissions from rice-vegetated soils. *Nat Commun* **11**: 1–5.

Scholz, V.V., Müller, H., Koren, K., Nielsen, L.P., and Meckenstock, R.U. (2019) The rhizosphere of aquatic plants is a habitat for cable bacteria. *FEMS Microbiol Ecol* **95**: 1–9.

Schönheit, P., Kristjansson, J.K., and Thauer, R.K. (1982) Kinetic mechanism for the ability of sulfate reducers to out-compete methanogens for acetate. *Arch Microbiol* **132**: 285–288.

Scilipoti, S., Koren, K., Risgaard-Petersen, N., Schramm, A., and Nielsen, L.P. (2021) Oxygen consumption of individual cable bacteria. *Sci Adv* **7**: eabe1870.

Seitaj, D., Schauer, R., Sulu-Gambari, F., Hidalgo-Martinez, S., Malkin, S.Y., Burdorf, L.D.W., et al. (2015) Cable bacteria generate a firewall against euxinia in seasonally hypoxic basins. *Proc Natl Acad Sci* **112**: 13278–13283.

Selle, B., Knorr, K.-H., and Lischeid, G. (2019) Mobilisation and transport of dissolved organic carbon and iron in peat catchments—insights from the Lehstenbach stream in Germany using generalised additive models. *Hydrol Process* **33**: 3213–3225.

Shi, L., Richardson, D.J., Wang, Z., Kerisit, S.N., Rosso, K.M., Zachara, J.M., and Fredrickson, J.K. (2009) The roles of outer membrane cytochromes of Shewanella and Geobacter in extracellular electron transfer. *Environ Microbiol Rep* **1**: 220–227.

Shinoda, Y., Sakai, Y., Uenishi, H., Uchihashi, Y., Hiraishi, A., Yukawa, H., et al. (2004) Aerobic and anaerobic toluene degradation by a newly isolated denitrifying bacterium, *Thauera* sp. strain DNT-1. *Appl Environ Microbiol* **70**: 1385–1392.

Shotyk, W. (1988) Review of the inorganic geochemistry of peats and peatland waters. *Earth-Sci Rev* **25**: 95–176.

Sikkema, H.R., Gaastra, B.F., Pols, T., and Poolman, B. (2019) Cell fuelling and metabolic energy conservation in synthetic cells. *ChemBioChem* **20**: 2581–2592.

Stackebrandt, E. and Ebers, J. (2006) Taxonomic parameters revisited: tarnished gold standards. *Microbiol Today* **33**: 152–155.

Sulu-Gambari, F., Seitaj, D., Meysman, F.J.R., Schauer, R., Polerecky, L., and Slomp, C.P. (2016) Cable bacteria control iron–phosphorus dynamics in sediments of a coastal hypoxic basin. *Environ Sci Technol* **50**: 1227–1233.

Táncsics, A., Szalay, A.R., Farkas, M., Benedek, T., Szoboszlay, S., Szabó, I., and Lueders, T. (2018) Stable isotope probing of hypoxic toluene degradation at the Siklós aquifer reveals prominent role of Rhodocyclaceae. *FEMS Microbiol Ecol* **94**: fiy088.

Teng, F., Darveekaran Nair, S.S., Zhu, P., Li, S., Huang, S., Li, X., et al. (2018) Impact of DNA extraction method and targeted 16S-rRNA hypervariable region on oral microbiota profiling. *Sci Rep* **8**: 1–12.

Thompson, L.R., Sanders, J.G., McDonald, D., Amir, A., Ladau, J., Locey, K.J., et al. (2017) A communal catalogue reveals Earth’s multiscale microbial diversity. *Nature* **551**: 457–463.

Thomsen, U., Thamdrup, B., Stahl, D.A., and Canfield, D.E. (2004) Pathways of organic carbon oxidation in a deep lacustrine sediment, Lake Michigan. *Limnol Oceanogr* **49**: 2046–2057.

Thorup, C., Petro, C., Bøggild, A., Ebsen, T.S., Brokjær, S., Nielsen, L.P., et al. (2021) How to grow your cable bacteria: establishment of a stable single-strain culture in sediment and proposal of *Candidatus Electronema aureum* GS. *Syst Appl Microbiol* **44**: 1–9.

Thorup, C., Schramm, A., Findlay, A.J., Finster, K.W., and Schreiber, L. (2017) Disguised as a sulfate reducer: growth of the Deltaproteobacterium *Desulfurivibrio alkaliphilus* by sulfide oxidation with nitrate. *mBio* **8**: e00671-17.

Trojan, D., Schreiber, L., Bjerg, J.T., Bøggild, A., Yang, T., Kjeldsen, K.U., and Schramm, A. (2016) A taxonomic framework for cable bacteria and proposal of the candidate genera *Electrothrix* and *Electronema*. *Syst Appl Microbiol* **39**: 297–306.

Tucci, M., Cruz Viggi, C., Esteve Núñez, A., Schievano, A., Rabaey, K., and Aulenta, F. (2021) Empowering electroactive microorganisms for soil remediation: challenges in the bioelectrochemical removal of petroleum hydrocarbons. *Chem Eng J* **419**: 1–15.

Urban, N.R., Brezonik, P.L., Baker, L.A., and Sherman, L.A. (1994) Sulfate reduction and diffusion in sediments of Little Rock Lake, Wisconsin. *Limnol Oceanogr* **39**: 797–815.

Varjani, S.J., Gnansounou, E., and Pandey, A. (2017) Comprehensive review on toxicity of persistent organic pollutants from petroleum refinery waste and their degradation by microorganisms. *Chemosphere* **188**: 280–291.

Vasquez-Cardenas, D., Vossenberg, J. van de, Polerecky, L., Malkin, S.Y., Schauer, R., Hidalgo-Martinez, S., et al. (2015) Microbial carbon metabolism associated with electrogenic sulphur oxidation in coastal sediments. *ISME J* **9**: 1966–1978.

Vassilev, I., Averesch, N.J.H., Ledezma, P., and Kokko, M. (2021) Anodic electro-fermentation: empowering anaerobic production processes via anodic respiration. *Biotechnol Adv* **48**: 1–13.

van de Velde, S., Lesven, L., Burdorf, L.D.W., Hidalgo-Martinez, S., Geelhoed, J.S., Van Rijswijk, P., et al. (2016) The impact of electrogenic sulfur oxidation on the biogeochemistry of coastal sediments: a field study. *Geochim Cosmochim Acta* **194**: 211–232.

Vogel, T.M. and Grbici-Galic, D. (1986) Incorporation of oxygen from water into toluene and benzene during anaerobic fermentative transformation. *Appl Environ Microbiol* **52**: 200–202.

Wagner, J., Coupland, P., Browne, H.P., Lawley, T.D., Francis, S.C., and Parkhill, J. (2016) Evaluation of PacBio sequencing for full-length bacterial 16S rRNA gene classification. *BMC Microbiol* **16**: 1–17.

Waite, D.W., Chuvochina, M., Pelikan, C., Parks, D.H., Yilmaz, P., Wagner, M., et al. (2020) Proposal to reclassify the proteobacterial classes Deltaproteobacteria and Oligoflexia, and the phylum Thermodesulfobacteria into four phyla reflecting major functional capabilities. *Int J Syst Evol Microbiol* **70**: 5972–6016.

Waite, D.W., Vanwonterghem, I., Rinke, C., Parks, D.H., Zhang, Y., Takai, K., et al. (2017) Comparative genomic analysis of the class Epsilonproteobacteria and proposed reclassification to Epsilonbacteraeota (phyl. nov.). *Front Microbiol* **8**: 1–19.

Wallner, G., Amann, R., and Beisker, W. (1993) Optimizing fluorescent in situ hybridization with rRNA-targeted oligonucleotide probes for flow cytometric identification of microorganisms. *Cytometry* **14**: 136–143.

Wang, X., Aulenta, F., Puig, S., Esteve-Núñez, A., He, Y., Mu, Y., and Rabaey, K. (2020) Microbial electrochemistry for bioremediation. *Environ Sci Ecotechnology* **1**: 1–7.

Wang, Y., Cui, D., Li, A., Yang, J., and Ma, F. (2016) Complete genome sequence of Chelatococcus sp. CO-6, a crude-oil-degrading bacterium. *J Biotechnol* **219**: 20–21.

- Watanabe, H., Tanji, Y., Unno, H., and Hori, K. (2008) Rapid conversion of toluene by an acinetobacter sp. Tol 5 mutant showing monolayer adsorption to water-oil interface. *J Biosci Bioeng* **106**: 226–230.
- Watanabe, T., Kojima, H., and Fukui, M. (2016) Identity of major sulfur-cycle prokaryotes in freshwater lake ecosystems revealed by a comprehensive phylogenetic study of the dissimilatory adenylylsulfate reductase. *Sci Rep* **6**: 1–9.
- Weelink, S.A.B., van Eekert, M.H.A., and Stams, A.J.M. (2010) Degradation of BTEX by anaerobic bacteria: physiology and application. *Rev Environ Sci Biotechnol* **9**: 359–385.
- Wenger, A.M., Peluso, P., Rowell, W.J., Chang, P.-C., Hall, R.J., Concepcion, G.T., et al. (2019) Accurate circular consensus long-read sequencing improves variant detection and assembly of a human genome. *Nat Biotechnol* **37**: 1155–1162.
- Weyer, C., Peiffer, S., and Lischeid, G. (2018) Stream water quality affected by interacting hydrological and biogeochemical processes in a riparian wetland. *J Hydrol* **563**: 260–272.
- Whiteley, A.S., Thomson, B., Lueders, T., and Manefield, M. (2007) RNA stable-isotope probing. *Nat Protoc* **2**: 838–844.
- Wickham, H. (2011) ggplot2. *WIREs Comput Stat* **3**: 180–185.
- Wilkes, H. and Schwarzbauer, J. (2010) Hydrocarbons: an introduction to structure, physico-chemical properties and natural occurrence. In *Handbook of Hydrocarbon and Lipid Microbiology*. Timmis, K.N. (ed). Berlin, Heidelberg: Springer Berlin Heidelberg, pp. 1–48.
- Williams, S.D., Ladd, D.E., and Farmer, J. (2006) Fate and transport of petroleum hydrocarbons in soil and ground water at Big South Fork National River and recreation area, Tennessee and Kentucky, 2002–2003, Scientific Investigations Report 2005-5104.
- Wisotzky, F. and Eckert, P. (1997) Sulfat-dominiertes BTEX-Abbau im Grundwasser eines ehemaligen Gaswerksstandortes. *Grundwasser* **2**: 11–20.
- Wu, S., Zhao, Y., Chen, Y., Dong, X., Wang, M., and Wang, G. (2019) Sulfur cycling in freshwater sediments: a cryptic driving force of iron deposition and phosphorus mobilization. *Sci Total Environ* **657**: 1294–1303.
- Yan, F. and Reible, D. (2015) Electro-bioremediation of contaminated sediment by electrode enhanced capping. *J Environ Manage* **155**: 154–161.

Yang, X. and Chen, S. (2021) Microorganisms in sediment microbial fuel cells: ecological niche, microbial response, and environmental function. *Sci Total Environ* **756**: 1–13.

Yang, Y., Wang, Z., Gan, C., Klausen, L.H., Bonné, R., Kong, G., et al. (2021) Long-distance electron transfer in a filamentous Gram-positive bacterium. *Nat Commun* **12**: 1–9.

Yilmaz, P., Parfrey, L.W., Yarza, P., Gerken, J., Pruesse, E., Quast, C., et al. (2014) The SILVA and “All-species Living Tree Project (LTP)” taxonomic frameworks. *Nucleic Acids Res* **42**: D643–D648.

Yin, H., Aller, R.C., Zhu, Q., and Aller, J.Y. (2021) The dynamics of cable bacteria colonization in surface sediments: a 2D view. *Sci Rep* **11**: 1–8.

Zhang, T., Gannon, S.M., Nevin, K.P., Franks, A.E., and Lovley, D.R. (2010) Stimulating the anaerobic degradation of aromatic hydrocarbons in contaminated sediments by providing an electrode as the electron acceptor. *Environ Microbiol* **12**: 1011–1020.

Zhou, J., Fries, M., Chee-Sanford, J.C., and Tiedje, J. (1995) Phylogenetic analyses of a new group of denitrifiers capable of anaerobic growth on toluene and description of *Azoarcus tolulyticus* sp. nov. *Int J Syst Evol Microbiol* **45**: 500–506.

Zhu, B., Wang, Z., Kanaparthi, D., Kublik, S., Ge, T., Casper, P., et al. (2020) Long-read amplicon sequencing of nitric oxide dismutase (nod) genes reveal diverse oxygenic denitrifiers in agricultural soils and lake sediments. *Microb Ecol* **80**: 243–247.

Ziółkowska, A. and Wyszkowski, M. (2010) Toxicity of petroleum substances to microorganisms and plants. *Ecol Chem Eng S* **17**: 73–82.

## Appendix 1: Supporting Information

*Table 7: Summary of PacBio sequencing results and number of reads in each sample*

Sample description	Barcode	Polymerase reads	Subreads	Bases	Mean read length	Mean of longest subread length	Mean no. of passes	No. of CCS	No. of reads after quality check
Stream Inoculum	lbc87	15231	233419	336409768	23192	1792	17	10004	6646
Stream Sed 0-3 mm	lbc78	10579	183320	233930697	23424	1597	17	7192	4314
Stream Sed 3-6 mm	lbc79	10537	162256	232016861	23136	1755	17	6772	4856
Stream Sed 6-10 mm	lbc80	6320	97806	140160855	23317	1744	17	4072	3052
Stream Sed 10-15 mm	lbc81	9912	153405	216712061	22978	1722	17	6482	5313
Stream Sed 20-25 mm	lbc83	11040	171688	246755751	23478	1762	17	6935	5421
Stream Sed 25-30 mm	lbc84	6795	109892	150476053	23340	1746	17	4511	3615
Stream Sed 30-40 mm	lbc85	6786	107432	149201724	23130	1712	17	4378	3532
Stream Sed 40-50 mm	lbc86	5389	81790	118230428	23024	1756	17	3469	2784
Stream Agar 0-3 mm	lbc69	12616	201507	285108383	23748	1778	17	7800	6415
Stream Agar 3-6 mm	lbc70	9321	144163	212224530	23880	1797	17	5972	4551
Stream Agar 6-10 mm	lbc71	22425	355376	512297692	23992	1751	17	14857	11814
Stream Agar 10-15 mm	lbc72	12548	194991	281808159	23572	1763	17	8174	6175
Stream Agar 15-20 mm	lbc73	12179	198807	276730098	23901	1770	17	7622	4864
Stream Agar 20-25 mm	lbc74	9293	148541	215470216	24345	1786	17	6105	4844
Stream Agar 25-30 mm	lbc75	12597	196279	286253375	23852	1783	17	8235	6567
Stream Agar 30-40 mm	lbc76	9258	151488	208560333	23727	1706	17	6080	4344
Stream Agar 40-50 mm	lbc77	31292	487709	713324966	23911	1782	17	20773	14448
Lake Inoculum	lbc57	14237	352163	567617032	41697	2061	n.a.	8249	6519
Lake Sed 0-3 mm	lbc69	25075	660287	1005600132	42035	1850	n.a.	16270	12662
Lake Sed 3-6 mm	lbc70	5416	135143	215303159	41601	2044	n.a.	3213	2479
Lake Sed 6-10 mm	lbc71	5888	145878	227472349	40459	1969	n.a.	3489	2748
Lake Sed 10-15 mm	lbc72	15505	391899	610784312	41259	1965	n.a.	9679	7379
Lake Sed 15-20 mm	lbc73	13440	333860	525058948	40909	2017	n.a.	7986	5974
Lake Sed 20-30 mm	lbc74	3852	97313	149927469	40785	2012	n.a.	2304	1732
Lake Sed 30-40 mm	lbc75	30724	778477	1219942204	41582	1982	n.a.	18882	14819
Lake Sed 40-50 mm	lbc76	25552	663325	1006048110	41284	1875	n.a.	16502	12207
Lake Agar 0-3 mm	lbc50	6353	155726	248057537	40862	2062	n.a.	3839	3286
Lake Agar 30-40 mm	lbc51	4038	112659	160245241	41738	1813	n.a.	2255	1776
Lake Agar 40-50 mm	lbc52	5621	156000	230824397	43128	1855	n.a.	3289	2606
Aquifer Inoculum	lbc89	5901	89627	132514181	23533	1797	17	2533	2900
Aquifer Sed 0-3 mm	lbc42	20016	326100	463916636	24366	1752	17	12821	10325
Aquifer Sed 3-6 mm	lbc43	3767	58708	85398814	23778	1774	17	2390	1908
Aquifer Sed 6-10 mm	lbc44	12214	186646	278905879	23941	1834	17	7619	5888
Aquifer Sed 10-15 mm	lbc45	10922	167380	249526677	23951	1809	17	6731	5359
Aquifer Sed 15-20 mm	lbc46	6063	94993	139763681	24170	1853	17	4022	3076
Aquifer Sed 20-25 mm	lbc47	19861	305738	456594242	24099	1802	17	12394	9576
Aquifer Sed 25-30 mm	lbc48	8750	135460	216957278	25900	2047	17	5752	3523
Aquifer Sed 30-40 mm	lbc49	11064	169347	259480344	24553	1885	17	7109	5184
Aquifer Sed 40-50 mm	lbc50	9965	151598	224609378	23635	1813	17	6294	4762
Aquifer Agar 0-3 mm	lbc36	11773	189380	275285689	24543	1763	17	7857	6169
Aquifer Agar 3-6 mm	lbc37	7767	122898	179747473	24303	1765	17	5063	4253
Aquifer Agar 6-10 mm	lbc38	4712	67029	114277676	25285	2184	17	3044	2520
Aquifer Agar 10-15 mm	lbc39	14696	231367	337398227	24131	1772	17	9100	6991
Aquifer Agar 15-20 mm	lbc40	12975	201385	298166430	24099	1796	17	8542	6225
Aquifer Agar 20-25 mm	lbc41	7696	123958	181112442	24697	1753	17	5131	4117

## Incubation in columns from River Eger sediment

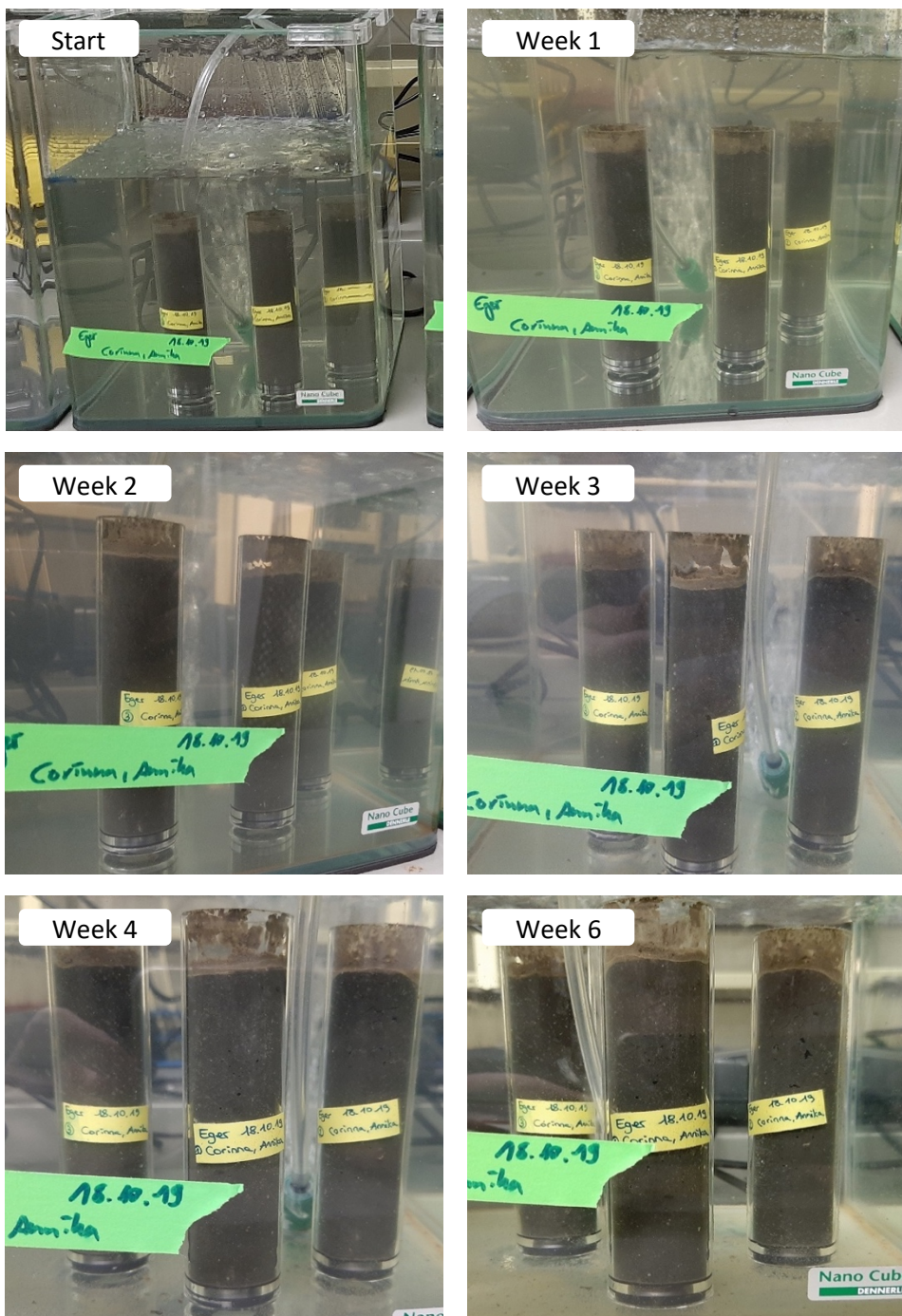


Figure 39: Visible changes over incubation time in upright flooded microcosms. The columns with internal agar pillar are made from river Eger sediment. The oxic zone of the sediment can be detected as upper light-brown sediment (1-3 mm), while the deeper layers remain anoxic, observable by the darker colour.

Table 8: Preparation of freshwater medium.

Solution A		Wolfe's Mineral Solution		
CaCO <sub>3</sub>	0.025 g	Add 1.5 g nitrilotriacetic acid to approximately 500 mL of water and adjust to pH 6.5 with KOH to dissolve, then add the following:		
NaHCO <sub>3</sub>	0.025 g		MgSO <sub>4</sub> x 7 H <sub>2</sub> O	3.0 g
Distilled water	900 mL		MnSO <sub>4</sub> -H <sub>2</sub> O	0.5 g
Solution B				
NH <sub>4</sub> Cl	5.3 mg		NaCl	1.0 g
KH <sub>2</sub> PO <sub>4</sub>	14 mg		FeSO <sub>4</sub> x 7 H <sub>2</sub> O	0.1 g
KNO <sub>3</sub>	100 mg		CoCl <sub>2</sub> x 6 H <sub>2</sub> O	0.1 g
MgSO <sub>4</sub> x 7 H <sub>2</sub> O	493 mg		CaCl <sub>2</sub>	0.1 g
CaCl <sub>2</sub> x 2 H <sub>2</sub> O	147 mg		ZnSO <sub>4</sub> x 7 H <sub>2</sub> O	0.1 g
Distilled water	1000 mL		CuSO <sub>4</sub> x 5 H <sub>2</sub> O	0.01 g
Dissolve carbonates in distilled water by stirring and add other components while stirring, adjust to pH 7.2 with KOH. Autoclave solutions separately.			AlK(SO) <sub>4</sub> x 12 H <sub>2</sub> O	0.01 g
			H <sub>3</sub> BO <sub>3</sub>	0.01 g
			Na <sub>2</sub> MoO <sub>4</sub> x 2 H <sub>2</sub> O	0.01 g
		Fill up to 1000 ml and adjust to pH 6.8.		
		Filter sterilize.		

To prepare freshwater medium, combine 900 mL Solution A with 100 mL Solution B and 1 mL Wolfe's Mineral Solution. Adjust to pH 7.2.

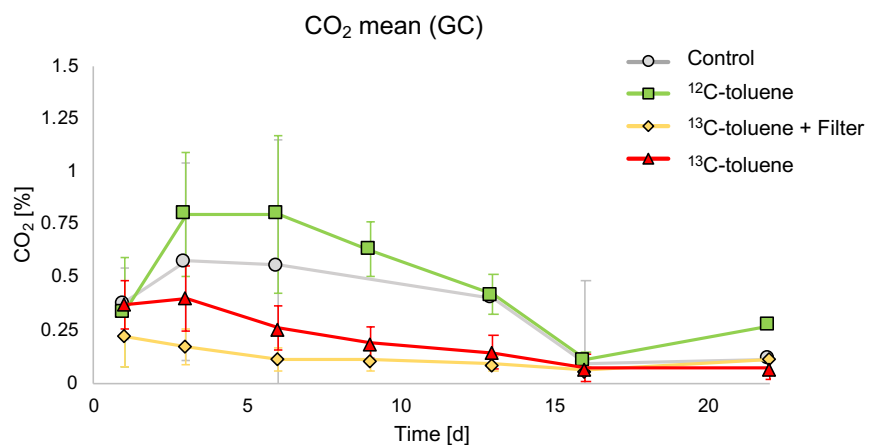


Figure 40: CO<sub>2</sub> concentrations in microcosm headspace (GC). Measurements were performed by gas chromatography (GC). Error bars show standard deviation of measurements from at least 3 biological replicates (up to day 13). GC measurements indicated initial CO<sub>2</sub> concentrations on day 1 for control, 12C-toluene- and 13C-toluene-amended microcosms of 0.38%, 0.33% and 0.37% CO<sub>2</sub>, respectively, with a maximum on day 3 with 0.57%, 0.80% and 0.40% CO<sub>2</sub> and decreasing concentrations until a minimum on day 16 with <0.11% CO<sub>2</sub>. Afterwards, CO<sub>2</sub> concentrations did not change, except in microcosms with 12C-toluene amendment, in which CO<sub>2</sub> concentrations slightly increased to 0.27%, probably due to reduced number of replicates (due to sacrificing). In comparison, microcosms with cable bacteria-free treatment reached a maximum CO<sub>2</sub> concentration of 0.22% on day 1, which decreased afterwards to ~0.10% after day 6.

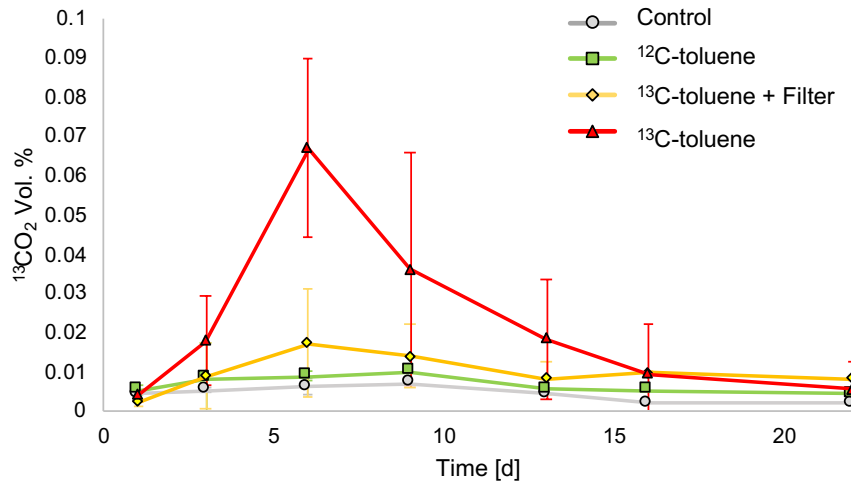


Figure 41: Volume %  $^{13}\text{CO}_2$  in microcosm headspace. Error bars show standard deviation of measurements from at least 3 biological replicates (up to day 13).

Table 9: Refractive index and calculated density from DNA-SIP experiment.

Origin Details	Fraction	Refr. Index	Density	Origin Details	Fraction	Refr. Index	Density
1_U_B <sup>12</sup> C Day 8 5-10 mm depth	1	1,4086	1.758	1_U_E <sup>12</sup> C Day 8 20-25 mm depth	1	1,4085	1.757
	2	1,4080	1.752		2	1,4074	1.745
	3	1,4072	1.743		3	1,4066	1.737
	4	1,4064	1.734		4	1,4058	1.728
	5	1,4055	1.725		5	1,4049	1.718
	6	1,4046	1.715		6	1,4040	1.708
	7	1,4038	1.706		7	1,4032	1.699
	8	1,4027	1.694		8	1,4025	1.692
	9	1,4020	1.686		9	1,4020	1.686
	10	1,4012	1.677		10	1,4009	1.674
	11	1,4002	1.666		11	1,4001	1.665
	12	1,3997	1.661		12	1,3997	1.661
	13	1,3956	1.615		13	1,3976	1.638
Origin Details	Fraction	Refr. Index	Density	Origin Details	Fraction	Refr. Index	Density
1_L_B <sup>13</sup> C Day 8 5-10 mm depth	1	1,4087	1.759	1_L_E_Wdh <sup>13</sup> C Day 8 20-25 mm depth	1	1,4095	1.768
	2	1,4076	1.747		2	1,4084	1.756
	3	1,4070	1.741		3	1,4073	1.744
	4	1,4061	1.731		4	1,4065	1.735
	5	1,4050	1.719		5	1,4054	1.723
	6	1,4043	1.711		6	1,4046	1.715
	7	1,4036	1.704		7	1,4037	1.705
	8	1,4026	1.693		8	1,4029	1.696
	9	1,4018	1.684		9	1,4018	1.684
	10	1,4010	1.675		10	1,4007	1.672
	11	1,4001	1.665		11	1,4001	1.665
	12	1,3988	1.651		12	1,3993	1.657
	13	1,3755	1.387		13	1,3799	1.438

Origin Details	Fraction	Refr. Index	Density	Origin Details	Fraction	Refr. Index	Density
1_F_B 13C + Filter Day 8 5-10 mm depth	1	1,4083	1.755	1_F_E 13C + Filter Day 8 20-25 mm depth	1	1,4090	1.763
	2	1,4076	1.747		2	1,4081	1.753
	3	1,4069	1.740		3	1,4072	1.743
	4	1,4060	1.730		4	1,4062	1.732
	5	1,4051	1.720		5	1,4054	1.723
	6	1,4042	1.710		6	1,4046	1.715
	7	1,4034	1.702		7	1,4037	1.705
	8	1,4025	1.692		8	1,4027	1.694
	9	1,4017	1.683		9	1,4019	1.685
	10	1,4008	1.673		10	1,4011	1.676
	11	1,4000	1.664		11	1,4004	1.669
	12	1,3988	1.651		12	1,3995	1.659
	13	1,3837	1.481		13	1,3836	1.480
Origin Details	Fraction	Refr. Index	Density	Origin Details	Fraction	Refr. Index	Density
2_U_B 12C Day 15 5-10 mm depth	1	1,4088	1.760	2_U_E 12C Day 15 20-25 mm depth	1	1,4089	1.762
	2	1,4078	1.750		2	1,4081	1.753
	3	1,4068	1.739		3	1,4073	1.744
	4	1,4061	1.731		4	1,4065	1.735
	5	1,4052	1.721		5	1,4055	1.725
	6	1,4044	1.713		6	1,4047	1.716
	7	1,4035	1.703		7	1,4040	1.708
	8	1,4025	1.692		8	1,4030	1.697
	9	1,4016	1.682		9	1,4023	1.690
	10	1,4008	1.673		10	1,4014	1.680
	11	1,4000	1.664		11	1,4005	1.670
	12	1,3991	1.654		12	1,3998	1.662
	13	1,3788	1.425		13	1,3910	1.564
Origin Details	Fraction	Refr. Index	Density	Origin Details	Fraction	Refr. Index	Density
2_L_B_Wdh 13C Day 15 5-10 mm depth	1	1,4092	0.944	2_L_E 13C Day 15 20-25 mm depth	1	1,4090	1.763
	2	1,4083	1.765		2	1,4081	1.753
	3	1,4072	1.755		3	1,4072	1.743
	4	1,4064	1.743		4	1,4062	1.732
	5	1,4053	1.734		5	1,4052	1.721
	6	1,4046	1.722		6	1,4046	1.715
	7	1,4038	1.715		7	1,4040	1.708
	8	1,4028	1.706		8	1,4029	1.696
	9	1,4021	1.695		9	1,4021	1.687
	10	1,4011	1.687		10	1,4012	1.677
	11	1,4003	1.676		11	1,4004	1.669
	12	1,3995	1.668		12	1,3997	1.661
	13	1,3799	1.659		13	1,3831	1.475
Origin Details	Fraction	Refr. Index	Density	Origin Details	Fraction	Refr. Index	Density
2_F_B 13C + Filter Day 15 5-10 mm depth	1	1,4092	1.765	2_F_E 13C + Filter Day 15 20-25 mm depth	1	1,4096	1.769
	2	1,4087	1.759		2	1,4088	1.760
	3	1,4076	1.747		3	1,4075	1.746
	4	1,4067	1.738		4	1,4068	1.739
	5	1,4059	1.729		5	1,4058	1.728
	6	1,4049	1.718		6	1,4049	1.718
	7	1,4043	1.711		7	1,4043	1.711
	8	1,4033	1.701		8	1,4034	1.702
	9	1,4024	1.691		9	1,4025	1.692
	10	1,4017	1.683		10	1,4016	1.682
	11	1,4010	1.675		11	1,4008	1.673
	12	1,4000	1.664		12	1,3999	1.663
	13	1,3819	1.461		13	1,3812	1.453

Depth: 5-10 mm

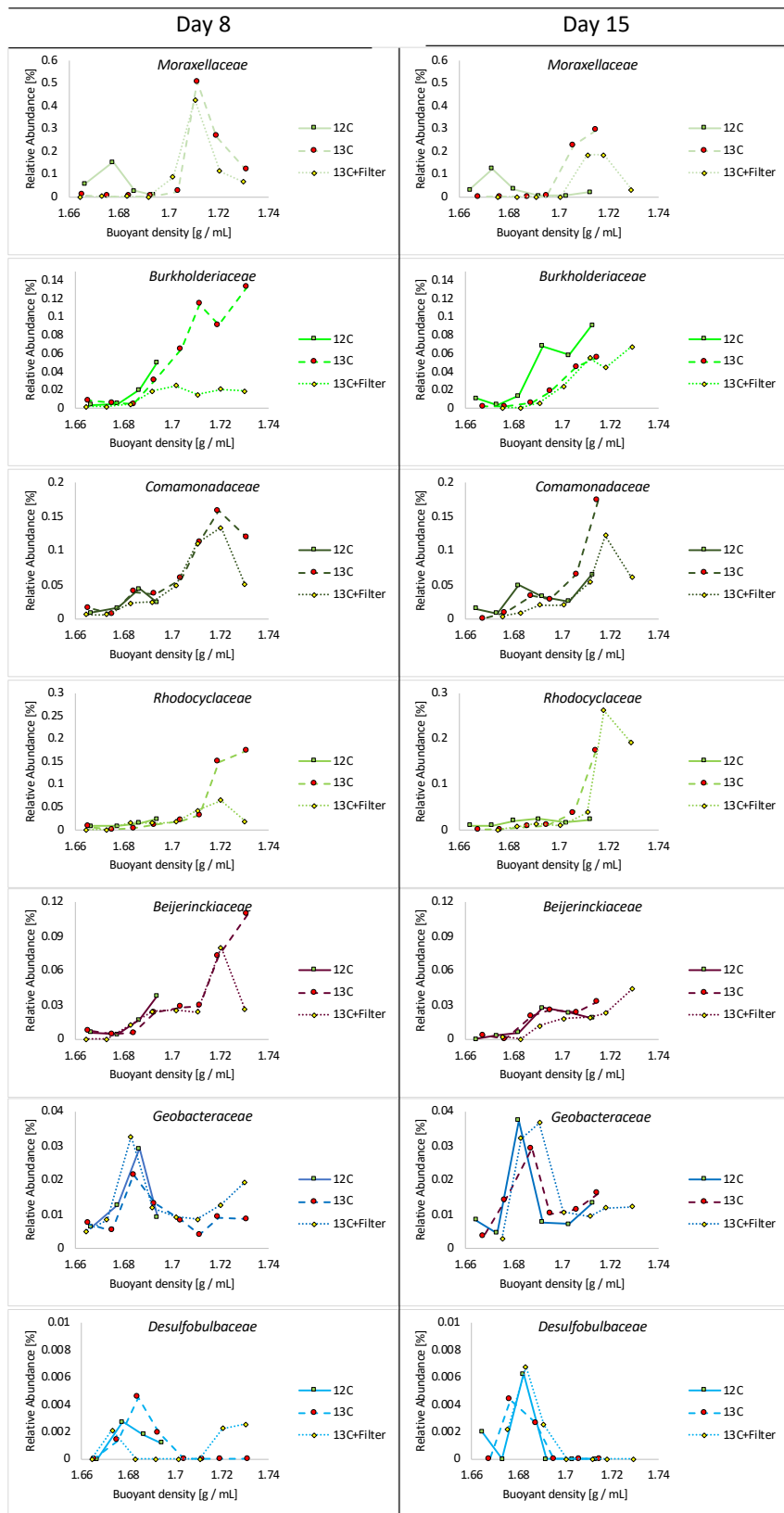


Figure 42: Relative abundance of selected families at 5-10 mm in SIP fractions over density. Data from day 8 are shown in the left panel, data from day 15 are shown in the right panel. Both show data from sediment depth 5-10 mm in the microcosms. Unlabelled toluene/12C: straight line; labelled toluene/13C: dashed line; labelled toluene and filter insertions/13C+Filter: dotted line.

Depth: 20-25 mm

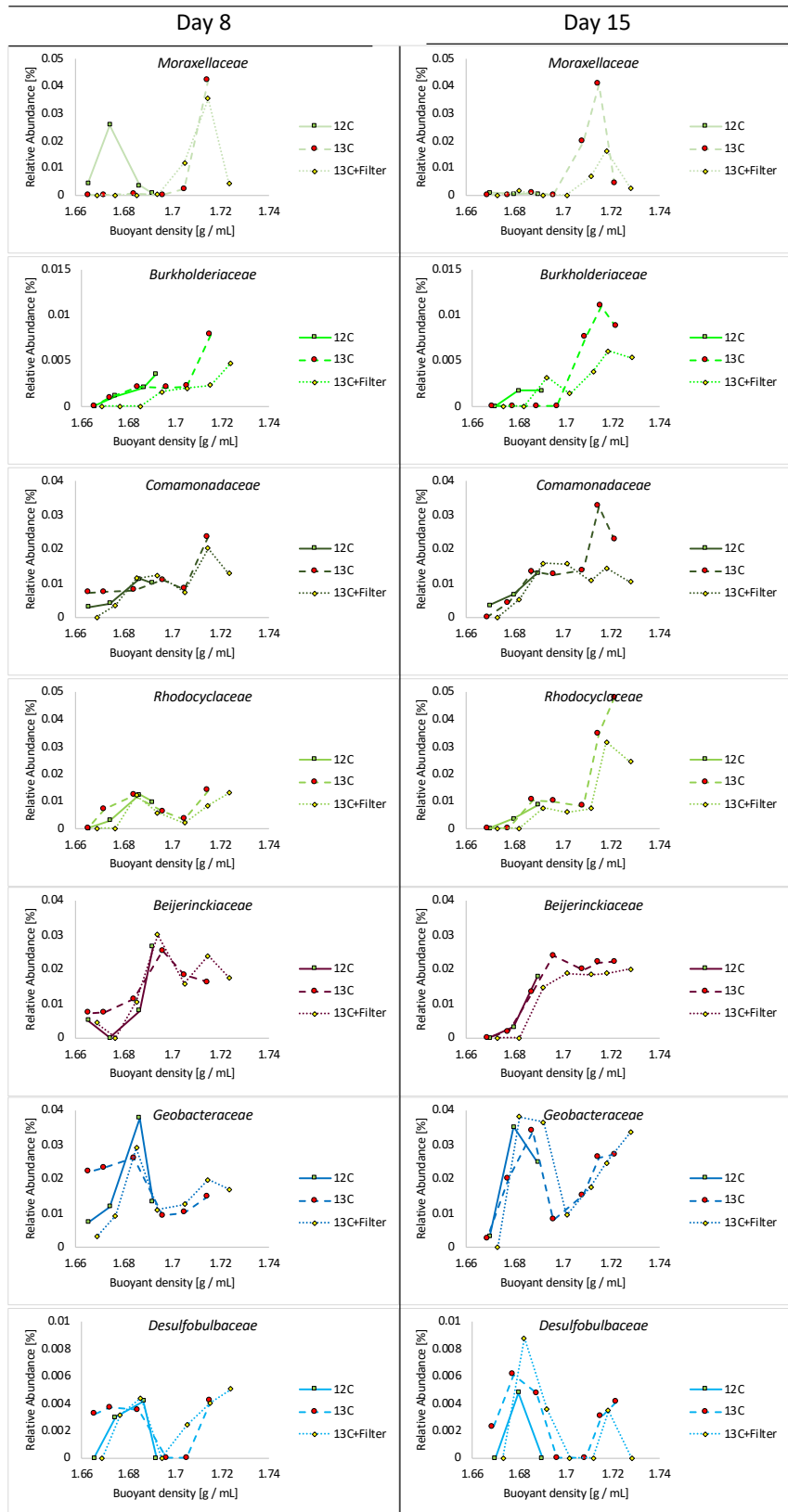


Figure 43: Relative abundance of selected families at 20-25 mm in SIP fractions over density. Data from day 8 are shown in the left panel, data from day 15 are shown in the right panel. Both show data from sediment depth 20-25 mm in the microcosms. Unlabelled toluene/12C: straight line; labelled toluene/13C: dashed line; labelled toluene and filter insertions/13C+Filter: dotted line.

**Table 10: Comparative enrichment of taxonomic groups in “heavy” fractions. Data from day 15 at 5-10 mm depth are shown and comparative enrichment was calculated by dividing relative sequencing abundance in  $^{13}\text{C}$ -microcosms by relative sequencing abundance in  $^{12}\text{C}$ -microcosms.**

	$^{13}\text{C}$ -toluene-amended microcosms			$^{13}\text{C}$ -toluene-amended microcosms + Filter		
	F6	F7	F8	F6	F7	F8
Other Phyla <1%	0.39	0.65	1.53	0.34	0.81	1.51
<i>Planctomycetes</i>	0.33	0.60	0.76	0.16	0.35	0.39
<i>Acidobacteriota</i>	0.22	0.75	0.82	0.40	0.93	0.83
<i>Thermoanaerobaculaceae</i>	0.09	0.38	4.96	0.17	0.52	3.53
<i>Holophagaceae</i>	0.19	0.77	0.82	0.34	1.20	1.20
<i>Actinobacteriota</i>	0.23	0.34	1.63	0.29	0.45	2.00
<i>Spirochaetes</i>	0.00	0.57	1.23	0.77	0.57	0.60
<i>Bacteroidota</i>	0.22	1.27	1.34	0.71	1.15	1.31
<i>Bacteroidetes vadinhA17</i>	0.34	1.81	1.01	0.84	1.78	1.09
<i>Chloroflexi</i>	0.23	0.58	2.08	0.27	0.56	1.95
<i>Anaerolineaceae</i>	0.34	1.01	0.88	0.49	1.38	1.25
<i>Firmicutes</i>	NA	1.56	0.00	NA	1.30	0.86
<i>Desulfobacterota</i>	0.11	1.27	0.69	0.32	1.02	0.68
<i>Desulfosarcinaceae</i>	0.49	1.31	0.67	0.47	1.33	0.51
<i>Geobacteraceae</i>	1.21	1.60	1.34	0.90	1.32	1.40
<i>Desulfobulbaceae</i>	NA	NA	NA	NA	NA	NA
<i>Gammaproteobacteria</i>	0.21	0.75	1.07	0.94	0.79	1.25
<i>Moraxellaceae</i>	13.56	48.42	0.30	8.54	39.62	0.00
<i>Gallionellaceae</i>	0.51	1.69	3.41	0.00	0.00	1.14
<i>Burkholderiaceae</i>	0.61	0.77	0.26	0.48	0.94	0.35
<i>Comamonadaceae</i>	2.66	2.53	0.87	1.88	2.09	0.61
<i>Rhodocyclaceae</i>	7.74	2.26	0.40	11.74	2.32	0.39
<i>Alphaproteobacteria</i>	0.94	0.82	0.84	0.66	0.75	1.04
<i>Xanthobacteraceae</i>	0.67	1.04	0.72	0.33	0.66	0.94
<i>Beijerinckiaceae</i>	1.76	0.99	0.92	1.22	0.82	0.66
<i>Myxococcota</i>	0.09	0.52	2.31	0.15	0.59	2.18
<i>Patescibacteria</i>	3.73	0.47	NA	1.63	1.04	NA
<i>Verrucomicrobiota</i>	4.00	1.46	0.77	0.97	0.40	0.32
<i>Pedosphaeraceae</i>	0.47	0.75	0.57	1.15	1.32	0.74
<i>Opitutaceae</i>	0.20	0.76	0.90	0.29	1.07	0.88

## Appendix 2: Bioinformatics Example

### Illumina 16S rRNA read (base 515 to base 806) analysis with Dada2 as denoising algorithm

```
library(dada2); packageVersion("dada2")
library(Biostrings); packageVersion("Biostrings")
library(ShortRead); packageVersion("ShortRead")
library(ggplot2); packageVersion("ggplot2")
library(reshape2); packageVersion("reshape2")
library(gridExtra); packageVersion("gridExtra")
library(phyloseq); packageVersion("phyloseq")

# Path to unzipped and demultiplexed fastq files # Mac
path <- <path to fastq>
path.rds <- <path th r-files>
filenames <- list.files(path, pattern = ".fastq", full.names = TRUE)

list.files(path)

# read in the names of the fastq files
# Only forward fastq files with format: SAMPLENAME_R1_001.fastq
fn <- sort(list.files(path, pattern="*_R1_001.fastq", full.names = TRUE))

# Extract sample names
sample.names <- sapply(strsplit(basename(fn), "_R"), `[, 1)

# Primers need to be trimmed off
F515 <- "GTGYCAGCMGCCGCGTAA"
R806 <- "GGACTACNVGGGTWTCTAAT"

rc <- dada2:::rc
theme_set(theme_bw())

nops <- file.path(path, "noprimers", basename(fn))
prim <- removePrimers(fn, nops, primer.fwd=F515, max.mismatch=3, orient=TRUE,
verbose=TRUE)

# Inspect read quality profiles
plotQualityProfile(fn[1:2])
plotQualityProfile(nops[1:2])

# Filter and trim
filt <- file.path(path, "filtered", paste0(sample.names, "_filt.fastq.gz"))
names(filt) <- sample.names

# truncLen=> 293 is total length
# filter after removing primers with removeprimers
# general filtering for Illumina iSeq Reads
out <- filterAndTrim(nops, filt, trimLeft=0, truncLen=272, minLen=250,
maxN=0, maxEE=2, truncQ=2, rm.phix=TRUE,
compress=TRUE, multithread=FALSE, verbose=TRUE)

# adapted filtering for Illumina iSeq Reads from SIP fractions
out <- filterAndTrim(nops, filt, trimLeft=0, truncLen=220, minLen=200,
maxN=0, maxEE=1, truncQ=2, rm.phix=TRUE,
compress=TRUE, multithread=FALSE, verbose=TRUE)

# Learn the Error Rates
err <- learnErrors(filt, multithread=TRUE)
plotErrors(err, nominalQ=TRUE)

# Sample Inference
dada <- dada(filt, err=err, multithread=TRUE)

# Inspect the merger data.frame from the first sample
head(dada[[1]])

# Construct sequence table
seqtab <- makeSequenceTable(dada)
dim(seqtab)
# Inspect distribution of sequence lengths
table(nchar(getSequences(seqtab)))
```

```

# Remove chimeras
seqtab.nochim <- removeBimeraDenovo(seqtab, method="consensus", multithread=TRUE,
verbose=TRUE)
dim(seqtab.nochim)
sum(seqtab.nochim) / sum(seqtab)

# Track reads through the pipeline
getN <- function(x) sum(getUniques(x))
track <- cbind(out, sapply(dada, getN), rowSums(seqtab.nochim))
colnames(track) <- c("input", "filtered", "denoised", "nonchim")
rownames(track) <- sample.names
head(track)

# Assign taxonomy
taxa <- assignTaxonomy(seqtab.nochim, file.path(path,
"silva_nr99_v138.1_train_set.fa.gz"), multithread=TRUE)
taxa <- addSpecies(taxa, file.path(path, "silva_species_assignment_v138.1.fa.gz"))

# Handoff to phyloseq
samples.out <- rownames(seqtab.nochim)
#setwd("~/OutputPhyloseq/")

metadata <- read.table("MetadataTest.txt", header = TRUE)
head(metadata)
samdf <- data.frame(metadata)
rownames(samdf) <- samples.out
ps <- phyloseq(otu_table(seqtab.nochim, taxa_are_rows=FALSE),
sample_data(samdf),
tax_table(taxa))

dna <- Biostrings::DNAStringSet(taxa_names(ps))
names(dna) <- taxa_names(ps)
ps <- merge_phyloseq(ps, dna)
taxa_names(ps) <- paste0("ASV", seq(ntaxa(ps)))
ps

# Visualize alpha-diversity
plot_richness(ps, x="sample.id", measures=c("Shannon", "Simpson"),
color="sample.site")

# Ordinate
# Transform data to proportions as appropriate for Bray-Curtis distances
ps.prop <- transform_sample_counts(ps, function(otu) otu/sum(otu))
ord.nmds.bray <- ordinate(ps.prop, method="NMDS", distance="bray")

plot_ordination(ps.prop, ord.nmds.bray, color="sample.site", title="Bray NMDS")
plot_ordination(ps.prop, ord.nmds.bray, color="sample.site", shape="sample.time",
title="Bray NMDS")

# Bar plot
top20 <- names(sort(taxa_sums(ps), decreasing=TRUE))[1:20]
ps.top20 <- transform_sample_counts(ps, function(OTU) OTU/sum(OTU))
ps.top20 <- prune_taxa(top20, ps.top20)
plot_bar(ps.top20, x="sample.id", fill="Family") + facet_wrap(~sample.site,
scales="free_x")

# Heatmap of top 300 most abundant bacteria taxa across all samples
data("ps")
bacteria <- subset_taxa(ps, Kingdom=="Bacteria")
bacteria <- prune_taxa(names(sort(taxa_sums(bacteria), TRUE)[1:300]), bacteria)
plot_heatmap(bacteria, sample.label="sample.id")

```

## Manuscripts and Conference Contributions

### Manuscripts

**Sachs C.**, Kanaparthi D., Kublik S., Szalay AR., Schloter M., Damgaard LR., Schramm A., Lueders T. (submitted 2022) Tracing long-distance electron transfer and cable bacteria in freshwater sediments by agar pillar gradient columns, *submitted to FEMS Microbiology Ecology*

**Sachs C.**, Macholett, A., Lueders T. (in prep) Exploring long-distance electron transfer and microbial community patterns in mining-impacted Fichtelgebirge freshwater sediments, *in preparation*

**Sachs C.**, Lueders T. (in prep) Long-distance electron transfer enhances toluene degradation capacity in a freshwater sediment microbial community, *in preparation*

### Conference Contributions

#### Oral

*5th Cable Bacteria Workshop – Virtual Event: “Cryptic sulfur cycling by cable bacteria in freshwater habitats”*. Sachs C., As K., Macholett A., Lueders T., 2020

*DHF, BayCEER, University of Bayreuth, Bayreuth, Germany: “Cable bacteria and biogeochemical redox gradients”*, Sachs C., 2019

*Annual Conference of the Association for General and Applied Microbiology 2018, VAAM Conference, Wolfsburg, Germany: “Filamentous Desulfobulbaceae as mediators of cryptic sulfur cycling in upland soils and aquifer sediments”*, Sachs C., Kanaparthi D., Lueders T., 2018

*4th International Workshop on Cable bacteria, Kalovig, Denmark: “Long-distance electron transfer in water-saturated soils and aquifer sediments mediated by filamentous bacteria”*, Sachs C., Kanaparthi D., Lueders T., 2018

#### Poster

*6th Joint Conference of the DGHM & VAAM – 72nd Annual Meeting of the DGHM & Annual Meeting of the VAAM, Leipzig, Germany: “Cryptic sulfur cycling by cable bacteria in freshwater habitats”*, Sachs C., Kanaparthi D., As K., Lueders T., 2020

*BayCEER Workshop 2019, University of Bayreuth, Bayreuth, Germany:* “Long-distance electron transfer in upright flooded column incubations from terrestrial sediment samples”, Sachs C., Kanaparthi D., Lueders T., 2019, **awarded with poster prize**

*Electromicrobiology 2019, Aarhus, Denmark:* “Long-distance electron transfer in upright flooded column incubations from terrestrial sediment samples”, Sachs C., Kanaparthi D., Lueders T., 2019

*17th International Symposium on Microbial Ecology (ISME), Leipzig, Germany:* “Filamentous Desulfobulbaceae as contributors to cryptic sulfur cycling in upland soils and aquifer sediments”, Sachs C., Kanaparthi D., Lueders T., 2018

*5th Joint Conference of the DGHM & VAAM, VAAM Annual Meeting 2017, 69th Annual Meeting of the DGHM, Würzburg, Germany:* “Tracking down patterns of long-distance electron transfer by filamentous bacteria in flooded soils and groundwater sediments”, Sachs C., Kanaparthi D., Lueders T., 2017

# Authorship Clarification

## Manuscripts featured in this thesis

- 1) Sachs *et al.*, *Tracing long-distance electron transfer and cable bacteria in freshwater sediments by agar pillar gradient columns. FEMS Microbiology Ecology*, Volume 98, Issue 5, May 2022, fiac042, <https://doi.org/10.1093/femsec/fiac042>. Corinna Sachs, Dheeraj Kanaparthi and Tillmann Lüders designed the experiments. Sampling at Flingern aquifer was performed by Corinna Sachs, Dheeraj Kanaparthi and Tillmann Lüders along with other members from Institute of Groundwater Ecology. Corinna Sachs performed sampling at all other locations with occasional aid from Dheeraj Kanaparthi and Gabriele Bartel. Corinna Sachs set up the microcosms and executed the experiments. Corinna Sachs did the microscopy and performed all microsensor measurements. During a lab exchange at Aarhus University, Corinna Sachs performed FISH and microscopy with aid from Andreas Schramm and microsensor measurements with aid from Lars Riis Damgaard. All preparations for PacBio sequencing, including library preparation, were done by Corinna Sachs, with support from Gabriele Bartel, Anna Roza Szalay, Michael Schloter and Susanne Kublik, who also performed the sequencing run at COMI, Helmholtz Zentrum München. All other laboratory work was done by Corinna Sachs. Data Analysis was performed by Corinna Sachs with input for bioinformatics received from Anna Roza Szalay. Corinna Sachs performed bioinformatics. Corinna Sachs performed visualization of results. Corinna Sachs wrote the manuscript with revisions from Tillmann Lüders, Dheeraj Kanaparthi, Michael Schloter, Susanne Kublik, Andreas Schramm and Lars Riis Damgaard. Sections of the submitted manuscript appear in sections of this thesis (Abstract and Chapters 2.1.1.-2.1.3, 2.2.1., 2.3., 2.5.1-2.5.3., 2.6.1-2.6.2, 2.8., 2.9.1., 2.9.3. 3.1., 4.1.).
- 2) Sachs, Macholett, Lüders, *Exploring long-distance electron transfer and microbial community patterns in mining-impacted Fichtelgebirge freshwater sediments*. Corinna Sachs designed the experiments. Corinna Sachs and Annika Macholett performed the sampling with aid from Ralf Mertel on one occasion. Corinna Sachs and Annika Macholett performed microcosm setup. Laboratory experiments were closely supervised by Corinna Sachs, primarily carried out by Annika Macholett with instructions from Corinna Sachs, and partly executed by Corinna Sachs. Index PCR and Illumina sequencing were performed by the team at the Sequencing Core Facility at Bayreuth University. Corinna Sachs performed the data analysis, bioinformatics and visualization for this thesis. Corinna Sachs wrote the sections of this thesis that might be considered for a manuscript (Chapters 2.1.5., 2.8.2., 2.9.2., 2.9.3., 3.2., 4.2.).

- 3) Sachs, Lüders, *Long-distance electron transfer enhances toluene degradation capacity in a freshwater sediment microbial community*. Corinna Sachs designed the experiments with input from Tillmann Lüders. Corinna Sachs performed sampling and microcosm setup. Experiments were carried out by Corinna Sachs. Gas chromatography and optode reading were performed by Ralf Mertel. HPLC measurements were performed by Corinna Sachs, aided by Anita Gößner. IRMS measurements were performed by Bayreuth University's Isotope Core Facility and index PCR and Illumina sequencing were performed by Bayreuth University's Sequencing Core Facility. SIP fractionation was demonstrated once by Tillmann Lüders and carried out by Corinna Sachs. All other laboratory work was performed by Corinna Sachs. Corinna Sachs performed all data analysis, bioinformatics and visualization. Corinna Sachs wrote the sections of this thesis that might be considered for publication (Chapters 2.2.2., 2.4., 2.7., 3.3., 4.3.).

## Acknowledgments

Firstly, I would like to thank Tillmann Lüders, in his role as my PhD adviser, for offering me the project and support. Thank you for giving me this great opportunity to explore the field of electromicrobiology, which also rekindled my personal interest in the data science side of microbiology. I am especially grateful to Dheeraj Kanaparthi for his mentorship and supervision throughout this work, for scientifically challenging me when needed, for inspiring me and for sharing his infinite knowledge about the microbial world with me. I also want to thank Gabi Bartel for taking me under her wing right from the start, and for always offering help (inside and outside the lab). My fellow MolEcol group members over the years (Anne, Anna, Baoli, Clemens, Dheeraj, Gabi, Laura, Lauren, Lu, Zhe) at -now-closed- IGOE were the best group mates anyone could hope for, and were always there to offer support and assistance in various forms (from hot chocolate to locating missing lab equipment) and share a coffee/tea, the occasional cake and a laugh.

I would like to express my gratitude to Andi Schramm and Lars Damgaard for their valuable input to the gradient columns-manuscript and for instructions and supervision during my lab exchange at Aarhus University. Thanks to international colleagues at various CB meetings over the years and for many lively discussions. I want to thank the team from COWI at Helmholtz, and especially Susanne Kublik for organizing and supporting PacBio sequencing during this project.

I was lucky to have started my PhD among the interdisciplinary researchers at IGOE, who not only conducted -scientifically and socially- relevant work in environmental research, but also created a welcoming workplace, filled with kind, encouraging and fun colleagues. Thanks especially to the breakfast group (Gabi, Günter, Anna, Marina, Aileen, Christina, Petra, Judith) for introducing me to archery and for always starting the day nicely, and to my -changing- office mates (Gabi, Anne, Laura, Dheeraj & Baoli) for many great and fun conversations, for sharing diving knowledge, for growing triops and for support with timesheets.

After IGOE closed, moving our lab to Bayreuth, midst my PhD work, was no easy task and I am thankful to the then newfound ÖMIK and BayCEER co-workers to have been welcomed. I am especially grateful for the rewarding experience to teach and to have had Annika as Bachelor student. I also appreciate Bayreuth University's accessible Ombudsperson system for offering guidance to grad students in need.

Not only the academic world contributed to finishing this thesis, there was a lot of support also outside of the lab. Thank you to my parents, who early on encouraged my interest in natural sciences, which led me on the path of pursuing a PhD in environmental research and thank you to my sister for

emotional support. I am also endlessly grateful to my friends for encouragement, having a beer from time to time and making life so much more colourful.

Lastly, thanks to Felix, for being there, for offering support, for kindness and understanding, and for sharing your life (and queso) with me.

This work was financially supported by the European Research Council (ERC) in the frame of the “POLLOX” project (Anaerobic Pollutant Degradation With Oxygen, under FP7-IDEAS-ERC, grant agreement 616644, Principal Investigator: Tillmann Joachim Lüders). I also acknowledge support by the Helmholtz Society, by the Danish National Research Foundation (DNRF136), and by the Department of Ecological Microbiology at Bayreuth University.

## Statutory Declaration / Eidesstattliche Erklärung

(§ 8 Satz 2 Nr. 3 PromO Fakultät)

Hiermit versichere ich eidesstattlich, dass ich die Arbeit selbstständig verfasst und keine anderen als die von mir angegebenen Quellen und Hilfsmittel benutzt habe (vgl. Art. 64 Abs. 1 Satz 6 BayHSchG).

(§ 8 Satz 2 Nr. 3 PromO Fakultät)

Hiermit erkläre ich, dass ich die Dissertation nicht bereits zur Erlangung eines akademischen Grades eingereicht habe und dass ich nicht bereits diese oder eine gleichartige Doktorprüfung endgültig nicht bestanden habe.

(§ 8 Satz 2 Nr. 4 PromO Fakultät)

Hiermit erkläre ich, dass ich Hilfe von gewerblichen Promotionsberatern bzw. –vermittlern oder ähnlichen Dienstleistern weder bisher in Anspruch genommen habe noch künftig in Anspruch nehmen werde.

(§ 8 Satz 2 Nr. 7 PromO Fakultät)

Hiermit erkläre ich mein Einverständnis, dass die elektronische Fassung der Dissertation unter Wahrung meiner Urheberrechte und des Datenschutzes einer gesonderten Überprüfung unterzogen werden kann.

(§ 8 Satz 2 Nr. 8 PromO Fakultät)

Hiermit erkläre ich mein Einverständnis, dass bei Verdacht wissenschaftlichen Fehlverhaltens Ermittlungen durch universitätsinterne Organe der wissenschaftlichen Selbstkontrolle stattfinden können.

.....  
Ort, Datum, Unterschrift